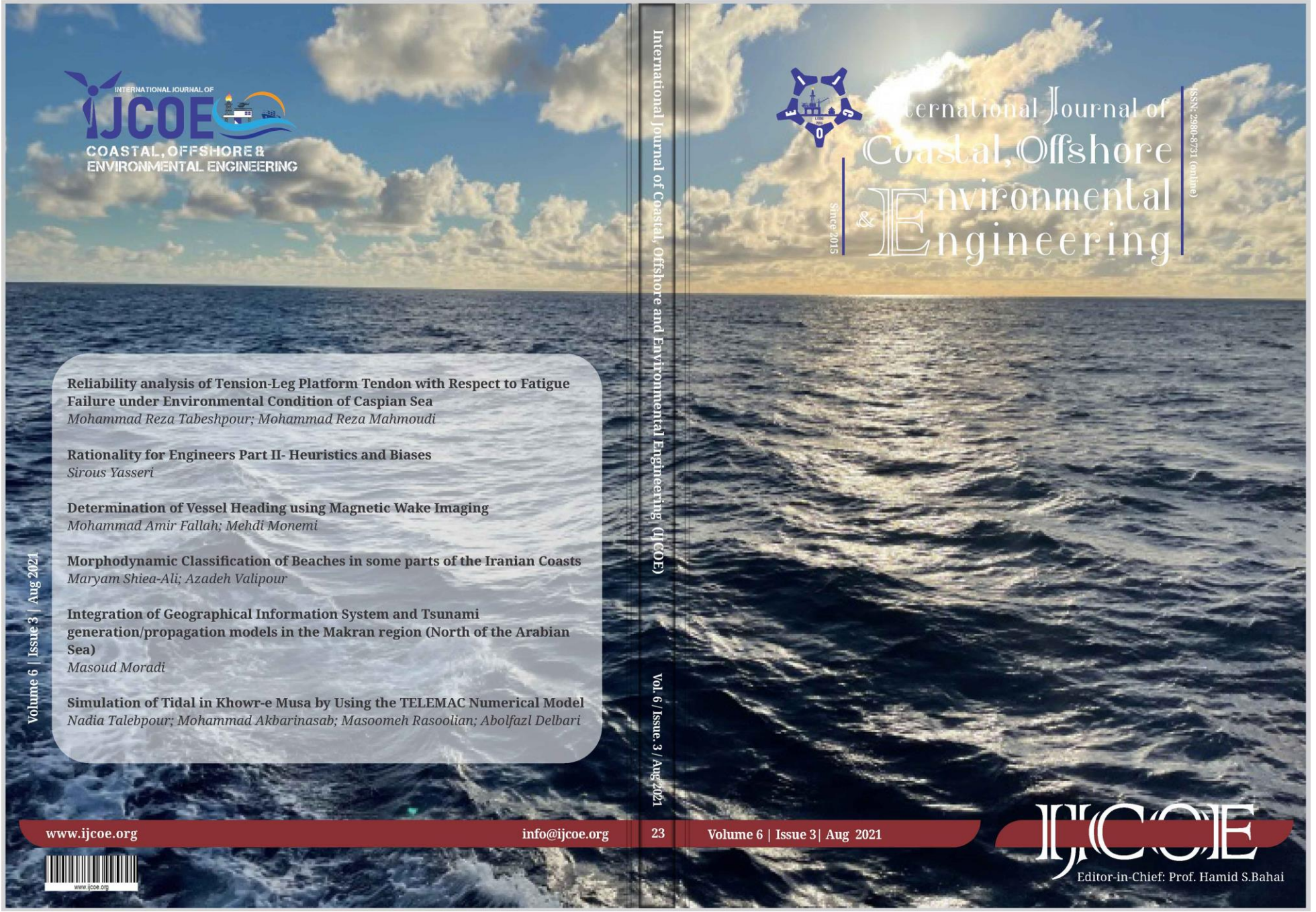

INTERNATIONAL JOURNAL OF
IJCOE
COASTAL, OFFSHORE & ENVIRONMENTAL ENGINEERING

Volume 6 | Issue 3 | Aug 2021

www.ijcoe.org info@ijcoe.org 23

International Journal of Coastal, Offshore and Environmental Engineering (IJCOE)
Vol. 6 / Issue. 3 / Aug 2021

International Journal of
Coastal, Offshore & Environmental Engineering

Since 2015
ISSN: 2980-8731 (online)

Volume 6 | Issue 3| Aug 2021

IJCOE

Editor-in-Chief: Prof. Hamid S.Bahai

International Journal of Coastal, Offshore & Environmental Engineering
Since 2015
ISSN: 2980-8721 (online)

In The Name of God

Message from the Editor-in-Chief

The IJCOE journal office was established in 2015,and its first issue was published in 2016. TheIJCOE covers a wide range of research in thefields of oceanography & ocean technology, aswell as marine industries & marine engineering.The editorial board of IJCOE consists of nearly130 of the greatest scientists and researchersfrom over 30 countries worldwide, and thejournal's review board comprises 1,000 membersfrom all five continents. The membership andapplication process for joining the editorial andreview boards of this journal is ongoing. IJCOE isa research-academic quarterly journal that haspublication and distribution permissions fromthe Press Organization and permission topublish scientific-research articles from theMinistry of Science, Research, and Technology(MSRT) with an "A" rating. It also holds a "Q1"rating from the ISC institute with an impactfactor (IF) of approximately 0.43 and isconsidered a "core journal" (prestigious andoutstanding journal). IJCOE is an open-accessjournal and allows the download and receipt ofaccepted articles in full text for free. It respectsand adheres to copyright and COPE regulations.The journal's office operates 24/7, providingservices to researchers. In addition to publishinga regular quarterly journal, IJCOE has 16 specialissues on specific topics in preparation. It alsoprovides conditions for publishing specializedbooks, references, and handbooks. Moreover, itis ready to cooperate with the secretariats ofreputable international conferences to publishtheir selected and outstanding articles. IJCOEevaluates, appraises, and publishes books,articles, and the scientific achievements andfindings of esteemed researchers and scientistsworldwide who are innovating and conductingin-depth research in the "important and strategicfield of the maritime technology & Oceanengineering." It welcomes any form of jointcooperation with universities, research institutes,and related research centers at the national,regional, and international levels, and extends ahand for collaboration.

Classification of Editorial Board in IJCOE

- Editor-in-Chief
- Director-in-Chief
- Deputy Editor
- Executive Managers
- English Text Editor
- Technical Editor
- International Editorial Board
- National Editorial Board
- Editorial Board Associate
- Editorial Board Assistant
- Guest Editorial Board
- Advisory Board
- Administrative Coordinator
- Honorary Board Member
- Methodology Advisor

Author Benefits

- Open Access
- Rapid Publication
- Thorough Peer-Review
- No Copyright Constraints
- Coverage by Leading Indexing Services
- Discounts On Article Processing Charges (APC)
- No Space Constraints, No restriction on the maximum length of the papers, number of figures or colors

INTERNATIONAL JOURNAL OF IJCOE COASTAL, OFFSHORE & ENVIRONMENTAL ENGINEERING

Aims of IJCOE

Hydrodynamics

Marine equipment

Structural mechanics

Ocean environmental predictions

Stochastic calculations Experimental

Automatic Control of Marine Systems

Scope of IJCOE

Marine Hazards

Ocean Acoustics

Naval Architecture

Ocean Engineering

Coastal Engineering

Marine Meteorology

Marine Earth Sciences

Underwater Technology

Marine Renewable Energy

Polar & Arctic Engineering

Marine Renewable Energy

Marine Geography & Geodesy

Marine Environmental Engineering

Automatic Control of Marine Systems

Hydro Physics & Physical Oceanography

Type of papers

- Case Studies
- Book Reviews
- Review Article
- Letters to the Editor
- Methodology Papers
- Editorials and Commentaries
- Response or Rejoinder Papers
- Perspective or Opinion Papers
- Conceptual or Theoretical Papers
- Meta-Analysis and Systematic Reviews
- Short Communications or Brief Reports
- Research Articles (Original Research Papers)

Scientific Research Journal

Ministry of Science, Research And Technology (MSRT)

Jurnal Ranking 2023: A

Ministry Of Science, Research And Technology (ISC)

Citation Impact 2022: 0.429

Quartile 2022 : Q1

Core Collection

IJCOE is a Member of

Cantact Us

Office 1 | Research Institute of Meteorology and Atmospheric Science

Address | Tehran, Shahid Kharrazi Highway, Pajoohesh Blvd, Research Institute of Meteorology and Atmospheric Science, Sand and Dust Storm International Research Center (SDS-IRC), No. 13, 1st floor.

Phone | +982144787652

Postal code | 13611-14977

website | www.rimac.ac.ir

Office 2 | Iranian National Institute for Oceanography and Atmospheric Science

Address | Tehran, Dr. Fatemi Gharbi St., Shahid Etemadzade St., No. 3, third floor.

Phone | +982166944873

Postal code | 13389 – 14118

website | www.inio.ac.ir

Email | Info@ijcoe.org

Website | www.ijcoe.org

Follow Us

www.ijcoe.org

INTERNATIONAL JOURNAL OF IJCOE COASTAL, OFFSHORE & ENVIRONMENTAL ENGINEERING

Volume & Issue:

Volume 6, Issue 3, August 2021

Number of Articles: 6

Content

INTERNATIONAL JOURNAL OF
COASTAL & OFFSHORE ENGINEERING IJCOE Vol.6/No. 3/Summer 2021 (1-6)

Available online at: www. Ijcoe.org

Reliability analysis of Tension-Leg Platform Tendon with Respect to Fatigue Failure under Environmental Condition of Caspian Sea

Mohammad Reza Tabeshpour[1*], Mohammad Reza Mahmoudi[2]

1. Sharif University of Technology, School of Mechanical Engineering, Tehran, Iran. tabeshpour@sharif.edu*
2. M.Sc. Graduated, Sharif University of Technology, School of Mechanical Engineering, Tehran, Iran.

ARTICLE INFO

Article History:
Received: 03 Mar. 2020
Accepted: 29 June. 2021

Keywords:
Tendon
Tension-leg platform
Fatigue
FORM
Monte Carlo sampling

ABSTRACT

The primary objective of this paper is probabilistic quantification of the fatigue life of tension-leg platforms (TLP) using reliability methods. The need for such methods stems from the significant uncertainty in the loads exerted on offshore structures. The scope of this paper is limited to the study of fatigue in TLP tendons. For this purpose, nonlinear time-history of force response of the TLP tendon under random-wave load is computed via MOSES software and the damage due to fatigue is estimated in accordance with the Palmgren-Miners rule. Assuming a Rayleigh distribution for stress variation and eight different sea states, the ultimate fatigue damage is computed by accumulating the damage over all individual sea states. This cumulative damage enters the limit-state function that is based on the Palmgren-Miners rule. Prevailing sources of uncertainty in this problem are those in the estimation of fatigue stresses, fatigue strength, and the Palmgren-Miners rule. Finally, reliability analysis is carried out for four different service lives using the first- and second-order reliability methods (FORM and SORM) and Monte Carlo sampling. The results indicate that FORM computes the probability of failure sufficiently accurate. It is concluded that the probability of failure increases drastically with the service life. The importance vector from the sensitivity analysis in FORM reveals that the model error is the most influential source of uncertainty on the probability of failure.

1. Introduction

TLP's are floating structures anchored to the sea bottom through vertical tensioned tendons. The tendons hold the platform in place and they remain tensioned due to the excess of buoyancy caused by the floating hull. The tendon system is a critical component for the TLPs, since its failure may lead to the collapse of the whole structure involving human lives, economic losses and damages to the environment. Thus, the tendon system has to be designed to withstand the possible occurrence of different limit states like fatigue. Since offshore structures are subjected to random wave loading, which may contribute to fatigue failure, analyzing and making realistic predictions of failure probability is necessary.

Chatterjee et al. [1] developed a computational tool to handle hydrodynamic and structural aspects of TLP together. They also generated relevant information for a nonlinear static local stress analysis of TLP components from a dynamic hydro-structural global analysis. Lotsberg [2], Banon and Harding [3], Amanullah et al. [4], Khan and Siddiqui [5] studied reliability of TLP tendons under conventional environmental forces. The reliability assessment of TLP tendons under less probable small duration impulsive forces such as that arising due to collision of ships, icebergs, big marine or sea creatures, etc. Siddiqui and Ahmad [6] studied fatigue and fracture reliability of TLP tendons under random loading of sea waves. In this study, fatigue reliability of TLP tendons are evaluated using two common methods, i.e., first order reliability method (FORM) and Mont Carlo simulation. A more detailed application of reliability methods in fatigue assessment of existing offshore structures can be found in Gerhard [7]. Tabeshpour and Malayjerdi [8] stated the effect of pitch degree of freedom on the dynamic response of tendons that can affect the stress in tendons. Such fatigue can lead to tendon failure [9]. In this research, reliability analysis is performed using an approximate method, which models the structure directly as a system rather than modeling of the structural system as a system of components.

2. Limit state function

Fatigue failure has been defined through the limit state function g(z) which is negative or zero at failure. $\underline{Z}$ is vector of basic variables describing load, material properties, geometry variables, statistical estimates and model uncertainties. The probability of failure or probability of limit state violation is defined as

$$P_f = P[g(z) \ll 0] = \int_{g(z)<0} f_z(z)dz \quad (1)$$

where $f_z(z)$ is the joint probability density function of vector z which is the product of individual probability density function of uncorrelated random variables. For fatigue of offshore platforms the major uncertainties involved are due to:

- Estimation of environmental parameters.
- Calculation of hydrodynamic and wind loads.
- Calculation of structural response.
- Calculation of local stresses (stress concentration factors) and stress intensity factors.

In the present study on fatigue reliability the following model has been employed for the formulation of limit state function.

2.1 Miner-Palmgren damage model

Equations in this approach, the fatigue strength is expressed in terms of S-N relation, which gives the number of stress cycles N with stress range S to cause failure. The S-N model generally used for high-cycle fatigue is given as

$$NS^m = A \quad (2)$$

where S is the stress range; m, A are empirical constants; and N is the number of cycles causing failure. The TLP is subjected to environmental loadings, which are random in nature. Consequently, the tendon stresses are random in nature. The estimation of fatigue damage under stochastic loading is commonly done by the Miner-Palmgren model. In this model it is assumed that the damage on the structure, per load cycle, D_j is constant at a given stress range S_j and is equal to

$$D = \frac{1}{N(S_j)} \quad (3)$$

Where $N(S_j)$ is the total number of cycles to failure at stress rangeS_j. The total damage accumulated in time T_s is thus given by

$$D = \sum_{j=1}^{N(T_s)} \frac{1}{N(S_j)} \quad (4)$$

Where $N(T_s)$ is the total number of stress cycles in timeT_s. In this formulation, it is assumed that the accumulated damage D is independent of sequence in which stress cycles occur.

Using the S-N curve, the accumulated damage, D, is given as

$$D = \sum_{j=1}^{N(T_s)} \frac{S_j^m}{A} \quad (5)$$

Since each stress range is a random variable $\sum_{j=1}^{NT_s} S_j^m$ is also a random variable. If $N(T_s)$ is sufficiently large, the uncertainty in the sum is very small and the sum can be replaced by its expected value. Therefore

$$E\left[\sum_{j=1}^{N(T_s)} \frac{S_j^m}{A}\right] = E[N(T_s)]E[S_j^m] \quad (6)$$

For a narrow-band Gaussian process, stress ranges are Rayleigh distributed. The mean value of the stress range follows directly as

$$E[S_j^m] = \int_0^\infty (2x)^m \frac{x}{\sigma_x} \exp\left(-\frac{1}{2}(\frac{x}{\sigma_x})^2\right) dx = (2\sqrt{2})^m \sigma_x^m \Gamma(1+\frac{m}{2}) \quad (7)$$

Hence, the accumulated damage is given as

$$D = \frac{1}{A} E[N(T_s)]E[S_j^m] \quad (8)$$

If we consider the environmental condition being described as a set of stationary short-term sea states, the total damage can be obtained by summing the accumulated damage over all sea states. Thus, the total damage D yields:

$$D = \frac{T_s}{A}\Omega \quad (9)$$

Where Ω is stress parameter given as

$$\Omega = (2\sqrt{2})^m \Gamma(1+\tfrac{m}{2}) \sum_{q=1}^{n} f_q \nu_{o_q} \sigma_q^m$$
$$\nu_{o_q} = \frac{1}{2\pi\sqrt{\frac{m_2}{m_0}}} \quad (10)$$
$$\sigma_q = \sqrt{m_0}$$

Where ν_{o_q} is the zero mean crossing frequency of stress process in q^{th} sea state, f_q is the fraction of time in q^{th} sea state, σ_q is the standard deviation of stress process in q^{th} sea state. m_q is the n^{th} moment of stress spectrum.

$$m_q = \int_0^\infty \omega^n S(\omega) d\omega \quad (11)$$

Failure occurs if $D > \Delta_F$ where Δ_F is the value of the Miner-Palmgern damage index at failure. Often Δ_F is taken as 1.

Letting $D = \Delta$, the time for fatigue failure T of a joint is obtained as

$$T = \frac{\Delta_F A}{\Omega} \quad (12)$$

In order to take into account the uncertainties associated with the above expression, the factors involved in the expression shall be modeled as random variables. The time to failure T_i of joint I may be given as

$$T = \frac{\Delta_F A}{B_i^m \Omega} \quad (13)$$

Where, Δ_F, A_i, B_i are random variable.

In the above Eq.(13), B_i describe the inaccuracies in estimating the fatigue stresses. The actual stress range is assumed equal to the product of B_i and the estimated stress range S. The uncertainties in fatigue strength, as evidenced by scatter in S-N data, are accounted by

considering A_i to be a random variable. The random variable Δ_F quantifies modeling error associated with Miner-Palmgren rule.

Uncertainty in fatigue stress estimates is assumed to stem from five sources. Attempts are made as follows to quantify the uncertainty contributed by each. A suggested model for B_i is [10]:

$$B = B_m B_s B_F B_N B_H \quad (14)$$

In which, each B_i is a random variable describing uncertainty as follows: B_M is fabrication and assembly operations; B_S is seastate description; B_F is wave load predictions; B_N is nominal member loads; B_H is the estimation of hot spot stress concentration factors. As the model error depends on various parameters it is found hard and time taking to determine it. Thus, according to the rules, a lognormal probability distribution function with specified mean and standard deviation is assumed for modeling error parameter [10]. The fatigue failure occurs when the random variable T_i is smaller than T_s where the T_s is the lifetime of the structure. Thus, the limit state function is

$$g(\underline{z}) = \frac{\Delta_F A}{B^m \Omega} - T_s \quad (15)$$

where

$$\underline{Z} = (\Delta_F, A, B) \quad (16)$$

The surface g($\underline{z}$) is the limit state surface, and z is the vector of basic random variables in the problem.

The failure probability is computed using First order reliability method and Monte Carlo simulation technique. If

$$z_1 = \Delta_F \quad z_2 = A \quad z_3 = B \quad (17)$$

Then the limit state function is

$$G(\underline{Z}) = \frac{z_1 z_2}{z_3^m \Omega} - T_s \quad (18)$$

And the probability of failure P_f is

$$P_f = P(T_i \ll T_s) = P[G(z) \leq 0] \quad (19)$$

The reliability or safety index is thus obtained by

$$\beta = \phi^{-1}(P_f) \quad (20)$$

Where ϕ^{-1} , is the inverse of the standardized normal distribution function.

1.1. System reliability

TLP tendons are made of welded elements that form a series system. If any its joints fails, the system fails. If the failure of any joint of any member in a series system were mutually independent, the system probability of failure P_{fsys} can be formulated in terms of welded joints failure probabilities P_{fj} form basic probability considerations:

$$P_{fsys} = 1 - \prod_{j=1}^{n} (1 - P_{fj}) \quad (21)$$

And reliability index as is:

$$\beta_{sys} = -\emptyset^{-1}(P_{fsys}) \quad (22)$$

where n is the number of joints.

2.2 Wide band correction

Fatigue stresses are assumed narrow band random process. However, if they are wide band random process then the stress parameter Ω has to be modified accordingly through a correction factor. In the present study, Wirsching's wide band correction factor (λ) has been applied to modify the expression of Ω Therefore, the corrected expression for stress parameter (Ω) is:

$$\Omega = (2\sqrt{2})^m \Gamma(1 + \frac{m}{2}) \sum_{q=1}^{n} f_q \nu_{o_q} \sigma_q^m \lambda_q \quad (21)$$

Where λ is Wirsching's wide band correction factor for q^{th} sea state [10]. Estimates of λ_q is obtained by the following empirical expressions given by:

$$\lambda_q(\varepsilon_q, m) = a(m) + [1 - a(m)](1 - \varepsilon_q)^{b(m)}$$
$$a(m) = 0.926 - 0.033m$$
$$b(m) = 1.587 - 2.323 \quad (22)$$

And ε_q is the spectral width parameter for q^{th} sea state. For a typical ocean structure problem if ε_q >0.5, then λ_q ≅0.79 for m =4.38 and λ_q ≅0.86 for m =3.

3 Environment

In this study, environmental condition is limited to random waves only. According to data from Iranian Institute of Oceanography and Atmospheric Science, time series of significant wave-height for Caspian Sea is extracted. Thus, eight seastates are obtained based on the probability distribution function that is fitted over mentioned data [12] (Table 1).

$$\sum f(H_s) \Delta H_s \approx 1 \quad (23)$$

And zero up crossing period T_z is estimated as [13]

$$T = 3.21(H_s)^{0.5} \quad (24)$$

Table 1. Caspian Sea Seastates

Seastate	Significant Wave height	T_z	Occurrence Probability
1	1.18	3.46	0.314329
2	2.15	4.67	0.270879
3	3.65	6.09	0.251491
4	5.15	7.23	0.102182
5	6.65	8.22	0.033753
6	8.15	9.10	0.009534
7	9.69	9.93	0.002394
8	11.15	10.651	0.000499

4 Numerical Study

ISSC TLP as described in Table 2 was chosen for reliability study for eight simulated seastates [14]. Dynamic analysis was performed with MOSES software for long-crested random wave idealizing the platform hull as rigid body anchored to the seabed acting like springs. The analysis was carried out using three-dimensional diffraction theory. This non-linear dynamic analysis considers hydrodynamic loading due to random sea represented by JONSWAP spectrum.

The effects of wind and current was ignored in this study.

The stress time-series of the tendons were carried out for 500 seconds with the time step of 0.5 sec. The response was assumed to follow a zero mean Gaussian process. This assumption would be violated particularly if springing and ringing, a higher order wave effects, were considered in the analysis. These major non-linearity causing effects were not being considered in the present study. Figure 2 shows schematic arrangement of tendons under each column.

The stress time-series were statistically analyzed and statistical parameters of stress response were obtained (Table 3). Reliability analysis was carried out using Miner-Palmgren damage model. A brief description of statistics of the random variables are summarized in Table 4.

The probability of failure and reliability indices for four different service lives obtained for long crested random waves using Miner-Palmgren damage model are shown in Table 5. The reliability computations were performed utilizing RT software [16]. Three methods were applied for reliability analysis: First and second order reliability method and Monte Carlo simulation. Two of the most commonly used reliability methods are first and second order reliability. The basic idea of these methods is to ease the computational difficulties through simplifying the calculations and approximating the limit-state function. The name of First Order Reliability Method (FORM) comes from the fact that the limit state function is approximated by the first order Taylor expansion and the Second Order Reliability Method (SORM) uses the second order Taylor expansion. In Monte Carlo simulation, probability of failure is calculated by generating random numbers according to the probability distribution function of the random variables. Therefore, the outcome of the Monte Carlo simulation is considered as the accurate solution for the comparison. In RT, the maximum iterations and coefficient of variation were set ten million and 2% respectively for convergence criteria. Also for system reliability analysis, it was assumed that each tendon was made of 40 welded elements forming a series system. Stress time-history should be calculated for each joint to obtain system reliability but for simplicity, it was logical to assume that the statistic variables of stress at joints were equal.

3 Discussion of results

Figure 3 and 4 show that the FORM results have close proximity with Monte Carlo simulation results. Although SORM uses accurate approximations in comparison with FORM, its computations are often more complicated and time taking. Therefore, FORM is equally sufficient for such problems as Monte Carlo simulation method. Thus, it can be recommended for economical and efficient computation of reliability or probability of failure.

Service life directly affects the probability of failure or reliability of a system. It is seen that as the service life increases, the corresponding probability of failure increases drastically. This is an expected trend.

Table 2. Platform and tendon characteristics [14]

Characteristic	Value
Column spacing	86.25 $[m]$
Column diameter	8.44 $[m]$
Pontoon height	10.5 $[m]$
Pontoon width	7.5 $[m]$
Vertical center of gravity	38 $[m]$
draft	35 $[m]$
Mass of platform	$40.5*10^6$ $[kg]$
Depth	800 [m]
Number of tendons	12
Total pretension	$137.2*10^6$ [N]
Length of tendon	765 [m]
Tendon outer diameter	600 [mm]
Tendon wall thickness	88 [mm]
Tendon young modulus	$2.1*10^{11}$ [N/m^2]

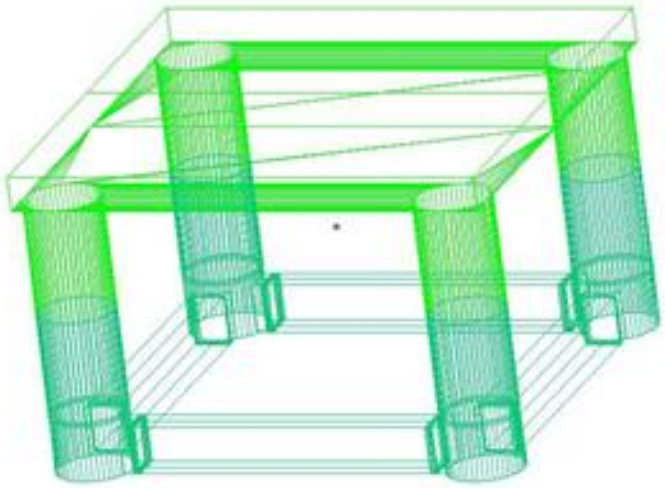

Figure 1: ISSC TLP

Table 3. Statistic for random response

Seastate	Occurrence Probability	RMS stress [MPa]	T_z
1	0.31432	2.28114	2.61E-01
2	0.27087	3.73885	5.93E-01
3	0.25149	3.741657	3.24E-01
4	0.10218	3.770279	3.49E-01
5	0.03375	4.742151	3.51E-01
6	0.00953	5.813777	2.08E-01
7	0.00239	7.486788	4.15E-01
8	0.00049	7.4988	1.24E-01

Table 4. Random variables statistics [6]

Variable	Distribution	Median / Mean	COV
Fatigue strength coefficient, A	lognormal	$\tilde{A} = 5.27 * 10^{12}$	0.63
Stress modeling error, B	lognormal	$\tilde{B} = 1$	0.2
Miner-Palmgren damage index error	lognormal	$\tilde{\Delta} = 1$	0.3
Fatigue exponent, m	constant	3	-

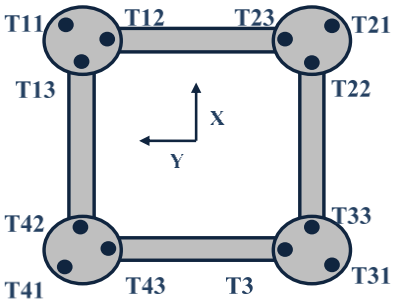

Figure 2: schematic arrangement of tendons

The system reliability analysis of TLP tendon is done assuming that it is consisted 40 elements. The results is shown in table 6. Acceptable range of reliability index based on rules is from 3.09 to 4.75 and of probability of failure from 10^{-6} to 10^{-3}. Therefore, the calculated values of probability of failure and reliability indices for joint and system are in accepted range [17].
Sensitivity analysis performed for random variables appearing in limit state function based on Miner-Palmgren damage model (Table 7). The sensitivity factors for Miner-Palmgren damage index α_Δ and fatigue strength coefficient α_A are negative hence, they are resistance variables and contribute to the resistance part of the limit state function. Sensitivity factor for stress modeling error or response uncertainty factor α_B is positive thus, it will contribute to load part of the limit state function. Therefore, an increase in Miner-Palmgren damage index and fatigue-strength coefficient will enhance the reliability of tendon. On the contrary, an increase in stress modeling error will reduce the reliability of TLP tendon. Furthermore, out of the two resistance variables, reliability is more sensitive to fatigue strength than Miner-Palmgren damage index.

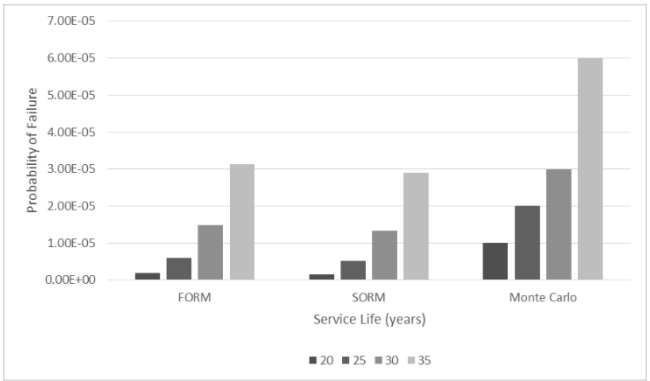

Figure 3: Effect of service life on Probability of failure

Table 5. Values of β and P_f for different service lives

Service life (years)	Monte Carlo		FORM		SORM	
	β	P_f	β	P_f	β	P_f
20	4.26489	1.00E-05	4.62554	1.87E-06	4.65572	1.61E-06
25	4.10748	2.00E-05	4.38029	5.93E-06	4.40615	5.26E-06
30	4.01281	3.00E-05	4.17645	1.48E-05	4.1987	1.34E-05
35	3.84613	6.00E-05	4.00267	3.13E-05	4.02188	2.89E-05

Table 6. Values of and for 20 years service-life

	β	P_f
Joint	4.62554	1.87E-06
System	3.79	7.48E-05

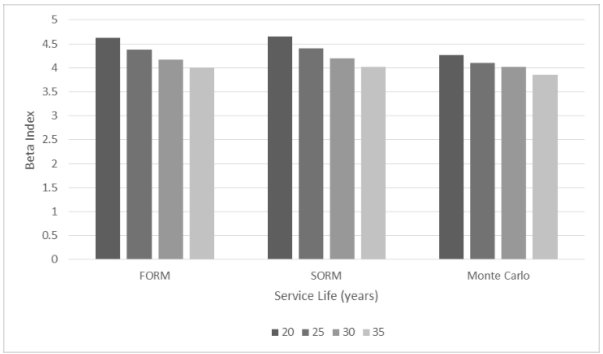

Figure 4: Effect of service life on reliability index

Table 7. **Sensitivity** factors

Sensitivity factor	α_Δ	α_B	α_A
Value	-0.65747	-0.33384	0.675491

4 References

[1]Chatterjee PC, Das PK, Faulkner D. (1997). *A hydro structural analysis program for TLPs. Ocean Engineering*; 24(4):313–34.
[2] Lotsberg I. (1991). *Probabilistic design of the tethers of a tension leg platform*. J Offshore Mech Arctic Eng.; 113:162–9.
[3] Banon H, Harding SJ. *A methodology for assessing the reliability of TLP tethers under maximum and minimum lifetime load*. Proceedings of the fifth international conference
[4] Amanullah M, Siddiqui NA, Umar A, Abbas H. (2002). *Fatigue reliability analysis of welded joints of a TLP tether sy*stem. International Journal of Steel and Composite Structure. 2(5):331–54.
[5] Khan RA, Siddiqui, N.A., Ahmad, Suhail, (2006), *Reliability Analysis of TLP tether under Impulsive Loading*, Reliability Engineering and System Safety 91 73-83.

[6] Siddiqui, N.A., Ahmad, Suhail, (2001). *Fatigue and fracture reliability of TLP tethers under random loading*. Marine Structure. 14, 331–352.
[7] Gerhard E., 2005. *Assessment of existing offshore structures for life extension*, Doctoral Thesis, University of Stavanger.
[8] Golafshani, A.A., Gholizad, A., (2009). *Friction damper for vibration control in offshore steel jacket platforms*. J. Constr. Steel Res. 65 (1). January, Elsevier.
[9] Tabeshpour MR, Ahmadi A, Malayjerdi E., (2018). *Investigation of TLP behavior under tendon damage*. Ocean Engineering 156, 580-595
[10] Wirsching PH. 1984. Fatigue reliability for *offshore structures*. J. Struct Div ASCE; 110(10): 2340-56.
[11] Siddiqui, N.A., and Ahmad, S., (2000). *Reliability analysis against progressive failure of TLP tethers in extreme tension*, Reliability Engineering and System Safety, Vol. 16, pp. 195–205.
[12] Mazaheri, S., Haji Valiei, F., (2012). *Wave Atlas Preparation for Persian Gulf, Oman Sea and Caspian Sea*, Iranian Institute of Oceanography and Atmospheric Science.
[13] Golshani, A.A., Chegini, V., Taebi, S., (2005), *Analysis of extreme wave and wind with different directions for Caspian Sea, Persian Gulf and Oman*, Technical report, Tehran, Iran,.
[14] Tan S., and Gie, (1981). *The wave induced motion of a tension leg platform in deep water*, 13th annual OTC Houston, USA.
[15] Mahmoodi, M.R. (2017) *Stability and dynamic response of tension leg platform in damaged condition (tendon removed) (experimental and numerical)*. Master thesis, Sharif University of Technology. Iran.
[16] Mahsuli, M., (2012). *Probabilistic models, methods, and software for evaluating risk to civil infrastructure. Doctoral thesis*, University of British Columbia.
[17] DNV Classification Notes 30.6, (1992), *Structural Reliability Analysis of Marine Structures*.

INTERNATIONAL JOURNAL OF
COASTAL & OFFSHORE ENGINEERING IJCOE Vol.6/No. 3/Summer 2021 (7-18)

Available online at www. Ijcoe.org

Rationality for Engineers

Part II- Heuristics and Biases

Sirous F. Yasseri*

* *Brunel University London; Sirous.Yasseri@Brunel.ac.uk*

ARTICLE INFO

Article History:
Received: 13 Apr. 2021
Accepted: 23 Aug. 2021

Keywords:
Decision Making
Rules Of Thumb
Fast And Frugal Heuristics
Intuition
Emergency Response
Engineering Judgment
Biases.

ABSTRACT

Two major research programs on the use of heuristics in decision-making exist, and each has its own set of followers. The first program was initiated by Kahneman and Tversky in the 70s. They primarily concentrated on the errors caused by using heuristics. This has now grown into many heuristics named after their associated biases. The second program was initiated by Gigerenzer and colleagues in Germany. Gigerenzer argues that although simple heuristics sometimes leads to "biased" decisions, they can deliver better answers in some situations. This is particularly true for uncertain or complex environments, where there is only a small data sample or there is no time to formally seek an optimized decision. Gigerenzer and colleagues have generated a substantial body of evidence that humans use simple heuristics, often with great results. Like Kahneman and Tversky, Gigerenzer's work has attracted researchers exploring the power of "Fast and Frugal" Heuristics, and how they are used by humans. This part, of the four-part paper, discusses Kahneman and Gigerenzer's findings concerning engineering decision making. Avoiding errors when using simple heuristics is discussed in Part IV.

1. Introduction

There are two ways that thought can enter the brain; one is through structured calculations, which is thinking in stages and applying rules; this is termed "Type 2". The second comes through perception and intuition, which is termed "Type 1". When you see a woman with an angry expression you can tell she is angry as easily as you can tell she is wearing a red dress. Perception predicts using patterns and this is closely linked with intuition. If you are asked the results of the multiplication of two long numbers, you need to follow the rules that you have learned. These are the two types of human thinking. Engineers as experts primarily use Type 1 thinking; it comes about by reinforced learning. If a situation is multi-faceted or complex, Type 1 thinking is not very useful. Perception, intuition, and practiced skills are type 1 thinking. For example, for driving a car or understanding languages, Type 1 will be more appropriate. Type 1 allows functioning within a complex environment and with conflicting information since it ignores much of the information. Engineers particularly populate their brains with rules required for Typ1 thinking and gradually refine them by feedback accumulated by their use. So that they do not need to labour on every decision, just the high-value ones. Mistakes happen when there is a mismatch between perception and reality. Perception is influenced by culture. For example, two distinct perceptions of social events exist, people from the east provide a behavioural explanation, while people from the west favour situational explanation.

Tversky and Kahneman's (1983) work led to the development of the above dual thinking mode termed the 'Dual-process Model". The dual concept encompasses a variety of theories with different approaches to the processes involved in thinking. These two co-existing processes have also been named "System 1" and "System 2" [21,31], intuitive and deliberative [35] associative and rule-based thinking [36], and fast and slow thinking [19]. Researchers who originally coined System 1 and System 2, now use Type 1 and Type 2 processes instead.

Kahneman's concept of thinking fast and slow [19] postulates that humans have two modes of thinking: a heuristic (intuitive) mode that is fast to act, and another mode that is slower, and more deliberative. The latter is the kind of thinking encouraged in critical thinking tests. The dominant "fast-acting" mode usually serves

the decision-maker well enough, as it helped our foraging ancestors to survive, so it has become embedded in our thinking processes. Fast thinking is effortless, associative, and experience-based. While slow thinking requires effort and the use of cognitive resources; it also uses symbolic and abstract rule manipulation. Not all fast and intuitive processes are genetically embedded but learned. In learning to drive one acquires a host of heuristics necessary for confident driving, such as assessing speed, keeping distance, etc. Engineers also learn quick intuitive responses that are reliable. However, on some occasions, when probabilistic reasoning is required, this fast and intuitive reasoning can lead to an erroneous (or biased) decision. These biases have been identified in a wide range of experiments by cognitive psychologists [19].

The concept that people have two co-existing, but separate sets, of decision-making processes, is described by Kahneman [19]:

System 1: This is impulsive, fast, emotional, and acts without deliberation – but relies on heuristics and past knowledge/experience.

System 2: This is a more cognitive, deliberate, thinking process that can take in a greater range of data than just our own experience.

This suggests that if our impulsive nature reacts strongest, this may lead individuals to pursue irrational decisions. For example, 'impulse buys', 'jumping to conclusions. *"Jumping to conclusions is efficient if the outcomes are likely to be correct and the costs of an occasional mistake are tolerable. But it could lead to a risky outcome when the situation is unfamiliar, or the stakes are high* [19].

We need System 1 to function, to free up some of our limited cognitive ability to permit more involved decisions. Without it, tasks such as driving would be very trying. Heuristics and cognitive error are especially relevant when responding to emergencies. In such a situation it may be a struggle to balance efficiency and accuracy, especially in large emergencies that require many fast decisions.

People who originated the idea of System 1 and System 2, abandoned this naming convention in favour of Type 1 and Type 2 to avoid giving the impression that the two systems are operating independently in the brain.

Engineers must think to earn a living. What they know matters, it is not just abstract reasoning. They may carry expertise from one field to another (causal knowledge) which is known as lateral thinking. Each engineering community has developed its own rules and best practices which are primarily experienced-based. Even if they are analytic, they are backed up by proof of the concept in practice. This is the wisdom of the crowd of well-practiced engineers. Here, the term crowd does not mean mob, rather a collection of diverse and informed (albeit partially) people where everyone thinks independently. When the problem is complex, rules are vague, and the environment is uncertain such a crowd performs better, however not unconditionally.

2. Biases Program

Herbert Simon [32] posed the question of how humans make decisions under uncertainty, limited information, and time constraints. He formulated a heuristics decision-making model which he called "Satisficing" [44]. Amos Tversky and Daniel Kahneman in the 1970s linked heuristics to cognitive biases. Their research is known as the "Heuristics and Biases Program". Psychologists and philosophers identified heuristics that were used by humans to make decisions in the past. The original ideas by Herbert Simon[32] were also taken up in the 1990s by Gerd Gigerenzer and others, which is further discussed in the next section.

Heuristics can lead to cognitive biases. What others call heuristics, Kahneman calls biases [19], i.e., he named heuristics by the biases they cause. Kahneman in his book lists 97 cognitive biases and explains how they could happen but does not explore why. In the following, some of the most common biases are described, and a longer list (but not exhaustive) is given in the Appendix to this part.

Confirmation Biases. These biases favour information that confirms our already held beliefs. These biases impact the way we gather information, namely, we only gather evidence [42] that supports our previously held opinions. They also influence how we interpret and recall information. For example, people will interpret news stories in a way that upholds their existing views. They will also remember details in a way that reinforces their attitude. During the election season, for example, people tend to seek positive information that favours their candidates. They will also look for information that casts a shadow on the opposing candidate. By not considering facts objectively, interpreting information incorrectly, and only remembering details that uphold our beliefs, will often lead us to miss important information. A divorcing couple only remembers the bad feeling of the last few months of the divorce proceedings, not the many happy years they had together.

"Till death do us part" is a common phrase exchanged between the bride and groom at a Christian wedding, indicating a commitment to their union. The confirmation bias when takes root has a promise of till death do us apart and getting rid of them is as traumatic as getting a divorce.

Galen was a renowned physician of Greek origin during the times of the Roman Empire (c. 130-210 A.D.). A famous quote attributed to him is a good

example of confirmation bias. "*All who drink of this remedy recover in a short time, except those whom it does not help, who all die. Therefore, it is obvious that it fails only in incurable cases*." We hear the same blind confidence when engineers talking about failure "My design is explosion-proof, and it undoubtedly works. Except when it does not. And, when that happens, it is not because our thinking is flawed, it is the fault of others who didn't follow the intention."

Confirmation bias serves as an efficient way to process information primarily due to the abundance of information humans are exposed to. A few common types of confirmation biases are:

- Biased Search for Information
- Biased Interpretation
- Biased Memory
- Biased Information Processing

Cognitive dissonance also explains why confirmation bias is adaptive. Cognitive dissonance is a mental conflict that occurs when a person holds two contradictory beliefs which cause psychological distress. To minimise dissonance, we adapt to confirmation bias by avoiding information that is contradictory to our views and seek evidence confirming our beliefs.

Representative Heuristics. The perceived likelihood that an object belongs to a particular group is based on how well that object is thought to represent it. Representative Heuristics occur when we believe the probability of an event occurring is based on a perceived similarity with another event. An example of a Representative Heuristic can be seen in "judging a book by its cover", which is an adage that warns us not to assume that similar packaging of a product or an idea will result in the same good outcome, as people tend to associate quality with the packaging, i.e., how it is presented. For the same reason, generic brands package their products to resemble well-known brands. We look for a similar situation we have seen before or similar decisions we have made in the past. Presentation is taken as the quality based on the similarity in packaging.

Using Representative Heuristic, an engineer's decision can be biased by failing to consider relevant and potentially critical evidence. For example, an engineer when predicting the outcome of an event may forget to consider the prevalence of that event. This bias may work differently when considering rare events with a small sample, compared to more common events where there may be larger numbers of atypical samples. This would lead to underestimating the likelihood of a very rare event, perhaps to the extent that thinking they are improbable. Representative bias directs an engineer's attention towards trusting in sets of information that appear to be more consistent. For example, some may believe that in a coin-flipping exercise a heads-and-tails sequence like THTTHT is more likely than TTTHHH because it appears more random [46]. Paraphrasing Popper looking for data to prove yourself wrong is a good way to come up with the right decision. Probability calculations are not like counting apples in a basket.

Affect Heuristics: This heuristic typically involves fast feelings based on prior beliefs. i.e., positive, and negative feelings are associated with certain stimuli in the brain. It happens when feelings take over the process of thinking [47]. The idea behind it is that an emotional response to a stimulus can affect the decision made. When people have little time to reflect and evaluate a situation thoroughly, they may base their decision on their immediate emotional reactions. The Affect Heuristic focuses on eliciting an automatic, fast, and reactionary response.

Advertisements can influence an emotional response, thus affecting purchase decisions. Fast-food companies design their ads to elicit a positive emotional response, that encourages people to view their products positively. People rarely take the time to evaluate the risk and benefit of everything that they see, and often the automatic, emotional response will dominate. Fast-food chains exploit the Affect Heuristic to create a positive emotional response towards their product [48].

Another name for this heuristic is "going with your gut", which causes emotions to influence decisions and perceptions of risk or reward. If you have good feelings about someone e.g., a politician, you are more likely to accept what they say is true, without fact-checking.

Availability Heuristics: This heuristic is about making judgments of the likelihood of an event using information that comes quickly to mind and acts as emotional tagging. In making decisions people typically rely on prior knowledge of an event; mostly they remember such an event. Thus, they tend to overestimate an event's likelihood simply because it comes quickly to mind. Such heuristics allow us to make decisions fast, but their accuracy may be questionable. However, this heuristic prevents us from considering alternatives.

Causes of bias may be the differences when retrieving from memory for different instances. For example:

✓ Salience (the probability of a car crash appears higher right after we have seen one).
✓ Familiarity (after being given a list of names of celebrities, we will tend to base our estimate of how many were male based only on the better-known among them, whom we can recall more easily).
✓ The relative ease of different search modes.
✓ Anything which requires the correct application of rules of probability.
✓ Seeing correlation when there is none.

✓ More publicized, disease events and products are easily recalled.

Availability Heuristics can be useful and accurate in many situations, however, if we can think of a similar situation that ended unfavourably, we are more likely to be cautious.

Two burglaries in your vicinity could change your view on the likelihood of being robbed. The experience of seeing an event may make accidents more vivid in your memory, thus making them seem more probable. However, the probability of an accident in one place is not increased by seeing one in another. Probably "seeing *is believing*".

Anchoring and Adjustment: Engineers often make an initial estimate (guess), based only on one part of the available evidence, and then adjusting it for the rest of the evidence. However, more often the initial guess is very stubborn, and the adjustment process seems to be sluggish, i.e., the initial estimate will not be altered by much. Once we reach a value that we deem plausible and believe to be reasonable, we stop adjusting. Thus, decisions with different starting points will yield different outcomes commensurate with the initial estimate. In a situation with limited information anchoring has the most influence.

An adage says, "don't drop anchor in the ''mockery'' of the past errors". Social ranking is another type of anchoring caused by believing that the truth comes from people who rank above us, while truth can come from both above and below.

Anchoring bias is frequently used in negotiations. You are in a car showroom, and you see a car you like. The showroom has priced the car at $32,000 but is prepared to sell at $28000. After discussing the details of the car, the salesman makes an offer to the customer of $30,000. This is the anchor. The customer hears the $30,000 price and thinks 'oh, that's way out of my price range'. However, at the same time, the customer has anchored their valuation of the car to $30,000.

The salesman then says, 'There is a promotion today, I can make a deal especially for you, I will go down as low as $28,000 if you buy it today.' The customer thinks 'That's an excellent deal, it's a bit out of my price range, but I can't miss out on this offer. Since he has anchored your price expectation at $30,000, anything below it sounds like a bargain. Street vendors and merchants in bazaars are highly skilled at anchoring their customers.

Don and Dan were two brothers who owned a gentleman's attire shop. Don's job was to look after the customers in the front, while Dan always busied himself with the accounts and orders out the back. Don helped customers to find a suit that they liked. When a customer inquiry about the price; Don shouts, "Dan what's the price on this suit?", Dan shouts back "which one?", Don says "the double-fronted blazer with gold buttons, matching trousers, and waistcoat in size 36." Dan shouts back "$825", and Don asks again "how much did you say?"; "$825" shouts Dan in a louder voice. Don tells the customer "$625". The customer heard $825 from Dan; however, the shop was willing to sell it for $525. But the customer is anchored and thinks $625 is cheap. Hence, the customer quickly pays up thinking he has got a bargain.

Simulation Heuristic is present when you are imagining how various scenarios will unfold. People often imagine how a conversation will go, or how they will be treated by others they meet, or what their friends or boss will think. These simulations, like movies in our heads, help us prepare and do a better job when the moment arrives. But they can also lead us to mistaken expectations. People may not react as we imagined, things may go in a much different direction, or we may misread the situation. Our preparations may fail because the outcome of our simulation has misled us into thinking that things would have to go as we had imagined.

Mental Accounting. Another name for this behavioural bias is the "two-pocket" theory. Some people mentally put their money into separate categories, namely dividing them into different mental accounts, depending on their source, or the intent of the account. A $10 lottery win may be ladled as "windfall" and earmarked to buy more tickets. In other words, putting different values on the same amount of money, based on subjective criteria. Regardless of the origin of the money or intended use, all monies are the same. To avoid this mental accounting bias, we should think of money as money when allocating it between our different accounts, be it for food, holidays, or savings.

Hindsight: Causes people to convince themselves after an event that they had accurately predicted the outcome before it happened. This can lead people to conclude that they can accurately predict other events. In hindsight, everybody is an expert, and we knew all along what would happen. When there is no expert, then everybody is an expert. When things go wrong (especially in emergencies), expert witnesses, peers, and senior colleagues often blame someone for not seeing the writing on the wall, forgetting that it was written in invisible ink and only became visible after the event.

Though engineers are not gamblers, they do share some of a gambler's optimism. According to Kahneman's theory of lottery [19], gamblers use different heuristics such as Representative, Availability, Anchoring, and Adjustment, and Framing of Decisions to select their lottery numbers. The Alternative Cognitive Theory of gambling emphasizes the gamblers' irrational beliefs according to *"entrapment, belief in hot and cold*

numbers, unrealistic optimism or perceived luckiness, superstitious belief, an illusion of control, near miss and a few more." [1]

3. Fast and Frugal Heuristics

Another heuristic program headed by Gigerenzer and colleagues in the 1990s took up Herbert Simon's idea [32]; they called it "Fast and Frugal Heuristics". According to their perspective, the study of heuristics requires formal models that allow predictions of behaviour to be made *ex-ante*.

Their program had three aspects:

1. What are the heuristics humans use? (The descriptive study of the "adaptive toolbox")

2. Under what conditions should humans rely on a given heuristic? (The prescriptive study of ecological rationality)

3. How to design heuristic decision aids that are easy to understand and execute? (the engineering study of intuitive design)

This program has shown that heuristics can lead to fast, frugal, and accurate decisions in many real-life situations, characterized by uncertainty. Fast and Frugal Heuristics, as defined by Gigerenzer [10] and Gigerenzer and Todd [13], are simple, task-specific decision strategies learned by experience. They do not require much information and do not involve appreciable computation. Fast and Frugal Heuristics consist of three building blocks which are:

- The way that information is searched for (the search rule).
- When the information search should be stopped (the stopping rule).
- How the processed information is integrated into a decision (the decision rule), and how to choose between two or more options.

"*Judgment and decision tasks are often too complex to be tractable even if time and cognitive capacity were without a limit*" [13].

Gigerenzer has built on Simon's [32] concept of bounded rationality. Simon [32] noted that "*people generally do not have the time, available information, or cognitive ability to optimize*". Simon [32] proposed the notion of bounded rationality as an alternative to optimizing normative models, suggesting that the quality of people's choices should be evaluated in a less "*black-and-white manner according to how reasonable the choices are given realistic constraints of the situation*" [32]. He proposed simple rules of thumb (i.e., heuristics) as a normative alternative to optimizing models of rationality - in his case, "Satisficing", a heuristic that involves choosing the first option that meets one's minimum criteria.

Simon [33] wrote: ''*Human rational behaviour is shaped by scissors whose two blades are the structure of task environments and the computational capabilities of the actor''*. This is equivalent to stating that rationality not only depends on internal criteria but also on the structure of the environment. This notion of ecological rationality looks at human rationality as the result of the adaptive fit between the human mind and the environment [12]. Ecological rationality is a special version of bounded rationality, which focuses on two questions:

1. What are the environmental regularities, and how frequently do they change?
2. How well can people adapt their use of specific strategies to a particular environment?

According to Gigerenzer [10], ''*The basic tenet of ecological rationality is that the rationality or irrationality of a judgment can only be decided by an analysis of the structure of the environment or the experimental task"*. That means that "*ecological rationality is about the fit between a particular heuristic and the environment within which it is applied*" [14). This view suggests different heuristics should be considered in environments with different informational structures [9]. Whether a heuristic is effective depends on how well it fits within the environmental information structure, that is, the ecological rationality. Ecological rationality does not mean that heuristics are good or not, but if they are useful relative to the environment. Thus, their success depends on how well they match the structure of a given environment [11].

Gigerenzer's vision of heuristics, which he calls Fast and Frugal Heuristics (FFH), "*begins with the assumption that the processes people use to make decisions are matched to the environments within which they make these decisions"* [10,33]. This concept is based on the hypothesis that there is a relationship between heuristics and the environments within which they are used. For example, if an FFH performs well in a particular environment, then people tend to use that heuristic within that environment; or if a heuristic is in wider use, then environments that favour that heuristic will tend to be also ubiquitous. Though these assumptions are not universally correct, adaptive assumption serves as a useful starting point for hypothesizing heuristics that people use in each environment [12]. Thus, it can be assumed that heuristics are adapted to the environments within which people find themselves, letting them make fast and effective decisions, even if there is a limitation on available information and cognitive capacity.

Gigerenzer & Todd [13] named the range of "*available heuristics as the mind's, 'adaptive toolbox', from which one can select the best tool, or strategy, for a given task in an uncertain world*." For example, the Recognition Heuristic is frequently used with

reasonable outcomes, as a rule of thumb [27]. Goldstein and Gigerenzer [14] asked students in the United States and Germany: *"Which city has more inhabitants, San Antonio or San Diego? Given the differences in background knowledge about American cities, one might expect that American students would do much better on this task than German students. Most of the German students did not even know that San Antonio is an American city*." Goldstein and Gigerenzer's [14] findings were the opposite of what one would expect: "*Whereas about two-thirds of the American students correctly inferred that San Diego has more inhabitants than San Antonio, all the German students got this question correct. How could this be? The German students' lack of recognition enabled them to use the RH, which, in general, says, "If one of two objects is recognized and the other is not, then infer that the recognized object has the higher value concerning the criterion." The American students could not use the RH because they had heard of both cities; they knew too much. This heuristic cannot be applied if the options are both known or both unknown*."

The RH allows for fast decisions and yields reasonable decisions in many environments because recognition is often systematic rather than random. Domains in which the RH works well include sizes of cities, performances of tennis players in major tournaments, or the productivity of authors. Conversely, the RH does not work well when, for instance, cities are compared concerning their mayor is male or female or comparing the average seasonal temperature.

Complex methods, use tools from logic or statistics that fuse many pieces of information, weighting them according to their perceived importance. It is not difficult to find a specific task for which a simpler method has an advantage over a more complex method. These simple heuristics rely on the concept that **less can be more**, like when a simpler decision strategy outperforms a more complex one or having fewer options leads to appropriate decisions [29]. This **less is more** is akin to the concept that humans do not maximize (i.e., consider all options) but rather 'Satisfice' (i.e., consider one or a few options to reach an acceptable, solution rather than the optimal one [32]. Evidence against pure rational behaviour which supports the less-is-more concepts has been found in many other decision situations such as medical treatment decisions [41]

Take the First (TTF) Heuristic [16]. According to this Heuristic, engineers ''rather than exhaustively generating all possible options and subsequently processing them deliberately [18], simply pick one of the initial options generated. In other words, the heuristic relies on the quality of options that comes to mind spontaneously.

Take the Best Heuristic (TTB). This Heuristic describes searches for cues in the order of their importance. TTB is a Cue Based Heuristic that does not use information integration to make an inference, but bases decisions on single cues. For example, when inferring the size of a city, the decision-maker could consider cues such as whether a city has an airport, a railway station, or is on a major bus route. TTB's search rules look for the cues based on their importance. The best choice should outperform relatively all other choices for the specific cue used. The search stops when one object has a higher positive cue value relative to all other choices. The validity of a cue is taken as the probability of making a correct inference under the condition that the cue discriminates, which means, one object has a positive cue value, while the other object a negative cue value. The search is halted when a cue is found that discriminates so that only one single cue is considered. Otherwise, the next-most valid cue is considered. According to this decision rule, the object that is favoured has a higher criterion value. If no discriminating cue can be found, then TTB takes a random guess. The cues within the heuristic are learned adaptively, as they are the most ecologically valid, and a range of simple heuristics are developed for different situations.

Conan Doyle said through Holmes "I never guess. It is a shocking habit - destructive to the logical faculty". But an "educated" or "inspired" guess is one of the tools in the tool bag, and like any other heuristic, if used in the right environment has a chance of success.

Research on Fast and Frugal Heuristics [4] has produced a significant amount of evidence showing that heuristics can often perform very well, by using just a fraction of the time and data., as they are designed to solve tasks and fit better. The heuristic tool bag of each engineer reflects his/her experience and is domain-specific. By focusing only on relevant pieces of information, heuristics may become portable from one situation to another. Heuristics may be the only tool for undecidable.

The difference between Kahneman and Gigerenwiser often appears to be framing rather than substance. The debate revolves around whether "biased" decisions are an error or "irrationality".

These Fast and Frugal Heuristics often fail the test of logical coherence, as pointed out by Kahneman. Gigerenzer and Todd [13] argue pursuing rationality, as an ideal, misses the point that much of our reasoning is powerful and accurate despite not being logically coherent. Gigerenzer and Todd [13] wrote "*we should replace the coherence criteria with an assessment of the real-world environment and heuristics are the way the mind uses to respond to the structure of the environment, i.e., ecological rationality, which is a*

result of the interaction between the heuristic and the environment."

4. Heuristics for Dealing with an Emergency

The limits of human rationality in decision making as discussed in Part I [44] become more apparent when time is limited and the pressure to act is high. However, knowledge about decision biases can improve emergency management. Simon's bounded rationality [32] concept is more visible during an emergency as it requires engineers to make critical decisions with limited information, time constraints, and often under high demand, and in an environment that is marked by multiple, often conflicting goals, such as resource allocation and priorities as well as preferences.

Natural disasters such as hurricanes, earthquakes, and floods have occurred frequently in recent years. Emergency supply chains are generally formed in response to the needs for the collection and distribution of relief supplies to the affected areas. This is different from commercial supply chains that are perfected by trial and error. In addition to the high expectation, emergency supply chains face challenges such as high expectations, poor information, inadequate communication, uncertainties in network capacity and coverage, limited resource availability, lack of coordination, and a frequent last-minute change of priorities in the shipment content, quantity, and destinations. A similar situation arises in other disasters, such as oil spills, large-scale offshore fires & explosions, aircraft crashes, and so on which require a different approach due to being localized.

Fast and Frugal Heuristics are useful tools when dealing with emergencies since they exploit evolved or learned human capabilities. Fast and Frugal Heuristics are task-specific decision strategies, and they are part of a decision maker's toolbox of cognitive strategies for decision making within a particular environment, which are adequate relative to the structure of that environment. Fast and Frugal Heuristics are composed of simple building blocks that specify how information is gathered, and when enough is gathered, the collected information is processed to develop robust decisions.

The adverse impacts of a disaster can be substantially mitigated if during the disaster accurate information regarding the available volunteers can be gathered, and victims' locations can be determined on time, enabling a well-coordinated and efficient response. This is more visible when there is a spike in requests and public resources are limited. The mismatch between victims and volunteers represents a challenge. Thus, it is important to improve the emergency services' coordination to enable them to efficiently share data, coordinate efforts, allocate the limited resources equitably and offer guidance on optimal resource allocation. These are outside of this paper's focus. The problem of resource coordination has attracted the attention of optimization researchers, and several algorithms on data mining approaches have been proposed to address this problem.

This complex nature of disaster makes it difficult to execute a recovery plan. It is not always possible to plan and optimize response for *every part* of a disaster area. In these situations, heuristics provide an optimal decision-making tool. In the following, a template is proposed for the management of emergencies, without the need to expend significant resources. The first step is to differentiate between critical and acute needs. It is beneficial to view these heuristics as a checklist for planning optimal disaster recovery.

1. *Evaluate the situation and your resources*. An inventory check should tell you if you can match the demand, or where, when, and how much additional resource is required.

2. *Visibility of response status* - Stakeholders should know which stage of the process they are involved in, what they are required to do, and what outcome their actions will have. The point of contact for most stakeholders should be identified.

3. *Match between response and the disaster*. The system should "communicate" to the stakeholders in a way they understand. The flow of processes should be commensurate with the situation on the ground, and stakeholders should be able to readily understand what is going on.

4. *Ready to change course*. Responders should be ready and able to undo mistakes.

5. *Consistency and standards.* Do not initiate changes unless you have a strong reason to do so, and then make your reasoning obvious to others.

6. *Error prevention.* Vigilance to spot errors *before the field agents do*. If this is not practical, then decisions should be validated in real-time.

7. *Recognition does not recall*. Make actions as intuitive as possible, without requiring the responder to remember instructions from a previous operation or consult their field manual.

8. *Flexibility and efficiency*. Allow responders to tailor the response as they see fit. To improvise

9. *Help the responder to recognize, diagnose, and recover from errors*. Clearly describe possible pitfalls, pinpoint the problem, and offer a solution.

10. *Monitor, review, and amend*. Collect data from the field agents and review it continually. Cross-check information from various sources to detect biases and propose corrective action if necessary.

Good communication is vital in an emergency. You never know what goes on in somebody's mind. When you attribute a belief or an opinion to others, most probably you hold that belief yourselves. Every action

may become comprehensible if meanings are attached to it.

Emergencies are "natural laboratories of errors" because of the number of decisions, constant need to switch between tasks, high emotional and cognitive loads, frequently hopping between demands by field agents, and sleep deprivation. Such high demands make emergency responders particularly vulnerable to cognitive missteps. Furthermore, there are limited opportunities for feedback on many emergency decisions, and the lack of feedback makes it challenging to calibrate one's decision-making process, which is a prerequisite for Adaptive Heuristics.

5. Conclusions

The brain does not faithfully transmit what you see. It provides you with an edited version which is a loose definition of what is going around you. The brain fills in missing information and gaps and serves you on a "need to know basis" without a controller to determine what you need to know. You need to be aware of this. Memories are pieces of information that the brain stitches together and sends to you when it considers they will be useful; they have more functional value than accuracy. Memory works like an archaeologist with scant information, just a piece here and a piece there, filling in the gaps by guesswork.

Two major heuristic research programs have been discussed, and a few common heuristics are explained in this part of the paper. The errors associated, and ways to guard against them, are presented briefly here, with a detailed discussion in Part IV [46]. The disciplined use of heuristics, considering their limitations and applicability, was also emphasized.

Heuristics are useful when used appropriately but can lead to biases in judgments. The important thing is to be aware of the bias. The dual representation of human decision-making assumes two types of thinking processes working together; one is fast and impatient, and the other slow and more deliberative. Type 1 replaces ambiguity with automatic guesses, mostly by pre-conceived stories. It creates stories that sound coherent and vivid, but no data to support them. Type 1 suppresses ambiguity by making stories from scanty data. Type 2 is the sceptic within, it weighs pros and cons, questions conclusions, and suspends judgment until a proper foundation can be established. When Type 1 thinking jumps in and makes mistakes, the Type 2 thinking process will slow us down and provide alternatives. We see the world much more coherently with Type 2.

Engineers are expected to think on their feet and appear on the scene ready and tooled up to deal with the situation; possibly while the situation still unfolding, such as during an offshore fire. A car mechanic checks how an engine is running, opens it up, fixes the engine, and puts it all back together so it works as well as new. The engineer is expected to do all these while the engine is running.

Although much of this part focuses on the way that heuristics can cause errors, most of the time, heuristics can provide substantial advantages, even though they may occasionally lead to error. For example, the Availability Heuristic, which directs us to follow the most immediately workable alternative, undoubtedly reflects the fact that an emergency demands fast decision-making more than perfect judgment. Non-optimal solutions often carry significant benefits, even though they may interfere with an accurate assessment of some situations.

There are no great differences between the two programs. Gigerenzer embraces heuristics with enthusiasm, while Kahneman is more cautious and gives a long list of errors arising from the unchecked use of heuristics. The primary emphasis of this article is the dual processing mode. Biases and heuristics have a substantial literature and research base. Their importance for engineers cannot be overestimated. For a quick reference, MacFarlane and Leigh (2014 25) provide a summary and brief description of the main ones that affect situational awareness and decision-making in crises, with a description of their main effects. A range of tools is described by MacFarlane [26] and MacFarlane and Leigh [25].

Acknowledgments The authors would like to thank Chris Millyard, Sassan Rezaei, Mehrdad Rahbari, Kabir Sadeghi, and Michael Vigne, Mohsen Mirza, Giles Thompson for their counsel and feedback, who have assisted to improve the quality and integrity of these papers. I am very much indebted to Mehrdad Rahbari for his patience and help with improving successive revisions.

This research did not receive any specific grant from funding agencies in the public, commercial, or not-for-profit sectors.

6. References

1- Ariyabuddhiphongs, V. (2010). Lottery Gambling: A Review, J Gambling Studies, Springer

2- Baron, J., and J. C. Hershey. (1988). "Outcome bias in decision evaluation." J. Personality Soc. Psychol. 54 (4): 569.

3- Benney, K. S., and L. A. Henkel. 2006. "The role of free choice in memory for past decisions." Memory 14 (8): 1001–1011.

4- Bennis, W. M., and Pachur, T. (2006). Fast and frugal heuristics in sports. Psychol. Sports Exerc. 7, 611–629.

5- Donovan, A., J. R. Eiser, and R. S. J. Sparks. (2017). "Expert opinion and probabilistic volcanic risk assessment." J. Risk Res. 20 (6): 693–710.

6- Finucane, M. L., A. Alhakami, P. Slovic, and S. M. Johnson. (2000). "The affect heuristic in judgments of risks and benefits." J. Behav. Decis. Making 13 (1): 1–17.
7- Fischhoff, B., and R. Beyth-Marom. (1983). "Hypothesis evaluation from a Bayesian perspective." Psychol. Rev. 90 (3): 239.
8- Gerrig, R. J., P. G. Zimbardo, P. G. Zimbardo, E. U. Psychologue, and P. G. Zimbardo. 2010. Psychology and life. Boston: Pearson.
9- Gigerenzer, G., and Goldstein, D. G. (1996). Reasoning the fast and frugal way: models of bounded rationality. Psychol. Rev. 103, 650–669.
10- Gigerenzer, G. (2008). Why Heuristics Work. Perspect. Psychol. Sci. 2008, 3, 20–29.
11- Gigerenzer, G., & Gaissmaier, W., (2011), Heuristic decision making. Annual Review of Psychology, 62, 451482.
12- Gigerenzer, G., Hertwig, R., & Pachur, T. (Eds.)., (2011), Heuristics: The foundations of adaptive behavior. New York: Oxford University Press.
13- Gigerenzer, G., Todd, P.M., & the ABC Research Group., (1999), Simple heuristics that make us smart. New York: Oxford University Press.
14- Goldstein, D. G., and Gigerenzer, G. (2002). Models of ecological rationality: the recognition heuristic. Psychol. Rev. 109, 75–90.
15- Hallowell, M. R., and J. A. Gambatese. 2009. "Construction safety risk mitigation." J. Constr. Eng. Manage. 135 (12): 1316–1323.
16- Hepler, T. J., and Feltz, D. (2011). Take the first heuristic, self-efficacy, and decision-making in sport. J. Exp. Psychol. Appl. 18, 154–161.
17- Hsee, C. K., and J. Zhang. (2004). "Distinction bias: Misprediction and mischoice due to joint evaluation." J. Personality Social Psychol. 86 (5): 680 Institution of Civil Engineers. 1998. RAMP: Risk analysis and management for projects. London: Thomas Telford.
18- Johnson, J., and Raab, M. (2003). Take the first: option-generation and resulting choices. Organ. Behav. Hum. Decis. Process. 91, 215–229.
19- Kahneman, D. 2011. Thinking, fast and slow. New York: Macmillan.
20- Kahneman, D., and D. Lovallo. (1993). "Timid choices and bold forecasts: A cognitive perspective on risk-taking." Manage. Sci. 39 (1): 17–31.
21- Kahneman, D., and Frederick, S. (2005). "A model of heuristic judgment," in The Cambridge Handbook of Thinking and Reasoning, eds K. J. Holyoak and R. G. Morrison (New York, NY: Cambridge University Press), 267–293.
22- Kardes, I., A. Ozturk, S. T. Cavusgil, and E. Cavusgil. (2013). "Managing global megaprojects: Complexity and risk management." Int. Bus. Rev. 22 (6): 905–917.
23- Koriat, A., S. Lichtenstein, and B. Fischhoff. (1980). "Reasons for confidence." J. Exp. Psychol.: Hum. Learn. Memory 6 (2): 107. Lam, K. C., D. Wang, P. T. Lee, and Y. T. Tsang. 2007. "Modelling risk allocation decision in construction contracts." Int. J. Project Manage. 25 (5)
24- Loke, W. H., and K. F. Tan. 1992. "Effects of framing and missing information in expert and novice judgment." Bull. Psychonomic Soc. 30 (3): 187–190.
25- MacFarlane, R. (2015) Decision-Support Tools for Risk, Emergency and Crisis Management. Emergency Planning College Position Paper Number 1. Easingwold: EPC http://www.epcresilience.com/EPC/media/MediaLibrary/Knowledge%20Hub%20Documents/J%20Thinkpieces/PP01-Decision-Making-Sep-2015.pdf
26- MacFarlane, R and Leigh, M. (2014) Information Management and Shared Situational Awareness Emergency Planning College Occasional Paper Number 12. Easingwold: EPC http://www.epcresilience.com/EPC/media/Images/Knowledge%20Centre/Occasional s/Occ12-Paper.pdf
27- Marewski, J. N., Pohl, R. F., and Vitouch, O. (2010). Recognition-based judgments and decisions: Introduction to the special issue (I). Judgment. Decis. Mak. 5, 207–215.
28- Ofir, C. 2000. "Ease of recall vs recalled evidence in judgment: Experts vs laymen." Organizational Behav. Hum. Decis. Processes 81 (1): 28–42.
29- Raab, M., & Johnson, J. (2007). Expertise-based differences in search and option-generation strategies. Journal of Experimental Psychology: Applied, 13, 158170.
30- Ross, L., D. Greene, and P. House. (1977). "The 'false consensus effect: An egocentric bias in social perception and attribution processes." J. Exp. Social Psychol. 13 (3): 279–301.
31- Stanovich, K. E. (1999). Who Is Rational? Studies of Individual Differences in Reasoning. Mahwah, NJ: Erlbaum.
32- Simon, H. A. (1956). Rational choice and the structure of the environment. Psychological Review, 63, 129–138
33- Simon, H. A. (1990). Invariants of human behavior. Annual Review of Psychology, 41, 1–20.
34- Sloman, S. A. (1996). The empirical case for two systems of reasoning. Psychol. Bull. 119, 3–22.
35- Sloman, S. A. (2014). "Two systems of reasoning, an update," in Dual-Process Theories of the Social Mind, eds J. Sherman, B. Gawronski, and Y. Trope (New York, NY: Guilford Press), 69–79.
36- Terrell, D. 1994. "A test of the gambler's fallacy: Evidence from parimutuel games." J. Risk Uncertainty 8 (3): 309–317.
37- Tversky, A., and D. Kahneman. (1971). "Belief in the law of small numbers." Psychol. Bull. 76 (2): 105.

38- Tversky, A., and D. Kahneman. (1973). "Availability: A heuristic for judging frequency and probability." Cognit. Psychol. 5 (2): 207–232

39- Tversky, A., and D. Kahneman. (1974). "Judgment under uncertainty: Heuristics and Biases, *Science,185*(4157),11241131. https://doi.org/10.1126/science.185.4157.1124

40- Walters, D. J., P. M. Fernbach, C. R. Fox, and S. A. Sloman. 2016. "Known unknowns: A critical determinant of confidence and calibration" Manage. Sci. 63 (12): 4298–4307.

41- Wegwarth, O., Gaissmaier, W., and Gigerenzer, G. (2009). Smart strategies for doctors and doctors-in-training: heuristics in medicine. Med. Educ. 43, 721–728.

42- Yasseri, S., (2015), Evidence-based practice in subsea engineering Underwater Technology, The International Journal of the Society for Underwater 32(4)

43- Yasseri, S., (2017), Thinking Like an Engineer, available on ResearchGate https://www.researchgate.net/publication/319644185_Thinking_like_an_engineer

44- Yasseri, S. (2021). "Rationality for Engineers: Part I- Setting the scene" International Journal of Coastal and Offshore Engineering, 5 (2), 22-33.

45- Yasseri, S., (2021), Rationality for engineers, Part III, International Journal of Coastal and Offshore Engineering, 5 (4).

46- Yasseri, S., (2022), International Journal of Coastal and Offshore Engineering, 6 (1).

47- Zajonc, R. B. (1980). Feeling and thinking: Preferences need no inferences. American Psychologist, 35(2), 151-75.

48- Zajonc, R.B. (1997). Emotions. In D.T. Gilbert, S.T. Fiske, & G. Lindzey. (Eds.), Handbook of Social Psychology, Fourth Edition (pp. 591-632). New York, NY: Oxford University Press.

Appendix

Cognitive biases and their impact on the risk management process

Bias	Definition	Problems or Flaws??	How to Avoid
Anchoring and Adjustment Bias [5, 39]	Relies on an initial piece of information but fails to adjust the conclusions sufficiently considering new information.	The framing of questions/interactions with leading information can anchor the decision-maker to that information. By using a starting point, DM may simply scale up or down from that initial position.	Avoid putting too much emphasis on a particular information time. The world dynamic is fluid and a compelling story a year ago might not be compelling anymore.
Affect Biases [6]	The tendency to use the incidental and integral emotional experience as the basis for decision-making.	DM uses emotional cues as salient and relevant information. DM also uses emotional cues when objective and emotional evaluations diverge.	The Affect Heuristic happens when you make a gut decision based on some sort of "feeling". To avoid this, you should apply quality controls in a systematic, consistent, and rigorous way.
Availability Bias [28, 38]	A tendency to use information that comes to mind quickly and easily. Assigning more importance to the information that one can recall easily. This heuristic is the core cognitive function of saving mental effort.	Undue influence of recent event(s) when estimating the likelihood of events because DM remembers this but not all past events. The availability heuristic describes behaviour that results from numerous shortcuts that our brain makes to process all information.	Awareness helps but cannot change one's thought process, it is essential to support and implement policies that recognize this heuristic in formulating a decision.
Attribution Bias, [38]	A tendency to blame others when things go wrong, instead of objectively analyzing the situation. Particularly, you may judge someone based on a stereotype or a perceived personality flaw.	In a car accident, when the other driver is at fault, you are more likely to assume that he/she is a bad driver than you rather than bad weather. A tendency to place blame on external events. If you have a car accident that is your fault, you are more likely to blame the brakes or the wet road rather than your reaction time.	Look at situations and the people involved in a non-judgmental way. Use empathy to understand why people behave in the way they do.
Base Rate Neglect [37].	Assessments of probabilities are based almost exclusively on new evidence, without adequate consideration of base rates.	This is a fundamental flaw in reasoning, resulting from our innate weakness in analyzing complex probability problems. It is an example of where our intuitive judgments or instincts can lead us astray.	This is due to assessing the likelihoods and subsequent probabilities ignoring the conditional probabilities. Make a habit of considering all relevant data. Understanding base rate neglect and the probability theory can help
Bandwagon Effect [15]	Individuals conforming to the majority opinion, believing in the crowd's wisdom.	Face-to-face interactions among group decision-makers could have coercing effects in voicing dissenting opinions or overrule the loudest voice in the room.	Conder the possibility that everybody could be wrong.
Choice-supportive Bias [3]	Recalling positive attributes more than negative ones when reconsidering past choices. Avoiding looking confused or wrong.	Selectively searching memory for information that supports the decision rationally and ignoring evidence to the contrary.	Regularly introduce new perspectives. Involve another expert halfway through.
Confirmation/my side Bias [15].	Evidence and information are interpreted to support current notions and expectations.	Strongly held beliefs and expectations, or when DM is made privy to the predetermined objectives and desired outcomes.	Do not interpret ambiguous information as supporting your position, and do not use it to construct a story. (This can also be called Reinforcement Theory).
Conservatism in Belief Revision [7].	Reluctance to revise one's opinions relative to Bayesian probabilistic predictions contrary to the evidence.	The tendency to favour prior data over new information. DM can be slow or reluctant to revise the initial judgments and may ignore the true value of any new evidence.	Explore the ways to refute the story that you have constructed rather than seeking to prove it.
Distance Bias [17]	The tendency to favour people who are closer to us in space and time. Out of sight out of mind.	People may unconsciously perceive someone that is not within proximity to them is of a lesser value, which can impact decision-making processes	Collect evidence as to the merit of people around you as well as at a distance.
False Consensus Effect [30]	Also known as Consensus Bias, is thinking your own behavioural choices and judgments are quite common and appropriate to existing circumstances. That is assuming that your personal qualities, characteristics, beliefs, and actions are relatively widespread.	False Consensus can occur when incorrectly believing that most peers agree with the decisions. These put people who are working in a remote location at a disadvantage. Believing incorrectly how well one's opinions align with the others.	Consider diversity; people are more different than we think.

Framing Effect [24]	Deciding based on how the information is presented, i.e., positive, or negative cues.	Decisions are made based on how the information or potential outcomes are expressed, not on objective probabilities.	Re-phrase the question. Look at the problem from a different angle. Remove some information and see if you reach the same decision.
Gambler's Fallacy [36, 37]	Believing that an event that has occurred recently is less likely to be random, i.e., assuming there is a correlation between independent trials	DM may misinterpret the likelihood of an event(s) that has recently occurred and ignore the element of chance.	Acquaintance with laws of probability help to avoid this bias. Make sure that you look at trends from probability vantage.
Illusion of Validity [23, 38]	Exhibiting unwarranted high confidence in their subjective judgments, predictions, and decisions.	This illusion can cause ignoring all possible outcomes adequately.	Generate options and evaluate them objectively.
Loss Aversion [38]	People give something of greater value simply because they own it. Loss hurts more than wins generates good feelings.	Losing something hurts people more than winning the same thing makes us happy. It is why we keep things for longer than we need them because losing hurts.	Awareness and asking for another opinion help.
Observer-expectancy Bias [8]	The expectations of an authoritative figure can impact the performance of an individual(s).	Seeking to provide assessments aligned with your perception of what responses are expected by others.	Consider that everyone is fallible or not in possession of all facts.
Optimistic Bias [20]	Ignoring probabilities and unduly believing in positive outcomes.	Giving more weight to personal opinions over probabilities.	Challenge your assumption.
Outcome Bias [2]	The tendency to judge previous decisions based solely on their outcomes, i.e., ignoring the chance element.	Ignoring probabilities, and incorrectly assuming that bad outcomes are the results of bad decision-making only, shifting from probabilistic judgments to subjective evaluations.	Consider the element of chance.
Primacy Bias [15]	The tendency to allow first impressions, and initial information or options to unduly influence subsequent decisions.	The initial information, observations, or other stimuli can skew decisions.	Give yourself time to investigate all aspects of the problem. The first impression may be right, but the burden of proof is on you.
Overconfidence [37, 39,40]	Placing too much faith in one's knowledge and opinions. Believing that one's contribution to a decision is more valuable than it is.	Failing to spot the limits to one's knowledge. Such a failure often yields the wrong decision. Engineers are more likely to display the Overconfidence Bias than the public, which is due to not being challenged often.	Overconfidence in genealogy has its roots in relying on some specific sort of information, which might not be fact-based. Or, information might not have been gathered systematically or suffered from missing data, or lack of trust in people who gathered information
Representative Heuristic [37, 39]	The tendency to allow probability to be influenced by the assessments of resemblance (i.e., the degree to which an event is judged as representative of another event) to save time and energy.	Engineers make snap decisions and assumptions in emergencies without thinking too much about looking for evidence. This bias can enter when the decision is based on one event only because of similarity or representativeness.	Look for evidence from all available sources
Similarity Bias [17]	Making judgments based on the perceived similarity of two situations.	Judging based on the similarity between current situations and other situations. The decision is based on how favourable or unfavourable the present situation is based on perceived similarity to the past situation.	Do not let previous experience shape the current situation. Gather more data and look for differences.
Sunk cost Effect. [22]	The bias to persist in a particular direction to avoid wasting the significant investment that has already been made is termed Sunk-cost Bias.	This bias applies more to risk management decisions made during construction activity.	Practitioners can show a lack of willingness to alter the course of action about managing risks when considerable resources already have been invested.
Survivorship [37, 39]	A tendency to focus too heavily on what remains standing, instead of considering what you cannot see.	It happens when we assume that success tells the whole story, and we do not adequately consider past failures. The road to success is strewn by corpses of those who failed.	Consider the thing you do not see, or you cannot see.
Von Restorff Effect [15]	Also known as the Isolation Effect, predicts that when multiple similar objects are present, the one that differs from the rest is most likely to be remembered!	People value a thing differently depending on whether it is placed in an isolation orbit or placed next to an alternative.	A certain choice can be made to look more attractive if it is placed next to an inferior alternative.

INTERNATIONAL JOURNAL OF
COASTAL & OFFSHORE ENGINEERING
IJCOE Vol.6/No. 3/Summer 2021 (19-25)

Available online at: www. Ijcoe.org

Determination of Vessel Heading using Magnetic Wake Imaging

Mohammad Amir Fallah[1*], Mehdi Monemi[2]

[1]Assistant Professor, Department of Engineering, Payame Noor University (PNU), Tehran, Iran; mfallah@shirazu.ac.ir*
[2] Assistant Professor, Department of Electrical Engineering, Salman Farsi University of Kazerun, Kazerun, Iran; monemimahdi@gmail.com

ARTICLE INFO

Article History:
Received: 03 Mar. 2020
Accepted: 29 June. 2021

Keywords:
Magnetic Wake
Vessel Heading
Magnetic Imaging
Magnetometer

ABSTRACT

The small microwave skin depth of sea water as well as the small penetration depth of laser signal in water impose limitations on the application of SAR and Lidar in sea surveillance systems. On the other hand, vessels travelling at sea bring about hydrodynamic anomalies in the sea water called as wake. These hydrodynamic disturbances can be detected by using some techniques such as airborne radio imaging and Extremely Low Frequency (ELF) electromagnetic signal processing. In practice, the motion of conductive sea water anomalies in the natural earth's magnetic field induces ELF magnetic wakes which can be measured via accurate magnetic sensors and detected through signal processing schemes. The physical properties of the hydrodynamic wake as well as those relating to the corresponding magnetic wake are directly related to the vessel parameters such as hull shape, speed and heading. In this work, we firstly derive and formulate the mathematical expressions relating to the aforementioned hydrodynamic and magnetic wakes. By employing derived expressions, a novel detection scheme is proposed based on constructing the 2-dimentional image of the vessel's magnetic wake through the magnetic signals captured from an array of magnetic sensors, and finally, the relation between the spectral image of the magnetic wake and the vessel heading is studied. We will show that our proposed scheme can detect the existence of a remote vessel as well as its heading from the constructed image with high accuracy, and moreover, it does not have common limitations of existing single-sensor based heading detection schemes.

1. Introduction

The hydrodynamic wave at the sea surface created by the movement of a vessel is visible for airborne radars, Synthetic Aperture Radars (SAR) and lidars [1-7]. Once a high-quality signal is measured through a sensor, the implementation of signal processing techniques is required in order to accurately distinguish the signal from remote vessel out of environmental noise and disturbances [8-10]. The employment of radar and lidar systems, even with efficient signal processing schemes, is not effective for many situations in the sea surveillance systems. The main reason for this inefficiency is the large power loss of high frequency electromagnetic waves in the sea water resulting in low effective detection range.

Traveling vessels bring about hydrodynamic anomalies called as wakes [10-14] in electrically conductive seawater across the ambient earth magnetic field, leading to the induction of magnetic wakes [15-19].

Efficient implementation of remote sensing schemes for vessels through electromagnetic signal measurement requires highly accurate magnetic sensors. Moreover, due to the large dimensions of hydro-physical changes, hydrodynamic harmonics in the seawater are considered as low frequency ones. Therefore, accurate magnetic sensors with accuracy of less than 1 pico-Tesla (pT) and low frequency measuring capability is essential for the implementation of efficient remote sensing techniques [20, 21]. The low frequency induced hydromagnetic wakes can be measured and detected through magnetic sensors positioned at the sea surface or under the sea surface. Although dimensions of marine vehicles are limited, the generated wakes may extend tens of kilometers and remain for several hours under certain conditions [10-13].

The Induced magnetic wake of a ship in an infinite depth sea was studied by Madurasinghe [17-19]. Zou and Nehorai [22-24] proposed a single-sensor detection scheme by using an airborne magnetometer flying above an infinite depth sea. The proposed detection method suffers from several drawbacks including the

detection limitation of the angle between the vessel heading and magnetic sensor trajectory (which should be lower than 19.47^0 in order to be detectable [22]), as well as the impossibility of distinguishing the positive heading angles from negative ones. In addition, in the airborne method, it is possible to track the aircraft and destroy it, but in the proposed single-sensor method, this problem is solved.

When a marine surveillance system observes the footprint of a vessel by capturing the magnetic wake samples through magnetic sensors, the next step is to process the received signal in order to detect the existence of a remote floating vessel or submarine as well as distinguishing the physical parameters of the traveling body such as heading, velocity, size, and hull shape. This post processing step is done by formulating the dependency of the magnetic wake to the vessel parameters. In order to overcome the drawbacks of the single-sensor heading detection scheme as stated above, in this work, we firstly derive and formulate the mathematical expressions relating to the hydrodynamic and magnetic wakes, and then a magnetic sensor array structure is proposed in order to measure the magnetic wake of the remote vessel. By employing the derived expressions, and based on different time delay of the magnetic wake signals measured through each element of the sensor array, the magnetic image of the vessel wake is constructed, and finally, the relation between the captured image of the magnetic wake and the vessel heading is studied. We will show that the vessel heading can be obtained from the spectral image of the magnetic wake in the presence of ambient Gaussian noise.

2. Mathematical Formulation

Consider the free space in the Cartesian coordinate system wherein the fluid surface corresponds to the plane $z = 0$ which is perfectly flat. We consider two electromagnetic media; the air and the fluid corresponding to the space regions $z > 0$ and $z < 0$ respectively. Electric conductivity, susceptibility and magnetic permeability of these layers are denoted by $(\sigma_a, \varepsilon_a, \mu_a)$ and $(\sigma_w, \varepsilon_w, \mu_w)$ respectively. Both media are immersed in natural earth magnetic field $\boldsymbol{B}_E$. By default, we assume that the vessel travels in the x-axis direction, and the z-axis is perpendicular to the fluid surface. The more general case wherein the vessel heading is an arbitrary direction (other than the x-axis) is later studied in Section 5.

Assuming the sea water is an irrotational fluid, which is acceptable at far distances away from the vessel, the induced magnetic wake at point (x, y, z) instigated by a moving vessel can be written as [17-19]:

$$\boldsymbol{H}(x,y,z) = \Re e \int_{-\pi/2}^{\pi/2} \boldsymbol{h}(\theta,z) A_\theta \, e^{-i(k_0 x cos\theta + k_0 y sin\theta)} \, d\theta \quad (1)$$

Wherein

$$A_\theta = \frac{2UVk_0^2}{\pi L} \text{ Koch}(\theta) \quad (2a)$$

$$k_0 = \left(\frac{g}{U^2}\right) sec^2\theta$$
$$\omega_0 = k_0 \cos\theta \quad (2b)$$

$$\text{Koch}(\theta) = \iint_S I_\kappa(x',y',z') e^{-ik_0 x' cos\theta} \, cosh\, k_0(z'+d) dx' dz' \quad (2c)$$

and

$$i = \sqrt{-1} \ , \qquad g = 9.8 \ {}^{m}/_{s^2}$$

wherein $\text{Koch}(\theta)$ is the Kochin function [12], $s(x', y', z')$ is the wetted part of the submerged portion of the vessel hull and $I_\kappa(x', y', z')$ represents the intensity of pressure distributed on the hull. The unknown term $\boldsymbol{h}(\theta, z)$ can be calculated by applying continuity conditions of normal component of **B** and tangential component of **H** in the surface between the air and the water which can be obtained as:

$$\boldsymbol{h}(\theta,z) = \boldsymbol{h}^a(\theta,z) = \boldsymbol{P} e^{\delta z} \frac{\boldsymbol{a}(\theta)}{(k_0^2 - \delta^2)} e^{k_0 z} \qquad \text{for } z < 0 \quad (3)$$

$$\boldsymbol{h}(\theta,z) = \boldsymbol{h}^w(\theta,z) = \left[\boldsymbol{P} \frac{\boldsymbol{a}(\theta)}{(k_0^2 - \delta^2)}\right] e^{\beta z} \qquad \text{for } z > 0$$

in which

$$\boldsymbol{P} = \frac{(\beta + k_0)}{(\beta + \delta)} \frac{\boldsymbol{a}(\theta).k}{(k_0^2 - \delta^2)} \left(\frac{\delta \cos\theta}{ik_0}, \frac{\delta \sin\theta}{ik_0}, 1\right) \quad (4)$$

$$\boldsymbol{a}(\theta) = \sigma_0 k_0 \{(\boldsymbol{B}_E.\boldsymbol{k}) - i(\boldsymbol{B}_E.\boldsymbol{i}\cos\theta + \boldsymbol{B}_E.\boldsymbol{j}\sin\theta)\}. (\boldsymbol{i}\cos\theta + \boldsymbol{j}\sin\theta - \boldsymbol{k})$$

$$\beta^2 = k_0^2 - \varepsilon_0 \mu \omega_0^2$$
$$\delta^2 = k_0^2 - \varepsilon_0 \mu \omega_0^2 - i\sigma_0 \mu \omega_0$$

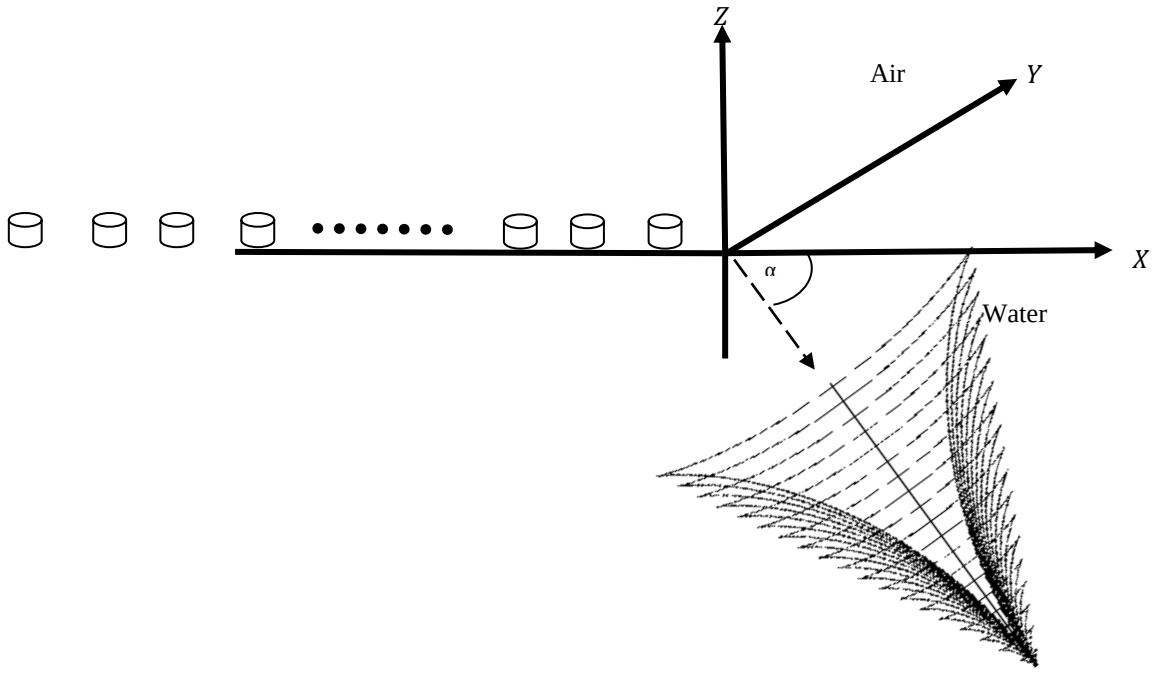

Figure 1. Configuration of the sensor array in the x-axis. The vessel is assumed to travel at the direction corresponding to the dashed line whose angle is α relative to the x-axis.

3. Spectral Analysis

In what follows we study the frequency spectrum of the magnetic wake as a means that sheds light on how the vessel heading can be distinguish from the spectral image of its magnetic wake. The spectrum of the magnetic anomaly is obtained by taking the spatial Fourier transform of magnetic wake in the points located on the plane parallel to the xy plane and located at the altitude $z = z_0$ which is expressed as follows:

$$\begin{aligned}\widehat{\boldsymbol{H}}(X,Y) &= \int_{-\infty}^{\infty}\int_{-\infty}^{\infty} \boldsymbol{H}^a(x,y,z_0)\, e^{-i2\pi(Xx+Yy)}\, dxdy \\ &= \frac{\boldsymbol{h}^a(\theta,z_0)A_\theta}{\left|\frac{\partial}{\partial\theta}(X-X_0)\right|\left|\frac{\partial}{\partial\theta}(Y-Y_0)\right|}\delta(\theta_x-\theta_y)\end{aligned} \quad (5)$$

where

$$X_0 = \frac{k_0\cos\theta}{2\pi} \quad , \quad Y_0 = \frac{k_0\sin\theta}{2\pi} \quad (6)$$

and (θ_x, θ_y) are obtained by solving the following equations:

$$X - X_0 = 0 \quad , \quad Y - Y_0 = 0 \quad (7)$$

The solution to equation (5) represents a locus on the $z = z_0$ plane describing the vessel's magnetic wake spectrum. Referring to (6) and (7), it is inferred that the spectrum consists of a number of impulses with intensity $\frac{\boldsymbol{h}^a(\theta,z_0)A_\theta}{\left|\frac{\partial}{\partial\theta}(X-X_0)\right|\left|\frac{\partial}{\partial\theta}(Y-Y_0)\right|}$ at points corresponding to $\theta = \theta_x = \theta_y$.

4. Sensor Array Configuration

Assume that M magnetic sensors are positioned along the x-axis as shown in Figure 1. The vessel is assumed to travel at the direction corresponding to the dashed line whose angle is α relative to the x-axis. This configuration has a time-spatial nature, in the sense that all magnetic sensors are fixed and simultaneously receive magnetic signal samples with sampling period $T_s = 1/f_s$ in time domain, and at M location points in the spatial domain. As the time passes, the xy-plane magnetic image is constructed through processing the received signals at the M location points and N time-steps. It is obvious that increasing the number of receiving sensors as well as the acquisition time leads to higher resolution of the magnetic image resulting in better detection probability. The image resolution in the spatial domain depends on the number of magnetic sensors positioned at the x axis, and on the other hand, the image clarity in time domain increases as time passes. Finally, the array can construct the magnetic image of the vessel wake and determine the vessel heading as described in the following section.

5. Determination of vessel heading

The shape of the magnetic wake is directly related to the vessel traveling direction and any change in the vessel heading leads to variations in the image of the wake; this is an important factor to be considered in the

estimation of the vessel heading. To show this key relation, assume that the angle between the vessel heading and the sensors array axis is denoted by α. It is evident that the received magnetic image in this case (denoted by $\boldsymbol{H}'$) is the same as that presented for $\alpha = 0$ (denoted by $\boldsymbol{H}$ as expressed in previous sections) except that it is rotated by α degrees in the counterclockwise direction. In what follows we prove that the spatial spectral Fourier transform for $\boldsymbol{H}'$ is also a rotation of that for $\boldsymbol{H}$ by α derees. Let define

$$\left(x', y'\right) = \mathcal{R}\{(x, y), \alpha\} \tag{8a}$$
$$\boldsymbol{H}'\left(x', y'\right) = \mathcal{R}\{\boldsymbol{H}(x, y), \alpha\} \tag{8b}$$

where the operator $\mathcal{R}\{\boldsymbol{f}(x, y), \alpha\}$ rotates $\boldsymbol{f}(x, y)$ by α degrees in the counterclockwise direction. According to (5), the spectrum of the received magnetic signal is expressed as:

$$\boldsymbol{\mathcal{F}}\{\boldsymbol{H}'\left(x', y'\right)\}\left(X', Y'\right) = \int_{-\infty}^{\infty}\int_{-\infty}^{\infty} \boldsymbol{H}'\left(x', y', z_0\right) e^{-i2\pi\left(X'x' + Y'y'\right)}\, dx'dy' \tag{9}$$

where $\left(X', Y'\right) = \mathcal{R}\{(X, Y), \alpha\}$. Now, from (8b) we can write:

$$\begin{aligned} &\left|\mathcal{F}\{H'\left(x', y'\right)\}\left(X', Y'\right)\right| \\ &= \left|\int_{-\infty}^{\infty}\int_{-\infty}^{\infty} H'\left(x', y', z_0\right) e^{-i2\pi\left(X'x' + Y'y'\right)}\, dx'dy'\right| \\ &= \\ &\left|\int_{-\infty}^{\infty}\int_{-\infty}^{\infty} H\left(x' \cos\alpha - y' \sin\alpha\, , x' \sin\alpha\right.\right. \\ &\left.\left. + y' \cos\alpha\, , z_0\right) e^{-i2\pi\left(X'x' + Y'y'\right)}\, dx'dy'\right| \end{aligned} \tag{10}$$

On the other hand

$$|dxdy| = \left|h_1 h_2\, dx'dy'\right| = 1 \tag{11}$$

where,

$$\begin{aligned} h_1^2 &= \left(\frac{\partial x'}{\partial x}\right)^2 + \left(\frac{\partial y'}{\partial x}\right)^2 = 1 \\ h_2^2 &= \left(\frac{\partial x'}{\partial y}\right)^2 + \left(\frac{\partial y'}{\partial y}\right)^2 = 1 \end{aligned} \tag{12}$$

Hence we have:

and finally, we conclude that

$$\begin{aligned} &\left|\int_{-\infty}^{\infty}\int_{-\infty}^{\infty} H\left(x' \cos\alpha - y' \sin\alpha\, , x' \sin\alpha + y' \cos\alpha\, , z_0\right) e^{-i2\pi\left(X'x' + Y'y'\right)}\, dx'dy'\right| = \\ &\left|\int_{-\infty}^{\infty}\int_{-\infty}^{\infty} H(x, y, z_0).\, e^{-i2\pi\left(x\left(X' \cos\alpha - Y' \sin\alpha\right) + y\left(X' \sin\alpha + Y' \cos\alpha\right)\right)}\, dxdy\right| = \\ &\left|\mathcal{F}\{H(x, y, z_0)\}\left(X' \cos\alpha - Y' \sin\alpha, X' \sin\alpha + Y' \cos\alpha\, , z_0\right)\right| = |\mathcal{R}(\mathcal{F}\{H(x, y), \alpha\})| \end{aligned} \tag{13}$$

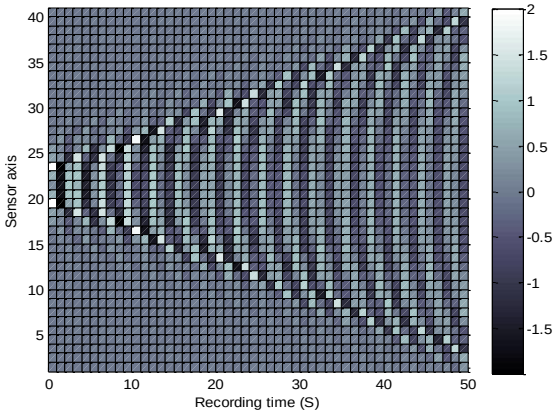

Figure 2. Magnetic wake amplitude (nT) at vessel speed 10 m/s recorded by 40-element multi-sensor arrangement with $N = 50$ time-steps and $f_s = 0.5\ Hz$ in a noiseless environment.

$$|\boldsymbol{\mathcal{F}}\{\mathcal{R}(\boldsymbol{H}(x, y), \alpha)\}| = |\mathcal{R}(\boldsymbol{\mathcal{F}}\{\boldsymbol{H}(x, y), \alpha\})| \tag{14}$$

In other words, adding the angle α between vessel trajectory and the sensors array axis leads to an image rotation equal to α in the spectral domain. Hence, determination of image rotation in spectral domain leads to the detection of vessel heading with respect to the array axis. Based on what stated, we propose the following heading detection scheme:

Algorithm 1: Determination of the vessel heading through constructing the spectral image of the magnetic wake

1- Let M and N be the total number of sensors and measuring time steps respectively.
2- For each $m \in \{1,2, \dots, M\}$ and $n \in \{1,2, \dots, N\}$, let $\widetilde{\boldsymbol{H}}[m, n]$ be the time domain magnetic signal measured by the m'th sensor at the n'th time step, where $\widetilde{\boldsymbol{H}}[m, n] = \boldsymbol{H}[m, n] + \sigma_{m,n}$ in which $\sigma_{m,n}$ is the corresponding Gaussian ambient noise.
3- Calculate the spatial Fast Fourier Transform (FFT) of $\widetilde{\boldsymbol{H}}_{MN}$ denoted by $\widetilde{\boldsymbol{H}'}_{MN}$ and depict the corresponding two-dimensional image of $\widetilde{\boldsymbol{H}'}_{MN}$.
4- Determine the direction of the wake by calculating the rotation angle α of $\widetilde{\boldsymbol{H}'}$ through simple image processing techniques.

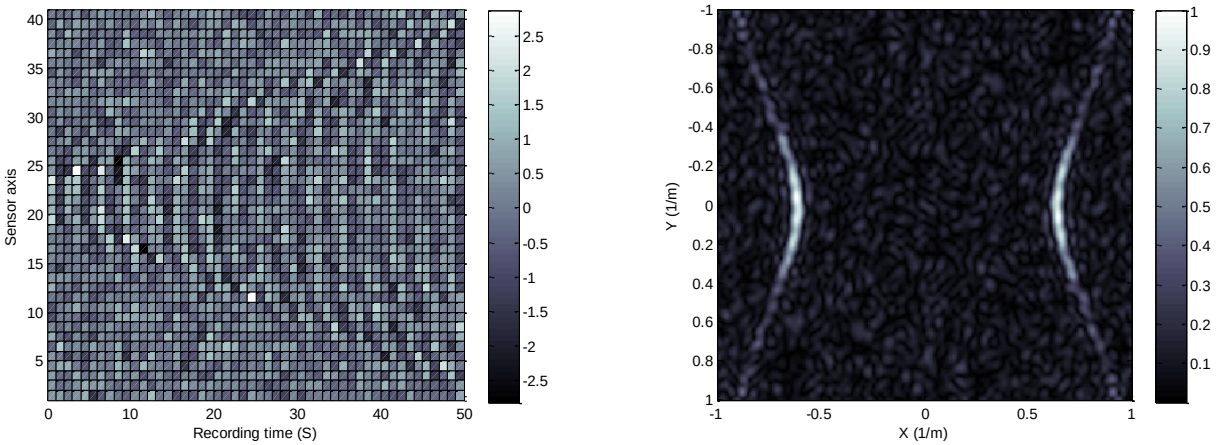

(a) **(b)**

Figure 3. (a) Magnetic wake amplitude (nT) at vessel speed 10 m/s, $\alpha = 0^{\circ}$ and SNR=0 dB recorded by 40-element sensor array arrangement with $N = 50$ time-steps and $f_s = 0.5\ Hz$. (b) Normalized spectrum of the corresponding magnetic wake.

In the following section, we study through numerical results how the proposed scheme results in the determination of the vessel heading in different practical scenarios.

6. Numerical Results

In this section, we study the determination of vessel heading by exploring the magnetic wake instigated from a vessel traveling at different speeds and directions in the presence of background Gaussian noise. The dielectric susceptibility, electric conductivity and magnetic permeability in the air and water are assumed to be $(\varepsilon_a, \varepsilon_w) = (\varepsilon_0, 81\,\varepsilon_0)$, $(\sigma_a, \sigma_w) = (0,5)$ and $(\mu_a, \mu_w) = (\mu_0, \mu_0)$ respectively [25-28].

It is assumed that all sensor elements of the array are omnidirectional and uniformly arranged along the x-axis. The results are obtained by simulating the proposed scheme for a Wigley's hull ship with length 180 meters, draft 10 meters and beam 20 meters sailing at 10m/s. The magnetic wake induced by the hydrodynamic wake of the ship is observed by a 40-elements sensor array system with 20 meters spacing between adjacent sensor elements. The sampling rate is $f_s = 0.5$ Hz and the number of measuring time-steps is $N = 50$. Figure 2 is the time-domain magnetic wake image of $\widetilde{\boldsymbol{H}}_{40\times 50}$ captured through Algorithm 1 in a noiseless environment for $\alpha = 0^{\circ}$. It is seen that the direction of the vessel movement is simply distinguished from the time-domain image and there is no need here to calculate the spectrum of $\widetilde{\boldsymbol{H}}$.

In order to evaluate the performance of our proposed scheme and investigate the superiority of the proposed sensor array configuration to conventional single-sensor methods in vessel heading estimation, several cases are simulated in the following.

First, we consider that the vessel sails at speed 10m/s and $\alpha = 0^{\circ}$ for the case when the signal to noise ratio

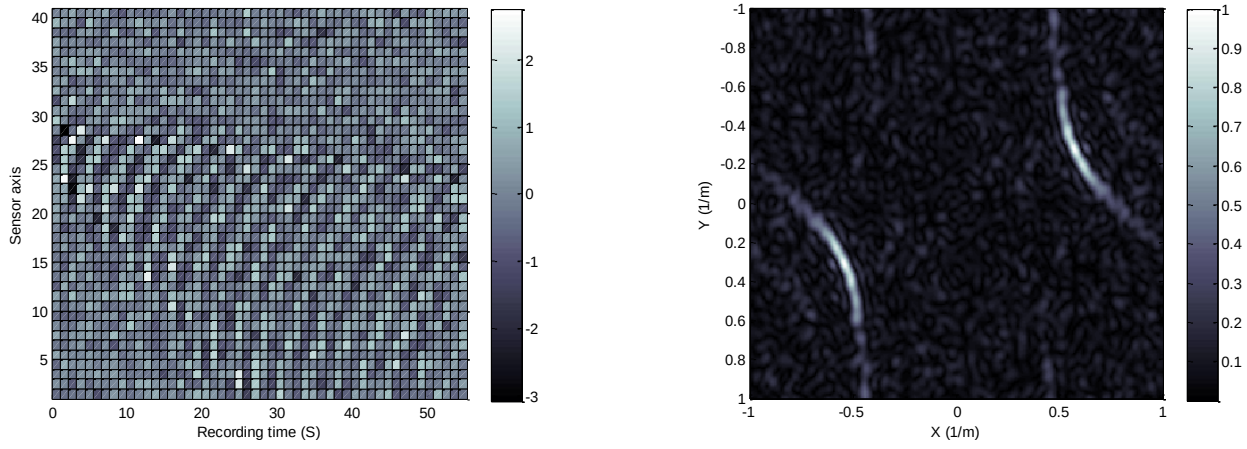

(a) **(b)**

Figure 4. (a) Magnetic wake amplitude (nT) at vessel speed 10 m/s, $\alpha = 25^{\circ}$ and SNR=0 dB recorded by 40-element array sensor arrangement with $N = 50$ and $f_s = 0.5\ Hz$ (b) Normalized spectrum of the corresponding magnetic wake.

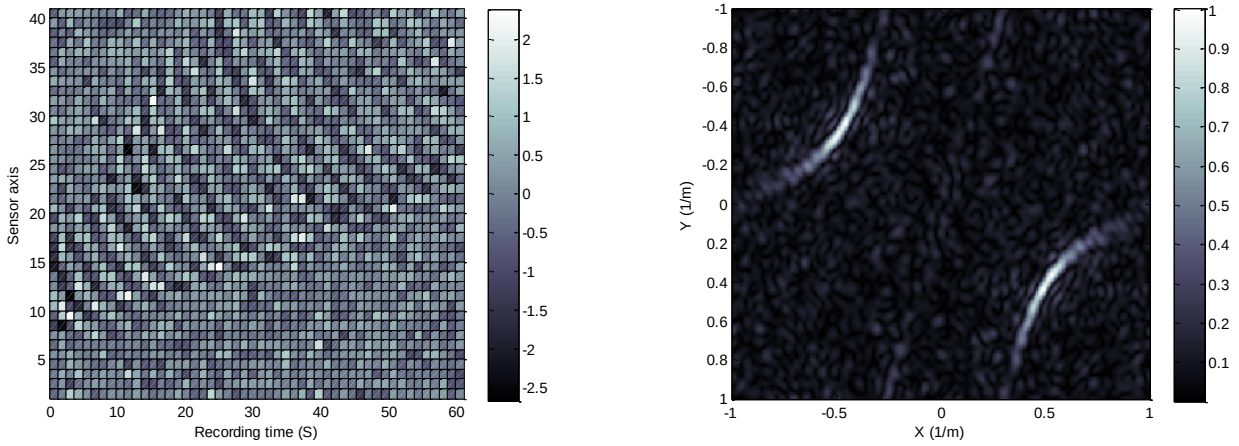

(a) **(b)**

Figure 5. (a) Magnetic wake amplitude (nT) at vessel speed 10 m/s, $\alpha = -35^{\circ}$ and SNR=0 dB recorded by 40-element array sensor arrangement with $N = 50$ and $f_s = 0.5\ Hz$ (b) Normalized spectrum of the corresponding magnetic wake.

(SNR) is 0 dB. The obtained time-domain magnetic wake signal captured by the sensor array system is shown in Figure 3(a), and the corresponding magnetic wake spectrum calculated by using 512 points FFT is presented in Figure 3(b). Note that although the presence of the wake is not so clear in the time domain, in the spectral domain however, we can observe a clear indication of the presence of the vessel and distinguish the corresponding heading. This can be justified by the existence of delta functions in (5) and noting that the noise power spectrum is randomly distributed in the region of spectral plane.

Figure 4(a) and 4(b) display the magnetic wake and its spectrum for the same scenario as in Figure 3 except that $\alpha = 25^{\circ}$ is considered here. The results show that that the limitation of conventional single sensor method in the vessel heading for $|\alpha| < 19.47^{\circ}$ ([22]) does not exist here by using the proposed array sensor configuration. As seen in Figure 4(b), the spectral image of the magnetic wake is rotated counterclockwise around the image center by $\alpha = 25^{\circ}$ as was pointed out in section 5. While the heading cannot be easily distinguished from the time-domain image in Figure 4(a), this is clearly detected in the spectral image in Figure 4(b).

Another advantage of the proposed detection scheme based on the spectral image construction through the sensor array configuration is to discriminate between positive and negative values of α which is impossible in the single sensor schemes [22]. Figure 5(a) and 5(b) show the magnetic time and spectral domain image of the magnetic wake for the same scenario as in Figure 4 wherein all parameters are the same as before except that heading direction corresponds to $\alpha = -35^{\circ}$. Compared to the pervious case, the spectral image in this case rotates clockwise, and it is clearly seen that, negative values of the angle corresponding to the heading is easily detected as well.

7. Conclusion

In this paper we proposed the heading estimation of remote vessels by processing the magnetic wake of the vessel through an array of magnetometers. More specifically, we proposed a scheme to construct the magnetic image of the vessel wake and then obtained the corresponding spectral domain image. We verified through numerical results that our proposed scheme can estimate the heading of a remote vessel with relatively high accuracy in the presence of background Gaussian noise and moreover, the proposed method was shown to overcome the limitations of conventional single-sensor heading estimation techniques.

8. References

1- O. Karakuş and A. Achim, (2021), *On Solving SAR Imaging Inverse Problems Using Nonconvex Regularization With a Cauchy-Based Penalty*, IEEE Transactions on Geoscience and Remote Sensing, vol. 59, no. 7, p.5828-5840, doi: 10.1109/TGRS.2020.3011631.

2- O. Karakuş, I. Rizaev and A. Achim, (2020), *Ship Wake Detection in SAR Images via Sparse Regularization*, IEEE Transactions on Geoscience and Remote Sensing, vol. 58, no. 3, p.1665-1677, doi: 10.1109/TGRS.2019.2947360.

3- K. -m. Kang and D. -j. Kim, (2019), *Ship Velocity Estimation from Ship Wakes Detected Using Convolutional Neural Networks*, IEEE Journal of Selected Topics in Applied Earth Observations and Remote Sensing, vol. 12, no. 11, p. 4379-4388, doi: 10.1109/JSTARS.2019.2949006.

4- Grishin, M.Y., Lednev, V.N., Pershin, S.M. et al., (2021), *Lidar sensing of ship wakes*, Phys. Wave Phen. 25,p.225–230, https://doi.org/10.3103/S1541308X17030104.

5- Alexey F. Bunkin, Vladimir K. Klinkov, Vladislav A. Lukyanchenko, and Sergey M. Pershin, (2011), *Ship wake detection by Raman lidar*, Appl. Opt. 50, p.86-89.

6- G. Yang, J. Yu, C. Xiao and W. Sun, (2016), *Ship wake detection for SAR images with complex backgrounds based on morphological dictionary learning*, IEEE International Conference on Acoustics, Speech and Signal Processing (ICASSP), p. 1896-1900, doi: 10.1109/ICASSP.2016.7472006.

7- G. Zilman, A. Zapolski and M. Marom, (2014), *On detectability of a ship's Kelvin wake in simulated SAR images of rough sea surface* , IEEE Trans. Geosci. Remote Sens., vol. 53, no. 2, p.609-619.

8- Yingfei Liu, Jun Zhao, Yan Qin, (2021), *A novel technique for ship wake detection from optical images*, Remote Sensing of Environment, Volume 258.

9- Liu, Yingfei & Deng, Ruru. (2018). *Ship Wakes in Optical Images*. Journal of Atmospheric and Oceanic Technology. 35. 10.1175/JTECH-D-18-0021.1.

10- M. Gilman, A. Soloviev and H. Graber, (2011), *Study of the Far Wake of a Large Ship*, J. Atmos. Oceanic Technol., vol. 28, p.720–733.

11- J. N. Newman, (1977), *Marine hydrodynamics*, MIT Press, Cambridge, Massachusetts.

12- Kostyukov, A. A., (1968), *Theory of Ship Waves and Waves Resistance*, Effective Communications Inc., Iowa City. p.241-243.

13- Tuck, E. O., Collins, J. I., and W. H. Wells, (1971), *On Ship Wave Patterns and Their Spectra*, J Ship Res 15,p11–21.
doi: https://doi.org/10.5957/jsr.1971.15.1.11.

14- D. F. Gu and O. M. Phillips,(1988), *On narrow V-like ship wakes*, J. Fluid Mech., vol. 275, p.301–321.

15- Weaver, J. T., (1965), *Magnetic Variations Associated with Ocean Waves and Swell*, Journal of Geophysical Research, 70: p.1921–1929.

16- Sanford, T. B.,(1971),*Motionally Induced Electric and Magnetic Fields in the Sea*, Journal of Geophysical Research, 76: p.3476–3492.

17- D. Madurasinghe,(1994), *Induced* electromagnetic fields associated with large ship wakes,Wave Motion, 20, p.283–292.

18- D. Madurasinghe, E.O. Tuck,(1994), The induced electromagnetic field associated with submerged moving bodies in an unstratified conducting fluid, IEEE Journal of Ocean Engineering, 19 ,p.193–199.

19- D. Madurasinghe, GR. Haack, (1994), The induced electromagnetic field associated with wakes-signal processing aspects. Proceedings of IGRASS 94, Pasadena, CA, p.2335–2357.

20- Yijin Xie, Huiyao Yu, Yunbin Zhu, Xi Qin, Xing Rong, Chang-Kui Duan, Jiangfeng Du, (2021), A hybrid magnetometer towards femtotesla sensitivity under ambient conditions, Science Bulletin, Volume 66, Issue 2, P.127-132.

21- Deans, Cameron & Marmugi, Luca & Renzoni, Ferruccio. (2018), Sub-picotesla widely tunable atomic magnetometer operating at room-temperature in unshielded environments, Review of Scientific Instruments. 89. 083111. 10.1063/1.5026769.

22- N. Zou and A. Nehorai, (2000), *Detection of ship wakes using an airborne magnetic transducer*, IEEE Transactions on Geoscience and Remote Sensing, vol. 38, no. 1, p.532-539, doi: 10.1109/36.823948.

23- O. Yaakobi, G. Zilman, T. Miloh, (2011), *Detection of the electromagnetic field induced by the wake of a ship moving in a moderate sea state of finite depth*,J. Engrg. Math. 70,p.17–27.

24- XiangmingGuo, Dongliang Zhao, Zhongqing Cao,(2016), *Detection of the Magnetic Field Induced by the Wake of a Moving Submerged Body Using Simple Models*, American Journal of Electromagnetics and Applications. Vol. 4, No. 2, p.20-25. doi: 10.11648/j.ajea.20160402.12.

25-Robert, P., (1988). *Electrical and Magnetic Properties of Materials*, Artech House.

26- Schon, J.H., (1996), *Physical properties of rocks: fundamentals and principles of petrophysics Calculated from field data at Otis MMR*, Cape Cod, Massachusetts.

27- Mavko, G., (1998). *The rock physics handbook: tools for seismic analysis in porous media*.

28 - Carmichael, Robert S., (1989), *Practical handbook of physical properties of rocks and minerals*.

INTERNATIONAL JOURNAL OF
COASTAL& OFFSHORE ENGINEERING IJCOE Vol.6/No. 3/Summer2021 (26-39)

Available online at: www. Ijcoe.org

Morphodynamic Classification of Beaches in some parts of the Iranian Coasts

Maryam Shiea[1*], Azadeh Valipour[2]

[1*]*Caspian Climate Company, Mashhad, Iran; m.shiea@gmail.com*
[2]*Department of Marine Science and Technology, Jouybar Branch, Islamic Azad University, Jouybar, Iran; a.valipour@yahoo.com*

ARTICLE INFO

Article History:
Received:20Nov. 2020
Accepted: 28Aug. 2021

Keywords:
Wave-Dominated
Wave-Tide
Beach State
Iran
Dimensionless Fall Parameter
Relative Tide Range

ABSTRACT

This research investigates the morphodynamic classification of beaches of Iran according to the dimensionless fall parameter (Ω) and the relative tide range (RTR). According to RTR parameter, the southern Iranian coast (Hormozgan province) is mixed wave and tide and the northern Iranian coast (Mazandaran province) is wave-dominated. By using some schemes, the beach states in the north regions of the eastern and central parts of the Mazandaran province are dissipative and in the western part it is intermediate. Also, in the south section in most of the regions of the Hormozgan province, the beach states are ultradissipative, but in some areas low tide terrace and low tide bar/rip occur.

1. Introduction

Despite the long history of research on the classification of beach morphodynamics, coastal classification can be useful in providing a conceptual framework for studying coastal environments, as well as predicting coastal morphology [1]. On the other hand, the relationship between coastal morphology and coastal risks (coastal crises and natural hazards) such as rip currents (based on beach state) is still a matter of great importance for coastal engineers and geomorphologists [2, 3, 4]. In the past years, coastal studies and the classification of morphodynamics have been carried out on various coastlines of the world with the help of various methods such as field experiments, numerical modeling in a variety of morphodynamic models [5, 6, 7, 8] and long-term field observations using video monitoring techniques [9, 10, 11, 12, 13, 14, 15]. One of these studies is the Wright and Short [16] research that relied on dynamic shore-based factors based on a 6-year observation period from the Australian coast. For these wave-dominated beaches, they presented a beach classification scheme in which three main beach states were identified as dissipative, intermediate, and reflective states (Figure 1).

Masselink and Short [17] have also identified a number of distinct morphological states or stages associated with various wave and tide regimes. In fact, they propounded the classification of natural beaches on the basis of four physical constraints: modal breaking wave height, modal breaking wave period, sediment characteristics of the upper beach face and mean spring tide range. These variables are quantified by two dimensionless parameters: the dimensionless fall velocity Ω and the relative tide range RTR [2]. Figure 2, is a simplified version of this kind of classification that consists of eight major beach types placed into three categories.

These different coastal models in this classification are defined using a dimensionless fall velocity parameter (DFVP), which was first proposed by Gourlay[18] and rewritten by Dean [19].

$$\Omega = H_b / W_s T \qquad (1)$$

where H_b = breaker height (m), T = wave period (s), and W_s =sediment fall velocity (m/s).Reflective beach states are expected to occur when $\Omega < 1$, intermediate beaches when $1 < \Omega < 6$, and dissipative beaches when $\Omega > 6$.

Masselink and Short [17] developed an empirical model to simulate the tide-induced migration of hydrodynamic processes across a beach profile and used the relative tide range RTR:

$$RTR = \frac{TR}{H_b} \qquad (2)$$

Where TR is the tide range (m) to quantify tidal effects.

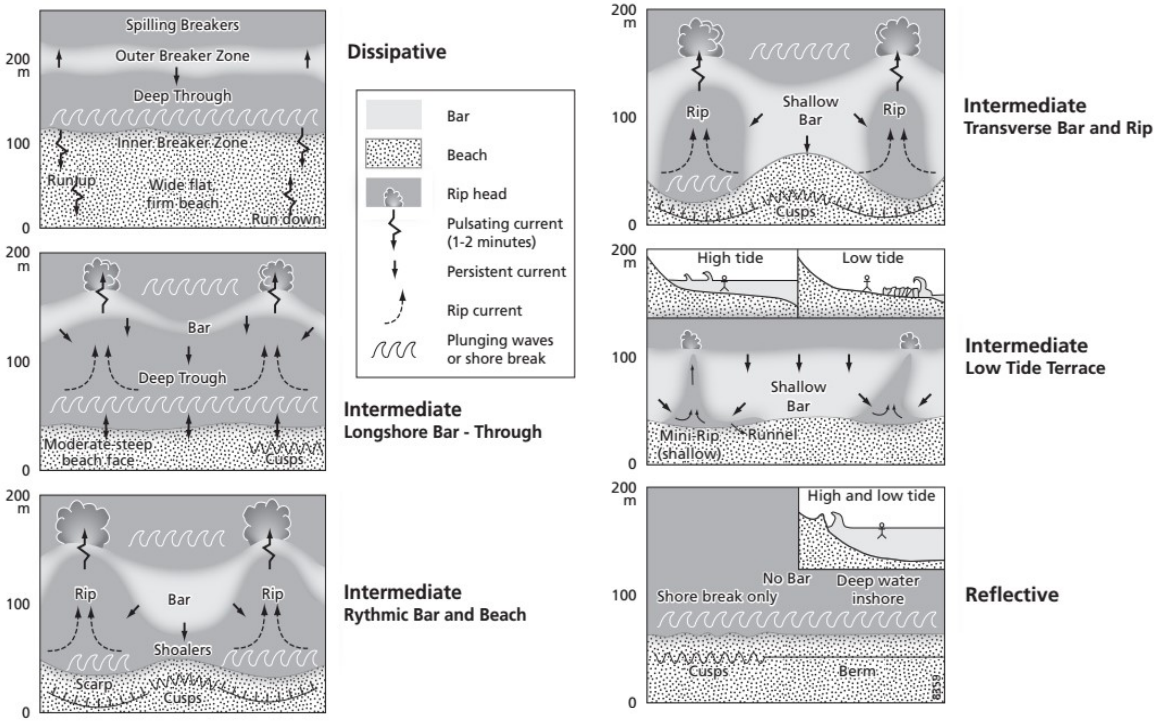

Figure 1. Plan and profile configurations of different kinds of wave-dominated beaches [2]

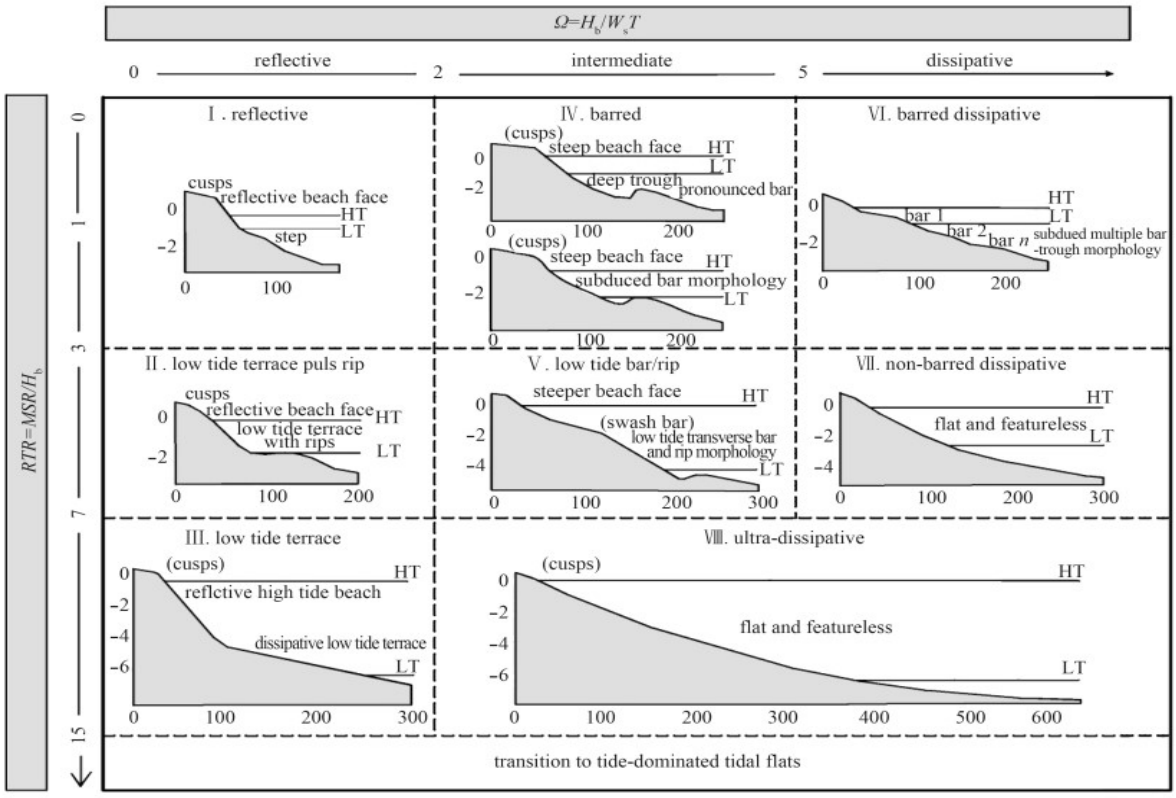

Figure 2. Conceptual beach model based on Ω and the relative tide range (RTR). When RTR< 3 and Ω< 2. When RTR> 3 the transition to tide-dominated tidal flats is entered [17]

Also, Masselink and Hegge [20] studied the morphodynarnic characteristics of three types of beach states by measurements of the morphology, waves, and longshore and cross-shore currents were conducted on two beaches on different macrotidal coastline of central Queensland (Australia). Summary of morphodynamic characteristics of these types of beaches shows in Table 1.

Short [21] presented Tide-modified and Tide dominated beaches models. Tide-modified beaches are divided into three states: Reflective +Low tide terrace (R+LTT), Reflective +Bars and Rips (R+LTR)

and Ultra-dissipative (UD). Also, Tide-dominated beaches are divided into three types: Beach +Sand riges (R+SR), Beach +Sand flats (R+SF) and Tidal Sand mud flats (RTSF).

The results of these studies showed that the morphological conditions and energy levels of the coast depend not only on the wave conditions but also on the range of tides and storms in each winter period.

In Iran, few studies have been conducted on the classification of beaches, which can be pointed to the research carried out by Khoshravan et al [22], based on sediments and geomorphologic evidence on the southern coasts of the Caspian Sea. Firoozfar et al[23] studied the changes of sea level on the southern coasts of the Caspian Sea by investigating the sediments and coastal profiles.

Rahbani et al [24] studied the south-eastern coastline of Iran (entrance of Coastal Makran) based on Shepard classification and using satellite imageries.

Kamranzad [25] investigated the wave characteristics in a 31-yearly period using localized ECMWF wind data and numerically model. The results of this study showed that the highest mean significant wave height occurs in the central strip of the middle parts of the Persian Gulf. While the monthly changes in wind and wave characteristics at different stations in the vicinity of the Strait of Hormuz is different.

Considering the mutual relationship between the beach states and the hydrodynamic and morphodynamic characteristics in beaches, determining the type of beach state in different regions of the northern and southern coastline of Iran plays an important role in the identification of characteristics of waves, currents, bed profile changes over time, coastal features and generally in the optimal coastal management of Iran. Therefore, in this study, beach states in some areas of the northern and southern coasts of Iran were classified according the methods of Wright and Short [16] and Masselink and Hegge [20].

For this purpose, first the beaches' slope was estimated by using Arc GIS, then the breaker height and the tide range were calculated. Sediment features were characterized to estimate the dimensionless fall velocity and determine the beach state. Next, the role of waves, tides and sediments in formation of Iranian coast were studied.

The study is structured as follows: In section 2 different characteristics of the study area were described. In section 3 we presented data and methodology for determining the beach state in differentstations. In section 4 the results were discussed by determining the hydrodynamic conditions and sediment characteristics. Also, spatial and seasonal changes in different coastal conditions were investigated and then the results of the studies were summarized in section 5 .

2. Study area

The studied regions in this research include 14 stations located in the Caspian Sea coast in the Mazandaran Province (between 53 ° 11' 34" E and 36 ° 49' 54" N until 51 ° 01' 30" E and 36° 01' 0"N) and the Hormozgan province coast located near the Strait-of-Hormuz and the Persian Gulf (between 54 ° 39' 18" E and 26 ° 30' 29" N up to 53° 9' 39" E and 27°4' 34"N). In Figure3 and Table 2 the name and location of the study areas are presented.

Generally, there are no gravitational tides in the north Caspian basin, and only weak radiational tides are observed whereas a semidiurnal type of tide is predominant in the middle and south Caspian basins and maximum tidal range of 21 cm was found in the southeastern part of the Caspian Sea[26]. Caspian Sea coast can be classified into three areas based on onshore sediments: (1) sandy beaches: west Guilan, central Guilan, and east Mazandaran (2) gravelly beaches: west Mazandaran (in some segments; not the entire coastline) and (3) muddy beaches: Golestan province [23].

On the other hand, the Persian Gulf is a semi-enclosed, marginal sea that is exposed to an arid, sub-tropical climate. Tidal range varies from 3 to 3.4 meters in the northwest of Persian Gulf and decrease to 0.8 to 1.2 meters in western part of Hormozgan province also reaches to 2.7 to 3 meters in the extreme southeast. The Persian Gulf is located between latitudes 24°to 30° N, and is surrounded by deserts [27].

3. Data and methods

In order to achieve the research objectives, field observations and measurements, laboratory measurements and numerical model results, and finally computational methods, had been used. Field operations were done initially in two steps: (1) photography of the coastal features and important coastal phenomena (such as erosion cliffs, sand bars, channels of rip currents), (2) coastal sediment sampling. In the next step, the spatial variations of thecoastal hydrodynamic and morphodynamic conditions in the northern and southern Iranian coasts were investigated by studying sediment variations, coastal features, and waves climate at each station.

Then, with regard to the characteristics of the waves and the calculation of the coastal slope, the calculation of sediment falls velocity (Ws), different beach states were determined in each station. The method for collecting morphological and hydrodynamic information at each of the stations on the northern and southern coasts is summarized in the table 3.

3.1. Wave breaker height

In this research the wave data from the modeling project (ISWM), which was done by the National Institute of Oceanography has been used. The patterns of wave breaking depend on the wave properties (wave height, wave period) and bed slope.

Table 1. Summary of morphodynamic characteristics of low tide terrace, low tide bar/rip and ultra-dissipative beaches [20]

Parameter/Process	Low Tide Terrace	Low Tide Bar/Rip	UltraDissipative
Ω	< 2(3)	2-5	>5(3)
RTR	3-15	3-7	3-15
High tide conditions and upper part of the intertidal profile			
Sediment size	>0.3 mm	0.2-0.4	<0.3
Tan β	>0.05	0.03-0.05	0.02-0.04
ε	<5	5-20	5-30
Breaker type	surging/plunging	Plunging	plunging/spilling
Attenuation coefficient	0.6-0.8	0.5-0.7	0.4-0.6
Dominant process	swash	swash/surf zone	swash/surf zone
Beach cusps	common	occasional	rare
Morphological change over lunar tidal cycle	Steepening during neap tides, flattening during spring tides	swash bar development, destruction and migration	minor, possible profile changes due to swash bar
Storm response	major erosion of steep upper part	erosion of upper part and of swash bar morphology	erosion upper part
Low tide conditions and lower part of the intertidal profile			
Sediment size	<0.2	<0.3	<0.2
Tan β	<0.03	0.02-0.04	<0.03
ε	>30	>20	>30
Breaker type	spilling	plunging/spilling	spilling
Attenuation coefficient	0.3-0.5	0.3-0.6	0.3-0.5
Dominant process	surf zone/shoaling	surf zone	surf zone/shoaling
Swash bars	occasional	Common	occasional
Rip currents	drainage rips at low tide	surf zone rips at low tide	absent
Tidal currents	important	minor importance	important
Morphological change over lunar tidal cycle	none	minor bar change	none
Storm response	deposition	deposition and destruction of bar morphology	deposition

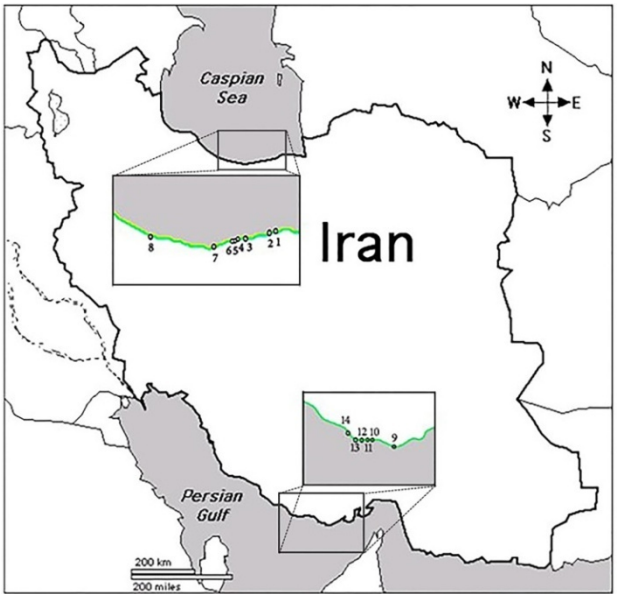

Figure 3. Map of Iran and locations of study areas and beach sites 1-14

Table 2. The names and locations of different stations in the study

NO.	Station name	Station location
Northern beaches		
1	Neka	Long:53° 11′ 34″ lat: 36° 49′54″
2	Farahabad	Long:53° 03′ 35″ lat:36° 47′57″
3	Larim	Long:52° 55′ 48″ lat: 36° 45′53″
4	Naftchal	Long:52° 48′ 06″ lat: 36° 44′16″
5	Mazandaran university	Long:52° 42′ 04″ lat: 36° 43′19″
6	Babolsar	Long:52° 40′ 06″ lat: 36° 42′57″
7	Noor	Long:52° 03′ 29″ lat: 36° 35′09″
8	Nashtarud	Long:51° 01′ 30″ lat: 36° 01′0″
Southern beaches		
9	Bostaneh	Long:54° 39′18″ lat:26° 30′ 29″
10	Charak	Long:54° 3′14″ lat:26° 44′ 27″
11	Gorzeh	Long:53° 53′5″ lat:26° 43′ 22″
12	Near Gorzeh	Long:53° 51′24″ lat:26° 42′ 23″
13	Chiruyeh	Long:53° 44′4″ lat:26° 42′ 6″
14	Moghdan	Long:53° 9′39″ lat:27° 4′ 34″

Weggel[28] based on some of experimental results proved the dependence of the breaking wave height on the bed slope as followed:

$$K = b(m) - a(m)\frac{H_b}{gT^2} \quad (3)$$

where

$$a(m) = 43.8(1.0 - e^{-19m}) \quad (4)$$

$$b(m) = 1.56(1.0 - e^{-19.5m})^{-1} \quad (5)$$

In these relations, m is the beach slope, T is the wave period, and H_b is the breaking wave height. Also, McCowan [29] showed that waves break when their height becomes equal to a fraction of the water depth:

$$H_b = kd_b \quad (6)$$

As a first approximation, the breaking wave depth can be obtained if the characteristics of the offshore wave are known by shoaling and refraction formulas in the case of straight and parallel contours [30]

$$H = H_0\left(\frac{C_0}{2nc}\right)^{\frac{1}{2}}\left(\frac{Cos\theta\circ}{Cos\theta}\right)^{\frac{1}{2}} \quad (7)$$

For shallow water, this relationship is approximately equal to:

$$H = H_0\left(\frac{C_0}{2\sqrt{gd}}\right)^{\frac{1}{2}}\left(\frac{Cos\theta\circ}{1}\right)^{\frac{1}{2}} \quad (8)$$

Now if the angle of wave breaking is assumed to be small$(\theta = 0)$, we use the McCowan's breaking criterion:

$$Kd_b = H_o\left[\frac{C_0}{2\sqrt{gd_b}}\ (\cos\theta_0)\right]^{\frac{1}{2}} \quad (9)$$

And so d_b can be written as:

$$d_b = \frac{1}{g^{\frac{1}{5}}k^{\frac{4}{5}}}\left(\frac{H_0C_0\cos\theta_0}{2}\right)^{\frac{2}{5}} \quad (10)$$

Table 3: Morphological and hydrodynamic information at each station on the northern and southern coast.

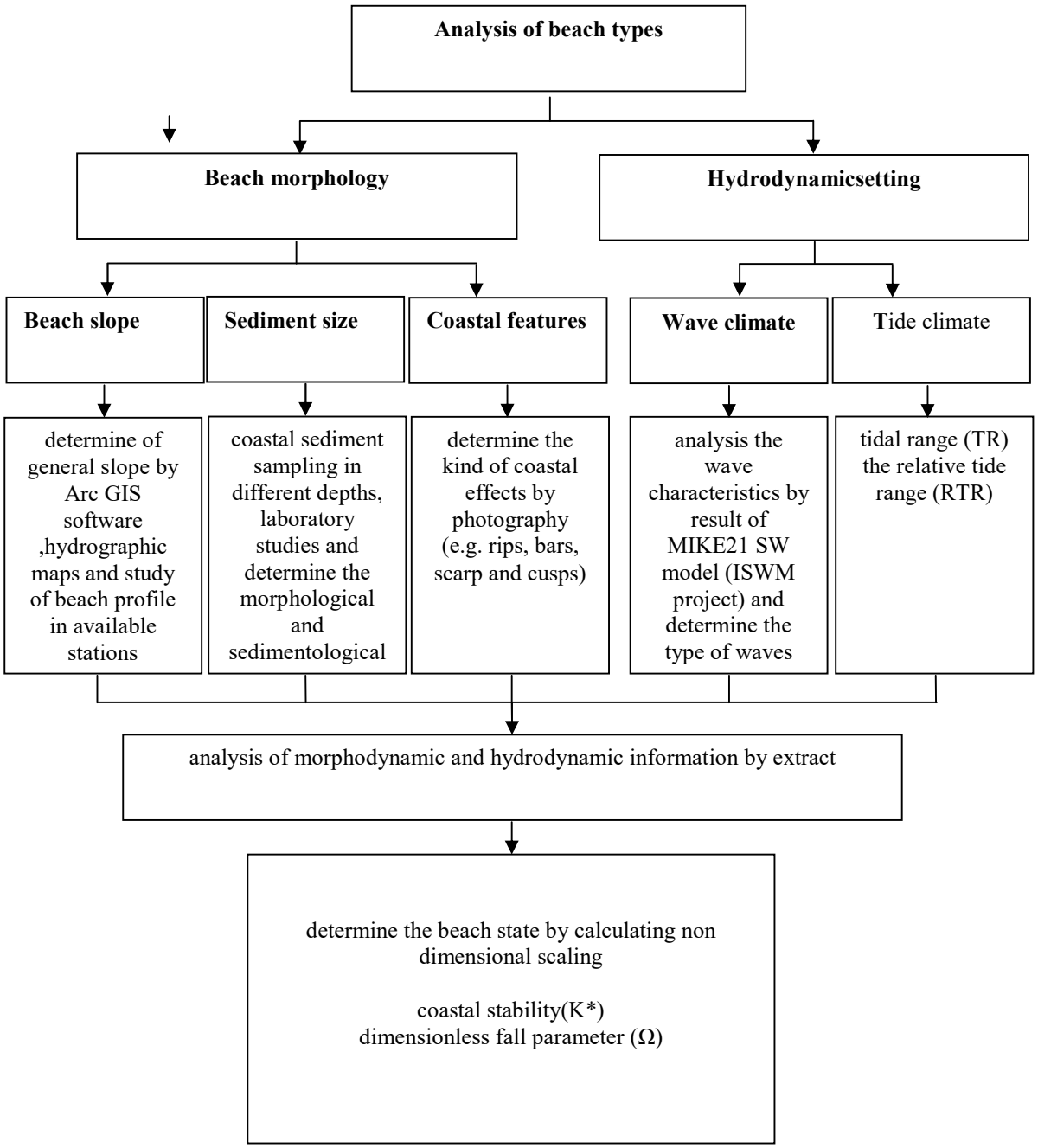

In the above relation$H_0$is the average height of deep water, $C_0 = \frac{gT}{2\pi}$is the velocity of the deep-water wave and θ_0 is the radiation angle of the dominant waves. The value of d_b obtained from the above equation is replaced in equation 6, and then the resulting $H_b$is compared with the numerical value of the hypothetical H_{bh}. It is necessary to determine the breaking wave height at each station. This operation is repeated consecutively to establish the relationship $H_b \cong Hbh$. Therefore, due to the implementation of such a trial-and-error method, the breaker index is calculated at each station.

Table 3 shows the characteristics and properties of waves in the northern and southern regions of Iran.

3.2 Sediment grain sizes

In order to investigate the effect of hydrodynamic conditions on sediment transport and bed form in the coastal zone, sediment sampling operations were performed at depths that covered the entire nearshore zone. A total of 56 sand samples were collected at 14 stations. Samples were taken from different depths (0, 2.5, 5 and 10 meters) of cross-shore profile with different morphological features such as beach face, surf domain, troughs and bars. Then sand samples were analyzed from different depths of the northern coasts in the Oceanographic laboratory and sedimentary information related to southern coasts in the Marine Geological Organization. In this way, specific gravity of sediment particles and diameter of

50% of sediments were determined from different depths then the average of these parameters were obtained from information about different depths. Finally, the average dimensionless fall velocity parameter and scale of morphodynamic features were determined and calculated in accordance with the sedimentation status of each station.

3.3 Beach morphology: Fieldmapping and imageinterpretation

In this study, with the help of images taken from coastal features in accordance with the characteristics of each beach state, comparing the features of different stations and monitoring the type of breaking wave, the morphological characteristics of the beach during the year were evaluated.

4.Results and discussion

Since tidal oscillations in the south Caspian basin are mainly caused by radiational effects and maximum tidal range is negligible in the central part of the southern Caspian, the effects of tides on the hydrodynamic conditions of the beach are ignored [26]. Also, the waves play an important role in this basin and so these coastal areas were considered as wave-dominated coast and the Wright and Short [16] method was used to determine the state of the northern coast in this study. On the other hand, in Iranian southern coastal areas, considering the effects of the tide on these coasts and the weak effects of waves compared to the northern coastal area, the Masselink and Short [17] classification was used.

4.1 Hydrodynamic conditions

According to figure 4, the information obtained from the wave roses showed that the prevailing wave direction over the western coast of Mazandaran province was northward; and in the central and eastern parts, was mostly northwest and wave height decreases from west to east. Therefore, on the western parts of the northern Iranian coast, hydrodynamic conditions were stronger than the central and eastern regions.

While on the southern Iranian coast, the wave characteristics at different stations in the vicinity of the strait of Hormuz are variable. Also, according to the definition of the Iribarren Number ε_b :

$$\varepsilon_b = \frac{\tan\beta}{\left[H_b/L_0\right]^{1/2}} \qquad (11)$$

(where tanβ is the beach gradient and$H_b$is breaker wave height, L is the water length and the subscripts $_0$ indicate deep water conditions) in all southern coast stations occur spilling breakers (Figure 5), while in the northern coast spilling breakers were often observed (Table 4). Although at station 8 (Nashtarud), surging breakers occur during in some periods (Figure 6).

4.2. Sediment characteristics

According to the information recorded in table 5 that show characteristics and properties of sediments, the mean sediment grain size increases discontinuously from east to west on the northern Iranian coasts. Also, morphodynamic conditions on the northern coasts showed the morphodynamic effects from station 1 to 7 are related to the dissipative state. On the other hand, the eastern parts of these coasts had low height berms, wide surf zone and low slope (compared with other coastal regions). The southern Iranian coasts did not follow a certain order, but in all of the stations in these coasts, the sediments consisted of more than 95% sand and less than 5% gravel.

4.3. Beach states

Due to the minimal effects of the tide in the Caspian Sea and the conditions mentioned about the waves, these coasts are considered wave-dominated (RTR<3). In this condition, to determine the beach state in the stations located in these area two dimensionless parameters, fall velocity parameter Ωand coastal stability were examined [31].

$$K^* = \frac{H_b^2}{gT^2 d_{50}} \qquad (12)$$

Where$d_{50}$is the median sediment grain size, g is acceleration due to gravity, T is the wave period.According Figure 7, the coastal conditions at seven stations in this area (Neka, Farahabad, Larim, Naftchal, Mazandaran University, Babolsar, and Noor) on average during the yearwere dissipative (D), while at the Nashtarud station was on intermediate state (Figure 8).

Along Iranian southern beaches, the spring tide range was TR ~ 0.8 - 1.13 m, and the wave period and breaker height ranged from T ~ 0.95 – 2.89 and H_b = 0.10 – 0.30 m. As a result, RTR ranges from 3 to 12 and all the beaches along the Hormozgan western coast were a tide-modified (see Short, 2006) and remain in this state throughout the year (Figure 9).

4.3.1. Wave-Dominated beaches (Iranian northern beaches)

4.3.1.1. Spatial variation in beach conditions

The poor hydrodynamic conditions with average breaker height of H_b ~0.585-0.772 m during the year, the gentle slope and fine sediments d_{50} ~ 0.116 – 0.158mm cause the beach state to be mostly on the dissipative state in the eastern and central area of the Caspian Sea coasts (from Neka to Noor). There were some similar morphodynamic features in almost all the seven dissipative stations which are in accordance with the value of Ω in each station had a different scale. Hence, the eastern coast of Mazandaran had lower berm levels and wider surf zone with a slope less than other the coastal areas.

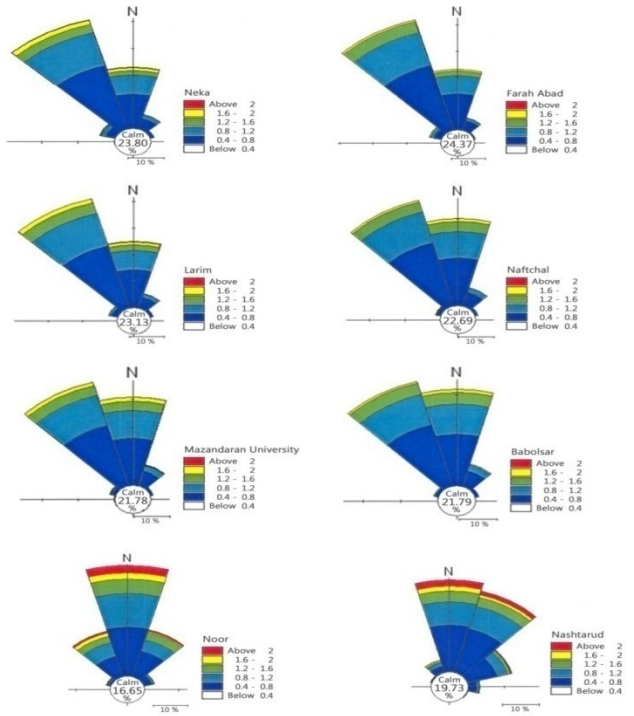

Figure 4. Wave rose of different stations of northern beaches

In the beaches that are not the fully dissipative state (all stations except for Naftchal), the crescentic bar was replaced shore-parallel sandbars when wave height decreased and these beaches were entered the intermediate state (RBB, LBT). Among these stations,there were more prominent bars and troughs in the bed of Noor and Farahabad stations. These sites also contained a mixture of undertow and rip currents system which changed in accordance with the prevailing morphodynamic conditions (Figure 10). While the beaches were fully dissipative state throughout the year (such as Naftchal) contained some subdued bars and troughs on the bed.

In the western stations such as Nashtarud with a steep slope in comparison with other stations (slope=0.0072), increasing the beach slope and stronger hydrodynamic conditions, especially increasing of sediment grain size had caused that this station was often on the intermediate (ridge-runnel or low tide terrace) during most of the year (85.2%) and beach profile was variable compared to other stations. Also, the type of breaker was predominantly spilling type (ε_b = 0.029) in this station, but when the beach returned to the reflective state the probability of occurrence of the surging type increased (14.79%). compared to the eastern and central beach regions this beach entered the ridge-runnel state with narrow and weak rip currents during the year.

4.3.1.2. Seasonal variation in beach conditions

For the study of seasonal variation of the beach state in the northern stations, the changing procedure of coastal hydrodynamic and morphodynamic effects were investigated during the year.

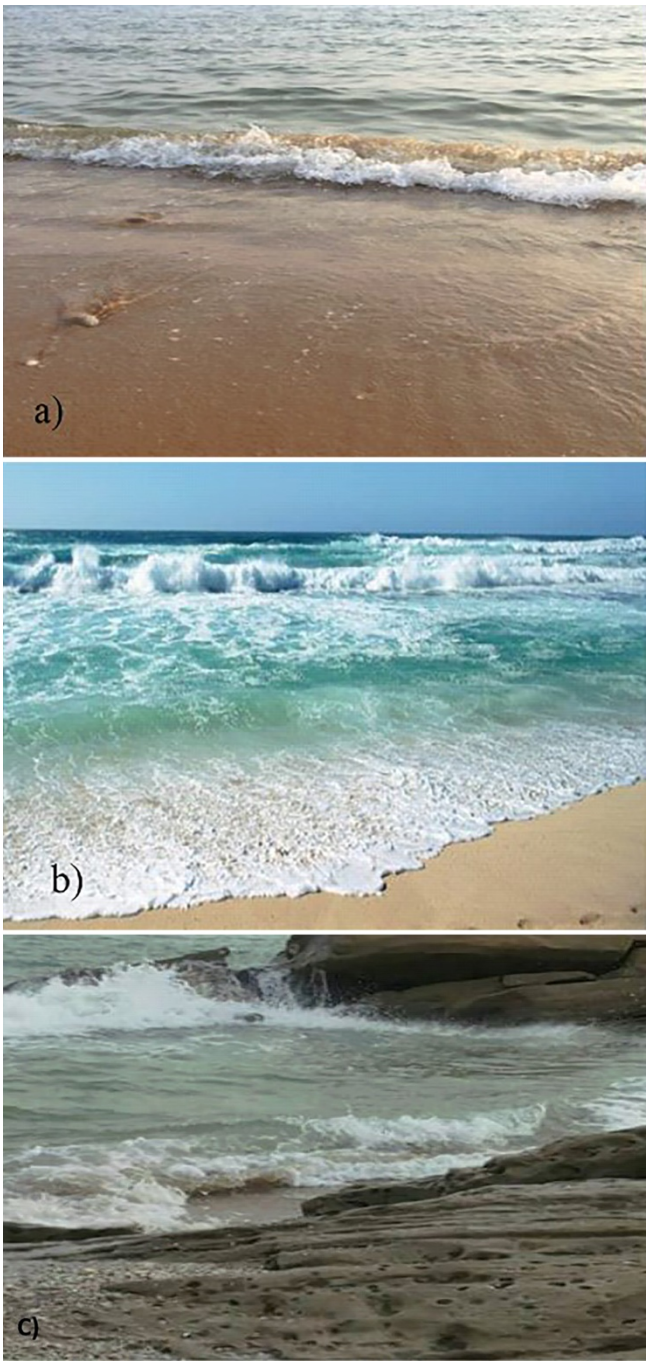

Figure 5. Spilling breakers at different stations on southern beaches a) Bostaneh (station 9) b) Charak (station 10) c) Moghdan (station 14)

According to Figure 11, diagram of the probabilities of annual occurrence of beach states for different stations of northern beaches showed that in all dissipative stations variations of beach state were small, so that the beach state was often in the dissipative state most of the year. But these changes were more evident in Nashtarud and regarding beach conditions had a good coordination with the intermediate beach state.

During winter when wave height increased, the profile of bed gradually changed as wave up rush and surf zone currents increased. These conditions also caused erosion and actually deepen of the rip channels. This process occurred while some bars sections were still

Table 3.Data of hydrodynamic properties of different stations in the study

NO.	Hs (m)	ε_b	T
Northern beaches			
1	1.128	0.018	2.69
2	1.093	0.023	2.68
3	1.131	0.025	2.69
4	1.125	0.026	2.69
5	1.14	0.024	2.71
6	1.17	0.021	2.74
7	1.375	0.042	2.98
8	1.312	0.029	2.91
Southern beaches			
9	0.487	0.018	2.897
10	0.254	0.179	1.717
11	0.168	0.056	0.956
12	0.223	0.090	1.226
13	0.273	0.013	2.480
14	0.281	0.013	1.494

connected to the beach. In this state, an increase in the height of the beach scarp was observed as the beachreached the transverse bar and rip (TBR) state. Given the severity of these rip currents when there were stormy conditions, the shoreline became more rhythmic. Based on field results, the beach state remained in this situation about 0.96% of the year (Nashtarud). Although this period was short, there was sufficient time for the beach to reach the transverse bar and beach (TBR) state. During summer wave height decreased gradually rip current velocity reduced and sediments moved from the bar to the beach. During this stage the surf zone width was reduced, the rip current channels were filled with sediment. So, the depth of the channels was reduced and the beach reached the ridge-runnel or low tide terrace (LTT) state, such that the rip currents became weak and the remaining narrow channels from these currents appearedas runnels on the beach profile. With the reduction of wave height and as more sediments transfer from the bars towards the beach, gradually all the runnels were filled with sediment and formed step-like effects in the base of the beach face. In this state the beach entered the reflective state (R). In general, the main impact on the beach profile was the bar connecting to the beach (terrace) and runnels. Other important effects in this area were the erosion scarps which distance between the base of these scarps from the shoreline increased and the height reduces in warm seasons (Figure 12).This phenomenon is most likely related to beach state changes towards the reflective state and sea level changes.

4.3.2 Wave-Tide beaches (Iranian southern beaches)

4.3.2.1 Seasonal variation in beach conditions

According to Figure 13, generally in all the southern stations the effects of waves were stronger in spring and winter, so the highest wave effects were created inApril, after that the wave height began to decrease and in October it was minimal.

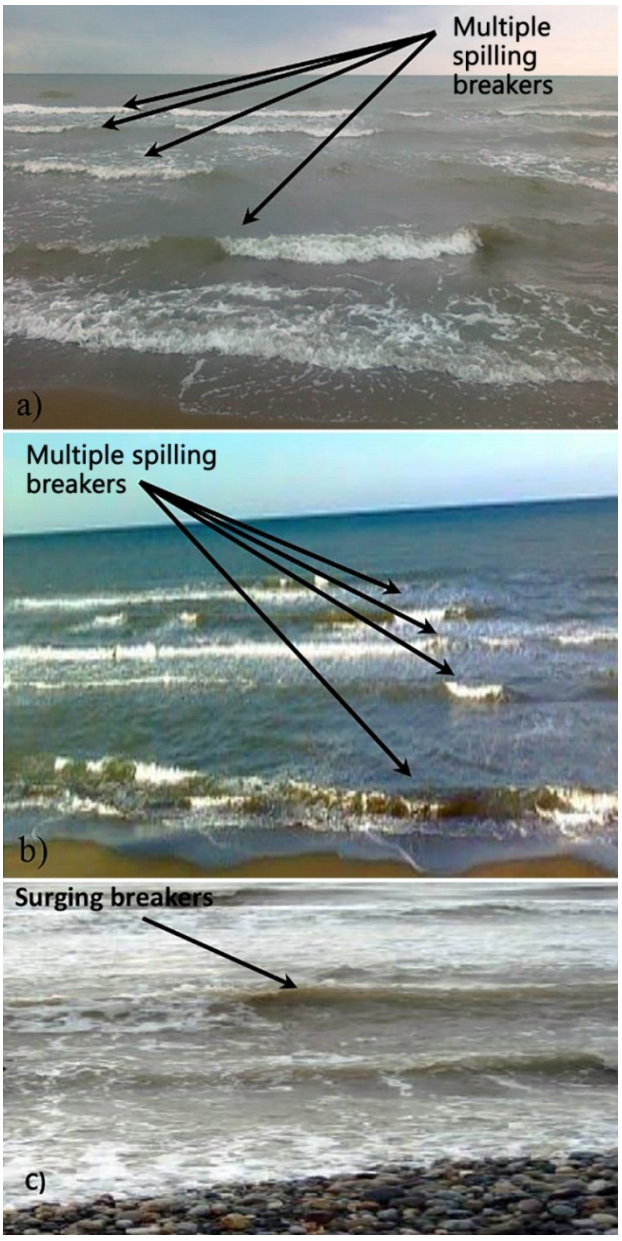

Figure 6. Breaker types on different stations in northern beaches a) Larim (station 3) b) Noor (station 7) c) Nashtarud (station 8)

Table 5. Sediment's characteristics of different stations in the study

NO.	D(φ)	d50(mm)	ρ(gr/cm3)	w (m/s)
Northern beaches				
1	2.66	0.158	2.67	0.0182
2	2.64	0.116	2.67	0.0186
3	2.77	0.146	2.713	0.0169
4	2.96	0.128	2.71	0.013
5	2.76	0.147	2.72	0.0171
6	2.85	0.138	2.75	0.0154
7	2.10	0.23	2.71	0.028
8	0.95	1.93	2.71	0.187
Southern beaches				
9	1.577	0.25	2.1	0.0023
10	1.14	0.64	2	0.0603
11	1.752	0.215	2.85	0.0282
12	2.678	0.12	1.5	0.0035
13	2.723	0.115	2.5	0.0099
14	1.759	2.5	2.5	0.197

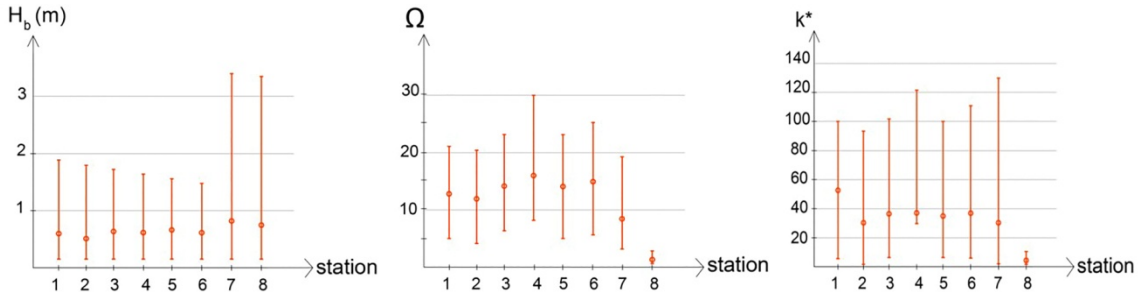

Figure 7. Range change of breaker height (H_b); sedimentation rate (Ω), coastal stability (k*) and mean of these parameters (•)at different stations of northern beaches

Figure 8. Examples of wave-dominated beaches in northern beaches a) Noor (station 7) b) Babolsar(station 6) c) Farahabad (station 2) d) Nashtarud (station 8)

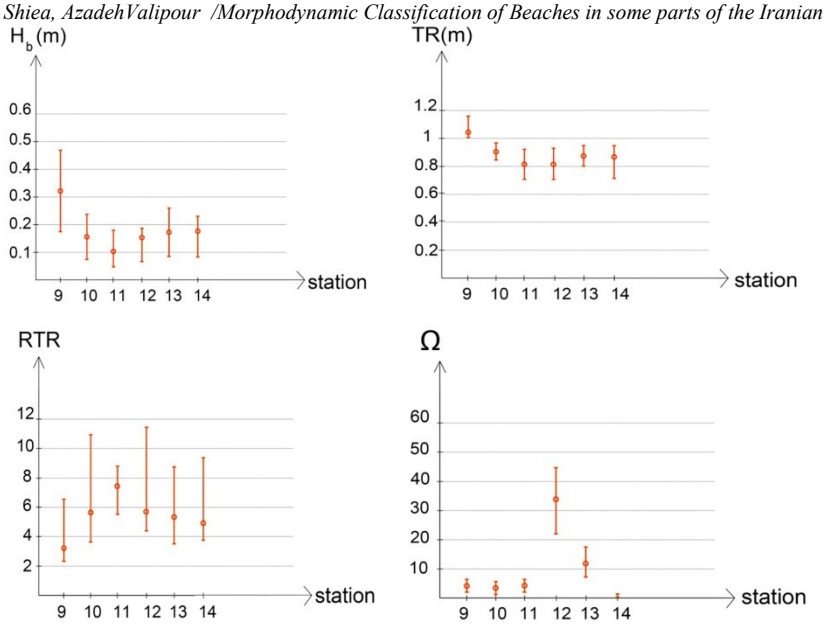

Figure 9. Range change of breaker height (H_b), tidal range (TR), relative tide range (RTR), sedimentation rate (Ω); mean of these parameters (•) at different stations of southern beaches

Figure 10.View of a topographic rip current and multiple longshore bar near Noor station

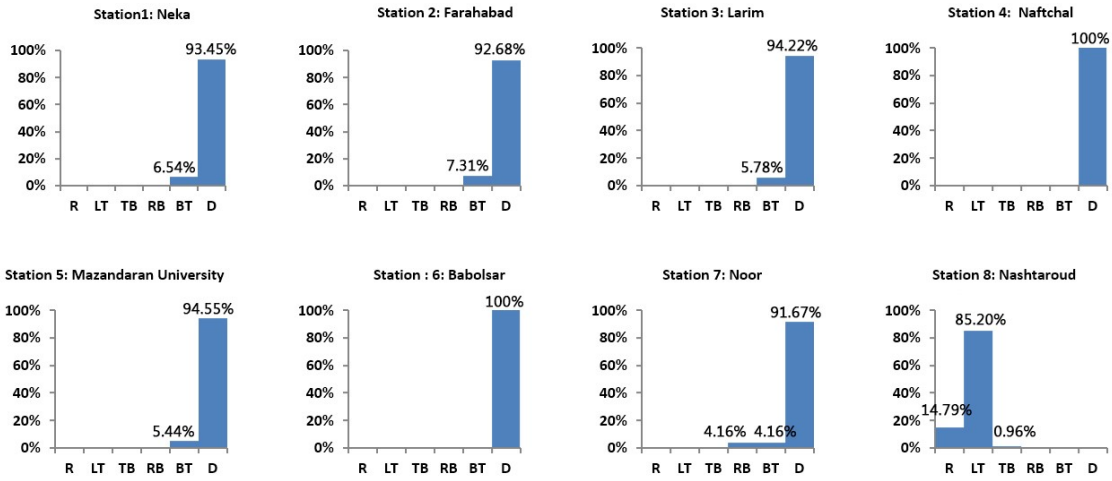

Figure11. Probabilities of annual occurrence of beach states for different stations of northern beaches

Figure12. View of an erosion scarp at Nashtarud station

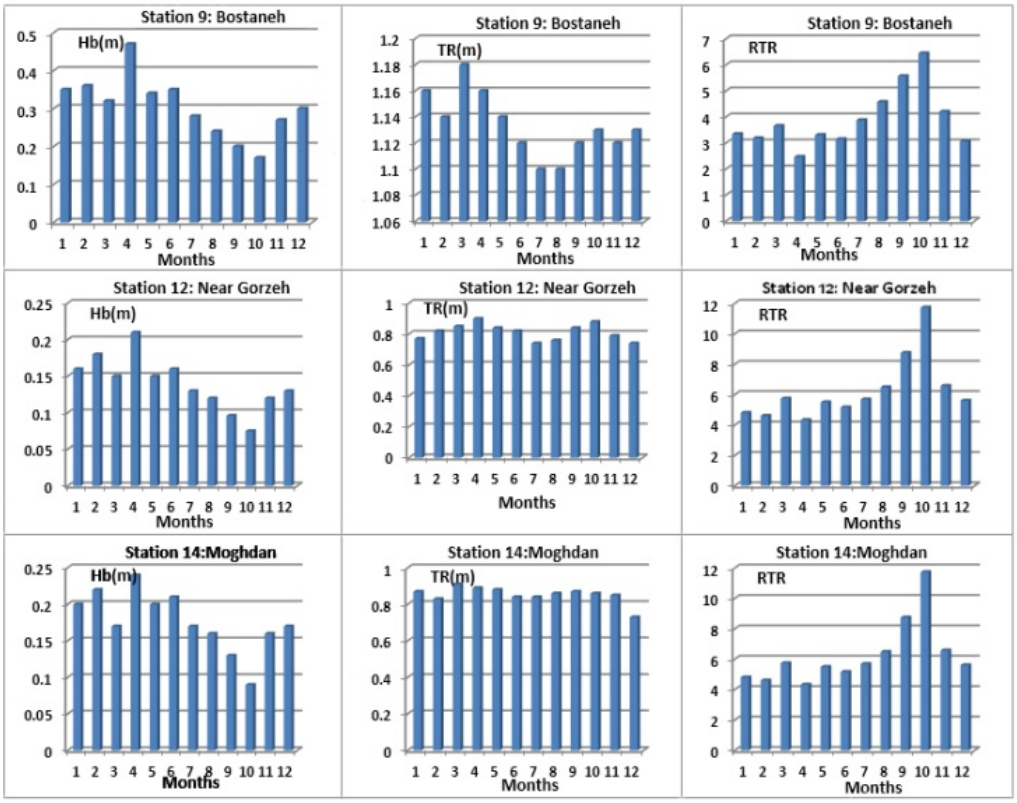

Figure13. Mean monthly of breaker height (H_b), tidal range (TR), relative tide range (RTR) during a year

On the other hand, tidal effects in fall and winter were at their maximum height. So that most amount of TR was observed in March. After March, tidal range decreased and in summer it was at its minimum, reaching its lowest in July (Figure 14).

Also, the study of the patterns' sediment grain size in all stations of the southern coast revealed that the sediment grain size did not follow a certain order.

However, despite the changes of tide and waves, the beach state for each station was almost fixed and unchangeable during the year.

4.3.2.2. Spatial variation in beach conditions

The results show that station 9 had the lowest slope (0.00277) and highest waves based on Figure 9 (H_b~0.175-0.47). Also, the intertidal sediment was 4.7% gravel and 95.3% sand. The average beach state during the year was low tide bar/rip beaches (75%), while 25% of the year the beach in this area was ultra-dissipative state.

At stations 10 and 14, the sediment particle diameter (in the upper part of the intertidal profile) was coarse

sand (0.64 mm) in station 10 and (very coarse sand) 2.5 mm in station 14 and this included 99.7% sand and 0.25% gravel. In these two stations the average beach state during the year was low tide terrace (92% at station 10) and became close to ultra-dissipative 8% of the year. However, at station 14 this state remained unchanged during the year, with the yearly incidence 100% low tide terrace (Figure 14).

In the three stations (11-13) located between Gorzeh and Chirooyeh Ports, the average beach state during the year was ultradissipative. This was primarily a result of the finer sediment (station 11 with d_{50}=0.215 mm, station 12 with d_{50}=0.12 mm and station 13 with d_{50}=0.115 mm) together with the relative tide range (RTR = 5-7), sedimentation rate (Ω = 5-35) and the slope of these beaches was less than 0.03.

In station 11, close to the Gorzeh area ultradissipative conditions occurred 75% of the time and low-tide bar/rip 25% of the time, while at station 12 and 13 ultra-dissipative conditions prevails 100%.

5. Conclusion

The northern coasts of Iran are adjacent to the Caspian Sea, the largest lake in the world, and are exposed to short waves that increase in height from east to west. The waves combined with the minimum of tidal amplitudes in this region, result in wave-dominated beaches. In the southern regions of Iran, which borders the Persian Gulf, the waves are lower compared to the northern region of Iran and the presence of tides effects in these beaches cause them to be tide-modified. These differences of hydrodynamic factors cause a variety of beach states in the northern and southern coastal areas of Iran.

Results of this study show that for the northern beaches, 10 out 11 stations are in the dissipative state while Nashtarod (station 8) is in the intermediate state (ridge-runnel or low tide terrace). By comparing the stations studied, it can be stated that, the most dissipative state can be observed in the Naftchal station and the least dissipative can be observed in the Noor and Farahabad stations. Also, there are very minimal changes during the year in the beaches in the stations in the dissipative state and so those beaches are in the dissipative state more than 90% of the year, while the intermediate beach ranges seasonally from reflective to transverse bar and rip.

On the southern beaches of Iran, a wide range of beach states are present in the study area: reflective, dissipative, and intermediate have been observed. However, the ultra-dissipative beaches (which are a part of the dissipative groups) at most of the stations undergo little annual change, while the stations with intermediate beach states such as low tide terrace beaches and or those with a bar, change during the year and can become close to the dissipative beach state. Based on the results of this study the most frequent beach states in the north and south of Iran are dissipative, with the southern coastal area being tide-modified with the ultra-dissipative state.

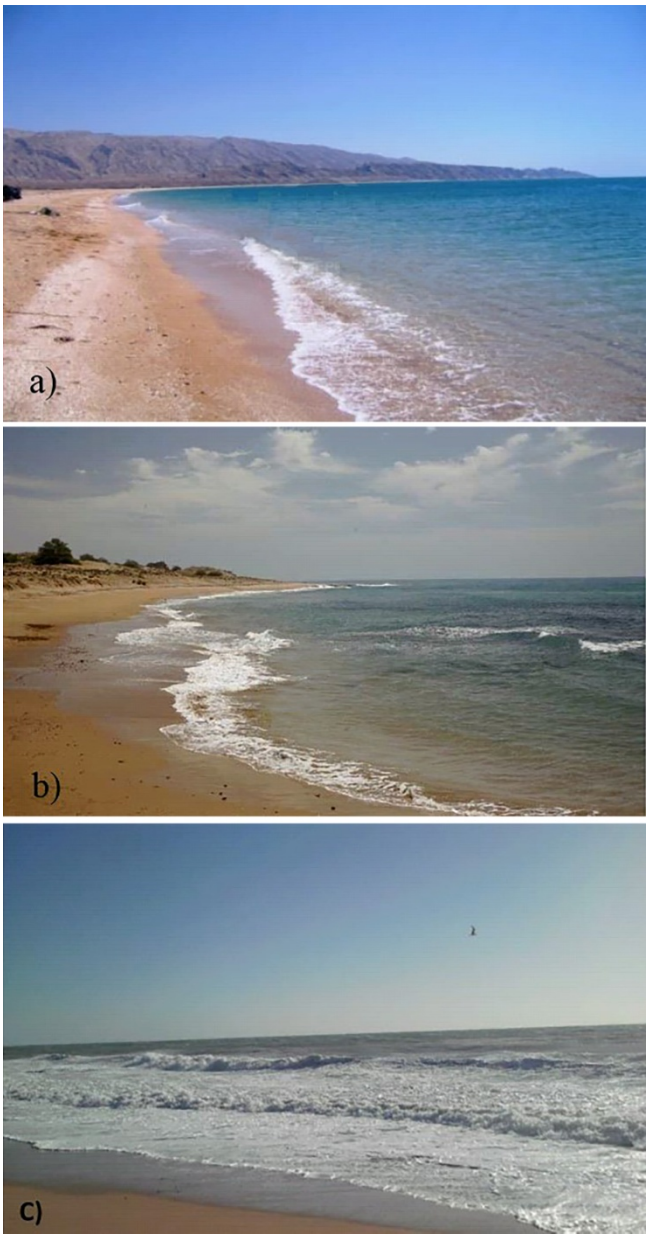

Figure 14.Examples of Wave-tide beaches in southern beaches a) Chiruyeh (station 13) b) Moghdan (station 14) c) Bostaneh (station 9)

are in the dissipative state more than 90% of the year, while the intermediate beach ranges seasonally from reflective to transverse bar and rip.

On the southern beaches of Iran, a wide range of beach states are present in the study area: reflective, dissipative, and intermediate have been observed. However, the ultra-dissipative beaches (which are a part of the dissipative groups) at most of the stations undergo little annual change, while the stations with intermediate beach states such as low tide terrace beaches and or those with a bar, change during the year and can become close to the dissipative beach state. Based on the results of this study the most frequent beach states in the north and south of Iran are

dissipative, with the southern coastal area being tide-modified with the ultra-dissipative state.

Acknowledgments
We are grateful to Professor A. Short for fruitful suggestions and valuable remarks. We would like to thank the Department of Physical Oceanography of the Iranian National Institute for Oceanography and Atmospheric Science (INIO) for providing wave and sediment data of the Mazandaran Province. In addition, we acknowledge the help of Dr. R. Lak from the Marine Geological Organization, Tehran, who provided us with the sediment data of the Hormozgan Province coast.

List of Symbols (Optional)

C_0	velocity of the deep water[m/s]
d_b	breaking wave depth [m]
d_{50}	median sediment grain size [mm]
g	acceleration due to gravity[m/s]
H_b	breaker height[m]
K^*	Coastal stability
L	water length[m]
m	beach slope
RTR	relative tide range
T	wave period [s]
TR	tide range [m]
W_s	sediment fall velocity [m/s]
θ_0	radiation angle
Ω	dimensionless fall velocity
ε_b	Iribarren Number

6. References

1-Scott, T., Masselink, G.y., Russel, P., (2011*), Morphodynamic characteristics and classification of beaches in England and Wales,* Marine Geology, Vol.286, p.1-20.
2- Short, A.D., (1999*), Beach and Shoreface Morphodynamics,* Chichester, United Kingdom: Wiley, p.379.
3-Short, A.D. and Hogan, C.L., (1994), *Rip currents and beach hazards: Their impact on public safety and implications for coastal management,* Journal Coastal Research, Special Issue No. 12, p.197-209.
4- Scott, T.M., Russell, P., Masselink, G. and Woolers, A., (2009), *Rip current variability and hazard along macro-tidal coast*, Journal of Coastal Research, SI 56, p.895–898.
5- Reniers, A.J.H.M., Roelvink, J.A., Thornton, E.B., (2004*), Morphodynamic modeling of an embayed beach under wave group forcing*, Journal of Geophysical Research, Vol.109, C01030. doi:10.1029/2002JC001586.
6- Garnier, R., Calvete, D., Falqués, A., and Caballeria., M., (2006), *Generation and nonlinear evolution of shore-oblique/transverse sand bars,* Journal of Fluid Mechanics, Vol. 567, p.327–360.
7- Dronen, N., and Deigaard, R., (2007), *Quasi-three-dimensional modelling of the morphology of longshore bars*, Coastal Eng, Vol.54, p.197–215.
8- Smit, M.W.J., Reniers, A.J.H.M., Ruessink, B.G., Roelvink, J.A., (2008*), The morphological response of a nearshore double sandbar system to constant wave forcing,*Coastal Engineering, Vol.55, p.761–770.
9- Van Enckevort, I.M.J. and Ruessink, B.G., (2003a), *Video observations of nearshorebarbehaviour. part 1: alongshore uniform variability*, Continental Shelf Research, Vol.23, p.501–512.
10- Van Enckevort, I.M.J. and Ruessink, B.G., (2003b), *Video observations of nearshore bar behaviour. part 2: alongshore non-uniform variability,* Continental Shelf Research, Vol.23, p.513–532.
11- Ranasinghe, R.; Symonds, G.; Black, K. and Holman, R.A., (2004), *Morphodynamics of intermediate beaches: a video imaging and numerical modelling study,* Coastal Engineering, Vol.51, p.629-655.
12- Quartel, S., Ruessink, B.G., Kroon, A., (2007*), Daily to seasonal cross-shore behaviour of quasi-persistent intertidal beach morphology,* Earth Surface Processes and Landforms, Vol.32, p.1293–1307.
13- Holland, K.T., Holman, R.A., Lippmann, T. C., Stanley, J and Plant, N., (1997), *Practical use of video imagery in nearshore oceanographic field studies*, Journal Oceanic Engineering, Vol.22(1), p.81-92.
14-Smit, M.W.J., Aarninkhof, S.G.J., Wijnberg, K.M., González, M., Kingston, K.S., Southgate, H.N., Ruessink, B.G., Holman, R.A., Siegle, E., Davidson, M., Medina, R., (2007), *The role of video imagery in predicting daily to monthly coastal evolution*, Coastal Engineering, Vol.54, p.539–553.
15- Klein, A.H.F. and de Menezes, J.T., (2001), *Beach morphodynamic and profile sequence for a headland bay coast,* Journal of Coastal Research, Vol.17, p.812–835.
16- Wright, L.D. and Short, A.D., (1984), *Morphodynamic variability of surf zones and beaches: A synthesis,* Marine Geology, Vol.56, p.93–118.
17- Masselink, G. and Short, A.D., (1993*), The effect of tide range on beach morphodynamics and morphology: a conceptual model,* Journal of Coastal Research, Vol.9(3), p.785–800.
18- GOURLAY, M.R., (1968), *Beach and Dune Erosion Tests*, Delft Hydraulics Laboratory Report M93 51M936, Delft.
19- Dean, R.G., (1973), *Heuristic models of sand transport in the surf zone,* Proc. Conf. Engineering Dynamics in the Surf Zone, Sydney, N.S.W, p.208–214.
20- Masselink, G. and Hegge, B., (1995*), Morphodynamics of meso- and macrotidal beaches:*

Examples from central Queensland, Australia, Marine Geology, Vol.129, p.1–23.
21- Short, A.D, (2006)*, Australian beach systems – Nature and distribution,* Journal of Coastal Research, Vol.22(1), p.11-27.
22- Khoshravan, H., Rohanizadeh, S., Malek, J., Nejadgholi, G., (2011), *Caspian Sea southern coasts zoning on the basis of sedimentary morphodynamic indicators,* Journal of the Earth and Space Physics, Vol. 37(3), p.1-15 (in Persian).
23- Firoozfar, A., Bromhead, E.N., Dykes, A.P., and Neshaei, M.L., (2012), *Southern Caspian Sea Coasts, Morphology, Sediment Characteristics, and Sea Level Change*, Proceedings of the Annual International Conference on Soils, Sediments, Water and Energy, Vol. 17, Article 12, p.123-150.
24- Rahbani, M. and Pakhirehzan, M., (2018*), Classifying east coasts of Hormozgan province using Shepard method and satellite imagery,* The Egyptian Journal of Remote Sensing and Space Sciences, Vol.21, p.335-344.
25- Kamranzad, B., (2018), *Persian Gulf zone classification based on the wind and wave climate variability,* Ocean Engineering, Vol.169, p.604-635.
26- Medvedev, I.P., Kulikov, E.A., Rabinovich, A.B., (2017), *Tidal oscillations in the Caspian Sea,* Oceanology, Vol.57, p.360–375.
27- Perrone, T.J., (1979), *Winter shamal in the Persian Gulf. Monterey, California,* technical report, Naval Environmental Prediction Research Facility, I.R.-79-06, p.180.
28- Weggel, J., (1972), *Maximum breaker height for design,* In: Proceedings of the 13th International Conference on Coastal Engineering,Vancouver, Canada, ASCE, p. 419–432.
29- McCowan, J., (1894), *On the highest wave of permanent type,* The London, Edinburgh, and Dublin Philosophical Magazine and Journal of Science, Vol.5, p.351–358.
30- Dean, R. G. and Dalrymple, R. A., (1991), *Water Wave Mechanics for Engineers and Scientists,* World Scientific, Singapore.
31- Sunamura, T., (1984)*, Quantitative predictions of beach-face slopes,* Geological Society of America Bulletin, Vol.95, p.242–245.

INTERNATIONAL JOURNAL OF
COASTAL & OFFSHORE ENGINEERING
IJCOE Vol.6/No. 3/Summer 2021 (40-48)

Available online at: www. Ijcoe.org

Integration of Geographical Information System and Tsunami Generation / Propagation Models in the Makran Region (North of the Arabian Sea)

Masoud Moradi[1*]

[1*]*Associate professor, Iranian National Institute of Oceanography and Atmospheric Science;* Moradi_msd@yahoo.com

ARTICLE INFO

Article History:
Received: 07 Dec. 2020
Accepted: 16 Sep. 2021

Keywords:
Tsunami
Propagation
Numerical Models
Data Management
GIS

ABSTRACT

Two numerical models of tsunami generation/propagation have been run in the Makran region. These models are one of the necessary components in the warning systems in this region. The outputs of these models are not in regular international data model standards. In order to get the best result from these models, the models' outputs must be managed in a database system. An ideal data management system for tsunami warning system has three essential parts included: data convertor, Geographical Information System (GIS) and Relational Database Management System (RDBMS). The schematics and properties of the proposed data management system have been shown in this paper. 3D, spatial, temporal and statistical analysis of tsunami models data exported to the proposed system based on GIS capabilities and data processing routines. Some examples of data analysis of tsunami propagation in the Makran region (north of the Arabian Sea) have been shown.

1. Introduction

Tsunamis have caused significant damage and casualties along the coastlines, even after spreading wide distances across open oceans. Emergency managers and governors need immediate operational tools to provide accurate tsunami forecasting as a quick and essay decision guide. Hazards from tsunamis are now mitigated by the instance of early warnings to evacuate coastal areas at risk. Observational networks will never be dense because the ocean is vast. It is technically difficult and costly expensive to establishing and maintaining monitoring stations in deep waters. These early warnings are based on seismic and tide gage data transferred to the warning stations, deep ocean recorders and simulated scenarios [1]. The uncertainty in bathymetric data affects the accuracy of numerical models. Integration of in situ measurement and numerical modeling techniques can provide more reliable tsunami forecasts [2]. One of the fastest techniques for tsunami early warning system is the utilization of pre-computed generation/propagation forecast database. In this method, seismic parameters and tsunami modeled parameters are used to search through a pre-computed forecast database and select the most appropriate scenarios which closely matches the observational and modeled criterion. In this regard, scenarios are an adequate tool for estimating the tsunami parameters in deep water, and they could be considered as an initial condition for further processing. Forecasting the maximum height of tsunami waves are calculated using statistical techniques which should be developed for a specific case study [3]. The results of tsunami scenario and statistical methods provide early warning tools for hazard assessment that help decision makers and emergency managers. These tools are used to forecast the tsunami amplitudes, and they assist emergency managers during tsunami warnings [1]. However, tsunami propagation modeling and forecasting systems clearly need data manipulation and here by there is no way to have a good data management system for tsunami warnings and also its hazard decision making and management.

Such as of many other oceanic phenomenon, knowledge of tsunami generation/propagation and decision for reducing its hazardous effects needs data and information. At the technical level, integrated management of the ocean and seas relies on two basic tools: modeling and data [4]. Within the decision-making process, modeling acts as a tool so that the environment modeling-decision making relationship is developed as a bridge between scientific research and policy analysis [5]. There is a significant gap between information needs on environmental decision making and information produced by the current systems of data collection and management [6]. Now most significant means of collecting, processing, storing and communicating data have been developed, but we still suffer from poor information when we attempt to make a decision for oceans and seas from the available data [4]. This gap can be filled in by appropriate monitoring, management and modeling of data [5]. However, availability of raw and modeled data is not a

sufficient condition to produce the required information about the oceans and seas. It is the utility or usefulness of data that contributes to production of information. Transfer of tsunami wave raw and modeled data into information involves several activities such as spectral, Statistical, spatial and temporal analysis [7]. Each of these activities contributes to retrieval of the required information from raw data. Spatial nature, large volume and organization of Tsunami modeled and raw data and information are the most important aspects in the Tsunami data management and visualization that directly support the good decision making for coastal protection against tsunamis. However, through the use of Geographical Information System (GIS) and the associated software; these data can be managed, compiled, and processed. Integration of GIS with environmental phenomenon modeling algorithms accomplishes a number of significant functions such as: planning, calibrating, modifying, data analysis and visualization [5]. GIS improves the ability to incorporate spatial details beyond the existing capability of numerical models [8].

This paper tries to bring forward a methodology for data management of tsunami generation/propagation model using GIS, and to show the importance of data management in tsunami warning systems and decision making for coastal protection. Makran region at the northern part of the Arabian Sea has been selected to carry out these prospective because it has the potential of Tsunami generation and also it is an important region for the Indian Ocean Tsunami Warning System.

2. Data and methods

2.1. Study area

The first Tsunami record in the Makran has been off the Makran Coast at Date 28th November 1945, Epicentre: 87.1 km, SSW of Churi (Baluchistan) Pakistan, Latitude: 24.500° N, Longitude: 63.000°E, Origin Time: 21:56 UTC (03:26 IST), Magnitude: Mw 8.0, Ms 7.8 (Figure 1) [9]. This was the last major tsunami-generating earthquake in the Arabian Sea. More than 4,000 people were killed in the devastation caused by the earthquake and tsunami on the coasts of Makran [10]. After this earthquake a great tsunami was triggered. The wave height of tsunami reached to 40 feet height in some coastal regions of Makran and caused great damage to the entire coastal region. In general, similar damages and mortality were observed along the coasts of Makran in Iran and Oman. The effect of tsunami damages and some mortality were also recorded at Muscat and Gwadar. The 6.5 feet height of tsunami waves were recorded in Karachi. The first wave was recorded at 5:30am, then at 7:00am, 7:15am and finally at 8:15am. The highest wave was observed at 8:15am. The tsunami had a height of 11.0 - 11.5 m in Kutchh, Gujarat. At 8:15am, it was observed on Salsette Island i.e Mumbai. It was recorded in Bombay Harbor, Versova (Andheri), Haji Ali (Mahalaxmi), Juhu (Ville Parle) and Danda [10, 11, 12].

The northward movement of Indian oceanic lithosphere has created the Makran Subduction Zone (MSZ). MSZ is often affected by the Iranian micro-plate at a very shallow angle of about 20 degrees [13]. The length of MSZ is more than 800 km along east-west direction. The MSZ includes very thick sedimentary columns that enter into the subduction zone with thickness of up to 7 km [14, 15]. The deeper structure of the MSZ, the wedge sediments and the subducted oceanic crust has been surveyed recently by wide-angle and seismic reflection [16]. Convergence rate between the Arabian and Eurasian Plates has been estimated to 30-60 mm/y. The thrust faults are oriented nearly perpendicular to the direction of convergence. There is no obvious topographic trench associated with the present accretionary front. The oceanic crust of this area have been formed during the Cretaceous (108-79 Ma), and no significant magnetic anomalies have been observed in relation to ocean floor spreading in the Oman Sea. The subducting plate has a northward dip of >20° till 270N, then bending down to an angle of ~300 (Figure 1) [10, 16, 17, 18].

The east-west oriented complex is one of the largest accretionary wedges on earth. It is more than 800 km long, bounded to the east and west by large transform faults which define the plate boundaries [19]. In Makran Accretionary Complex a fairly high earthquake activity should be expected, as in many of the other major accretionary complexes/subduction zones around the world but the Makran zone is remarkably low in seismicity [20, 21]. The earthquake epicenters during the last century is shown in Figure 2 [10]. Although large earthquakes along MSZ are infrequent, the potential for a devastating tsunamis in the Northern Arabian Sea cannot be ignored.

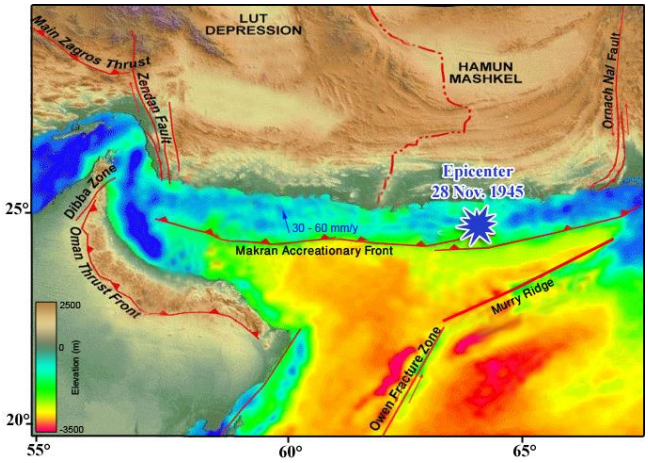

Figure 1. Major faults and the Zone of Tectonic Subduction in the Northern Arabian Sea (from: Fruehn et al, 1997).

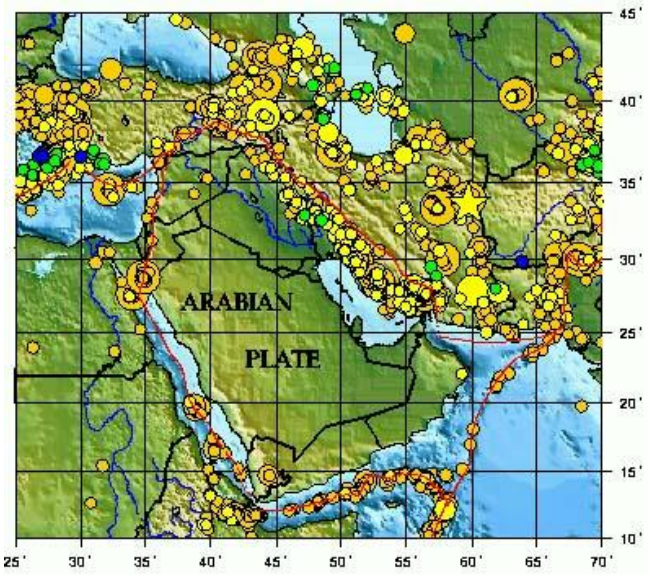

Figure 2. Distribution of earthquake epicenters along the boundaries of the Pakistan, Afghanistan, Iran and Arabian microplates (from: Mokhtari and Farahbod, 2005).

2.2. Tsunami propagation models

The 2004 tsunami tragedy in Indian Ocean highlighted the need to develop technical capabilities on tsunami modeling as a highly-needed capability in the field of tsunami hazard assessment. Very few institutions in Southeast Asia, the Pacific, and the Indian Ocean are presently skilled in conducting their own tsunami modeling. Models by Imamura and Hashi [22], Satake and Tanioka [23], Lynett et al [24], Imamura et al [25] and also European JRC (Joint Research Center) Tsunami Propagation model [26], MOST (Method of Splitting Tsunami) model [27], AVI-NAMI [28], SiTPros (Siam Tsunami Propagation Simulator) model [29] are the most reliable tsunami generation/propagation models for the Indian ocean region. In general, all of these models examine the influence of both initial conditions and analytical approximation on the results of hydrodynamic simulations. They carry out numerical simulations using both the Non-Linear Shallow Water (NSLW) equations, which assumes a less strict condition on the ratio of water depth to wavelength and take into account the frequency dispersion of the wave [30, 31]. These models usually can estimate tsunami height, inundation and arrival time information.

Intergovernmental Oceanographic Commission (IOC) has introduced the AVI-NAMI (http://avi-nami.ce.metu.edu.tr/) and SiTPros (http://www.schuai.net/SiTProS/) tsunami generation/propagation models as a quick and simple operational models for decision makers, who are interest in quick response action against natural hazards [32]. Here, these models were selected for tsunami generation/propagation in the Makran region, and the results are presented.

2.3. Data management methods

AVI-NAMI and SiTPros use the bathymetry of the area as one of the input data. The bathymetry of the area is usually stored as data file that consists of three values: X coordinate, Y coordinate and the depth values. However, data files must be converted into an evenly spaced grid before using as input file of the models. Grid files contain header lines that provide information about the size and limits of the grid, followed by a list of Z values. The Z values are stored in roe-major order stating with the minimum Y coordinate. The value of the lower left corner of map is the first Z value in the grid file. The second Z value is the next adjacent grid node in the same row.

The first output file of the models is the initial wave in the sea which contains the water surface height at each grid point of the bathymetry data. Simulated wave height at each time step for all grid points is saved in a separate grid file. Hence, there will be N grid file for N time steps simulation. The detailed information of processing routines of the models has been shown in the Figure 3.

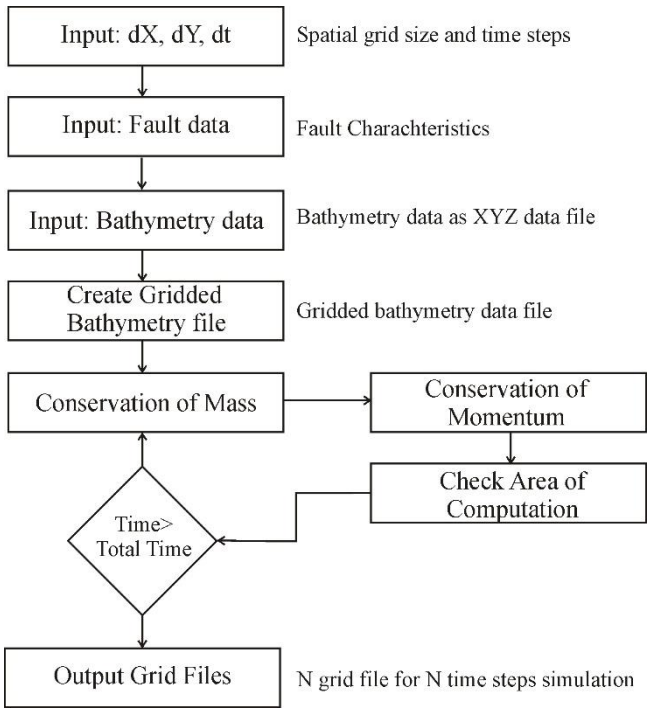

Figure 3. Processing routines of tsunami propagation models used in this paper.

3. Results and discussion

The AVI-NAMI and SiTPros models require the bathymetry of the area as well as the fault characteristics and earthquake parameters as input data. The data concerning the fault consists of the following parameters: The coordinates of the starting point and the end point of the fault, the width of the fault in meters, the dip direction, dip angle, slip angle in degrees, the dislocation and the depth of earthquake

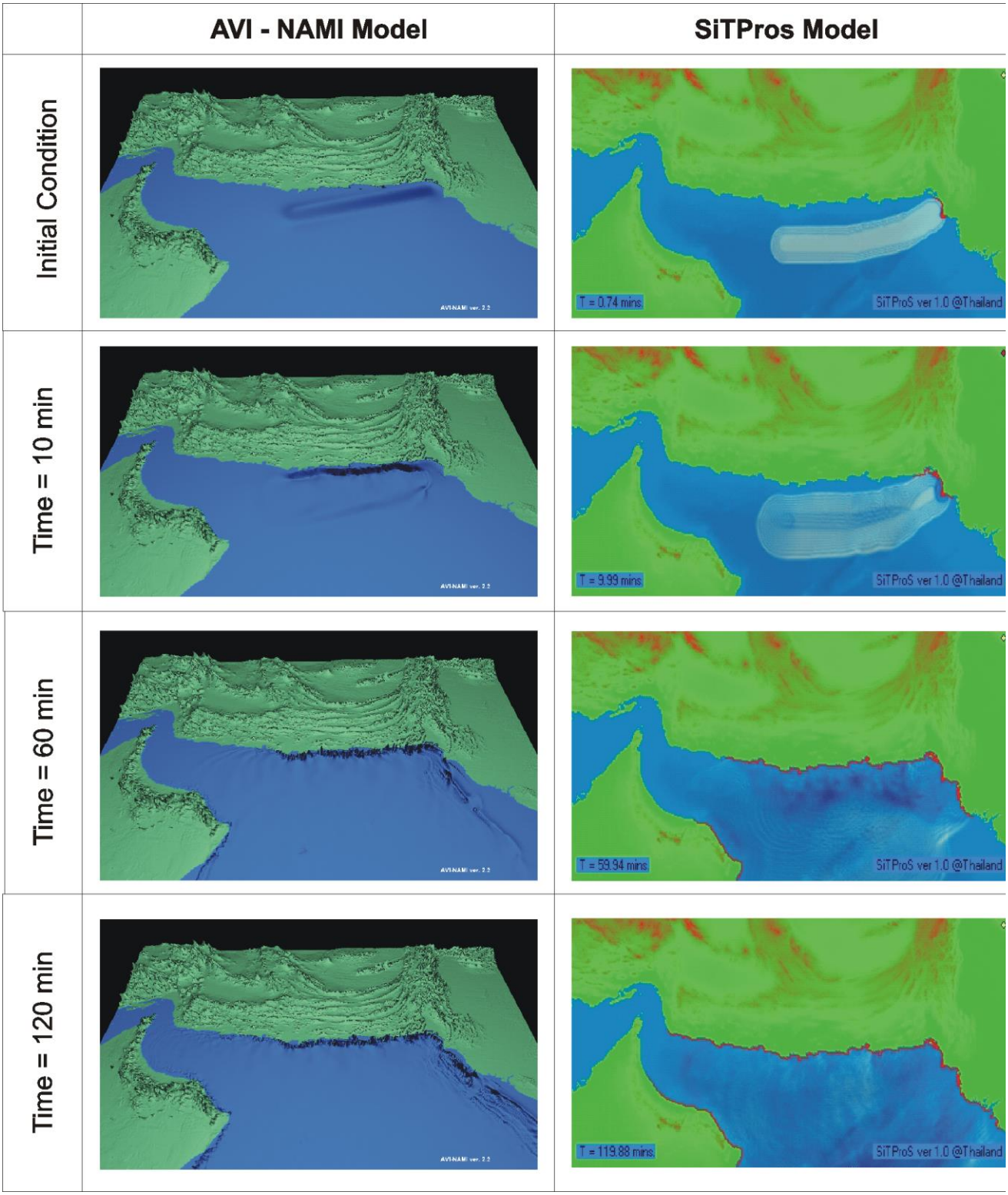

Figure 4. Propagation of a hypothetical tsunami in the Makran region using two numerical models.

epicenter in meters. As noted above, the only earthquake generating tsunami has been occurred along the Makran Accretionary Fault (MAF) on Nov. 28 1945, and hence characteristics of this fault and an earthquake like the last one tsunami generator have been selected for the ocean bottom rupture parameters for tsunami generation/propagation in the Makran region using these two models. The ETOPO2 bathymetry data is available for the whole world with a good resolution (2 minutes) through the NOAA website. The models were run using these data as input parameters for two hours of simulation for the Makran region (Figure 4).

In order to get the best results, the output files are needed to be converted into diagrams or graphs so that

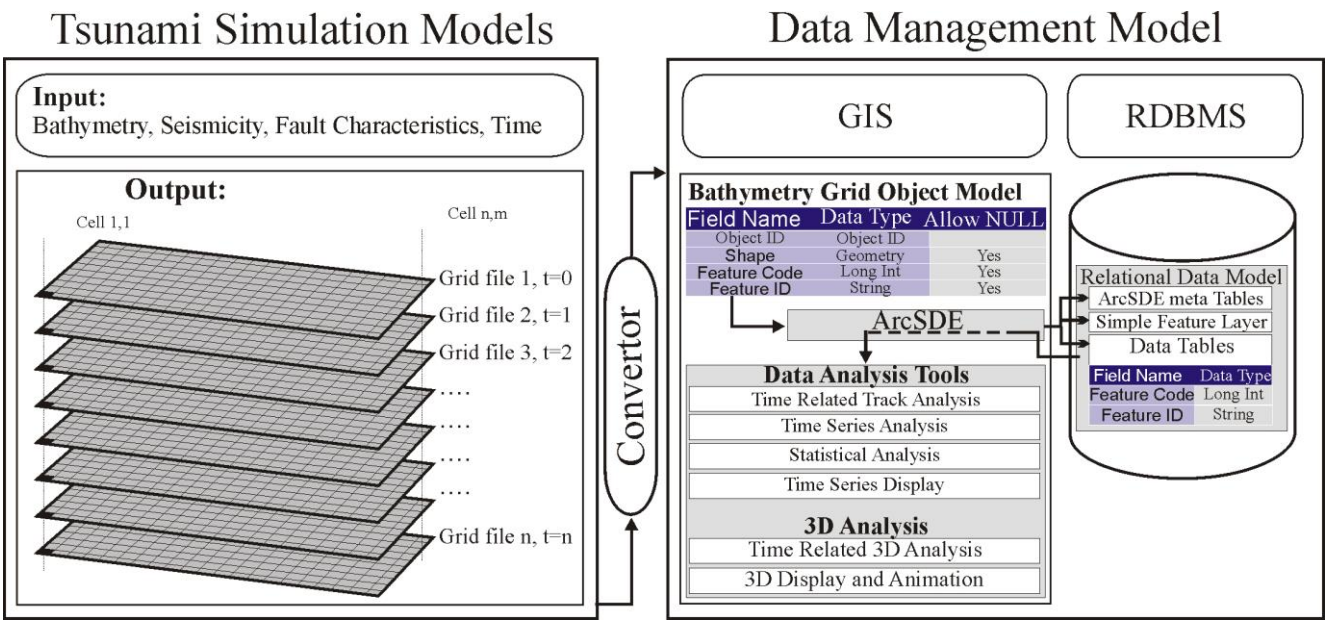

Figure 5. Schematic view of the proposed combined modeling and data management system for tsunami propagation and data analysis.

the interpretation and the comparison of different data can be achieved easily and also comparison of the real time data and the numerical analysis of the tsunami can be done which is a way of checking the accuracy of the simulation. Conversions of numerous output grid data files of the tsunami models to the required information will generate some problems in the warning systems include:

- data could not be searched one by one
- Data are saved in too many files which confused the users
- Users have to work with too many files to get the required informations
- Data visualization must be done for separate files one by one, and comparisons of all time steps simulation results need the processing of all output grid files
- Time series data analysis for a grid point must be run for that point in all output grid files which requires the programming and advanced training
- GIS application for these grid files is a time wasting procedure and it should be done for each simulation run
- We have to use few softwares for output grid file processing and this method will confuse the warning system operators
- Archiving, updating and maintenance of the output files is very troublesome and the warning system operators must be take care about the simulation outputs missing.

Relational Database Management Systems (RDBMS) are the best solution for time series and girded data [33]. RDBMS can joint with GIS softwares for data management and analysis. In this software system, data are saved in different tables which have logical and mathematical relations that provide the data accessibility based on different query algorithms [34]. A grid map just like the bathymetry grid is created that contains a unique code for each grid cell. This grid map will be used for spatial data management and visualization. All cell characteristics data are stored in an internal database of the GIS and tabular data, which are the results of the simulation, are stored in a RDBMS. Data structures in these data tables provide a one to many relations between each map grid cell and tabular data, and hence each grid cell contains the related time series data resulted from simulation. In this tabular relation, the ID field of grid cells and tabular data in RDBMS is a unique key and used for data query by SQL.

The warning system operators can extract data for each grid map cells easily when the GIS-RDBMS systems were established. The GIS component of the system gets the ID and other characteristics data of the selected grid cell, and sends it to the RDBMS using SQL and finally tabular data will be queried from database. SQL provides an interface to relational tables that allows user to select rows based on the values contained in the fields. A SQL statement can range from simple to complex, allowing user to compose virtually any type of query from basic column types. The result of a query is a set of rows meeting the criteria established by the SQL statement. In this study, SQL Server and ArcGIS have been selected for RDBMS and GIS softwares respectively, and ArcSDE has been selected for these two software bridge. The overall schema of the proposed system has been shown in Figure 5. In this system, a software

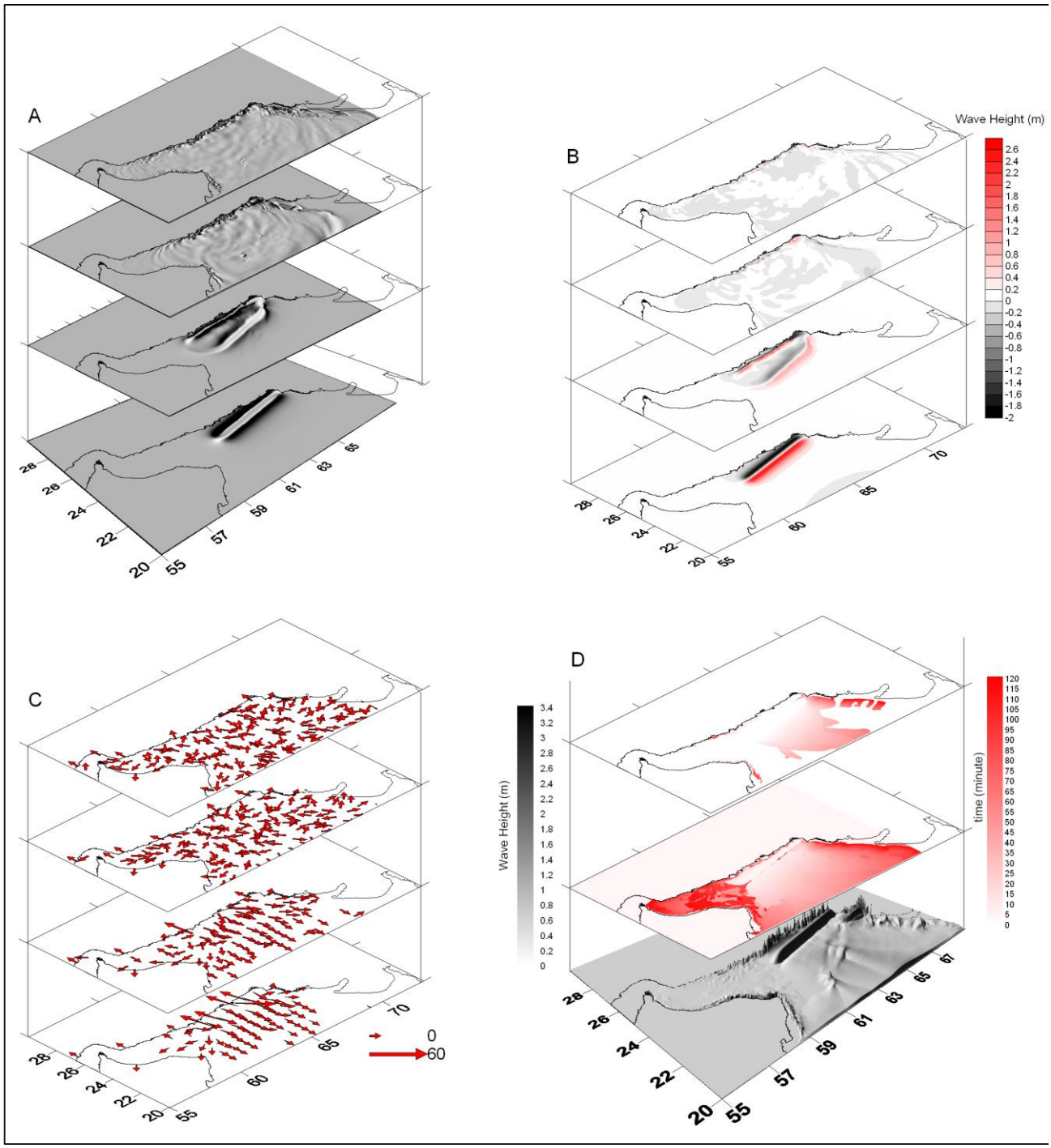

Figure 6. 3D analysis of tsunami propagation model in the Makran region. (a) 3D view of wave propagation at different times. (b) Maximum wave height at different times. (c)- Wave vector of tsunami propagation at different times. Layers in figures A to C from bottom to top show the tsunami wave characteristics at 0 (initial condition), 10, 60 and 120 minutes following tsunami generation. (d) Miscellaneous plots of propagation characteristics: from bottom to top, maximum wave height of tsunami after 120 minutes of modeling; arrival time of maximum wave height; and arrival time of the first 2.5 meter and more wave tsunami.

convertor processes all the simulation output grid files and convert them to time series tabular data with a unique ID for each grid cell data and then insert TS data to the SQL server.

The output grid files of these models were converted to a proposed data management system (Figure 5). Furthermore, some statistical analyses include time series plots and 3D views of the hypothetical tsunami were done using GIS capabilities (Figure 6 and 7). 3D model of tsunami propagation shows that the Strait of Hormuz and Persian Gulf are not in tsunami domain (Figure 6a). The maximum wave height will affect the east and north-east of the Makran region coasts. In these regions propagation and rollback of sea water at coastal areas is extremely high during this hypothetical tsunami (Figure 6b, c). However, 3D data analysis shows that the maximum wave height will be

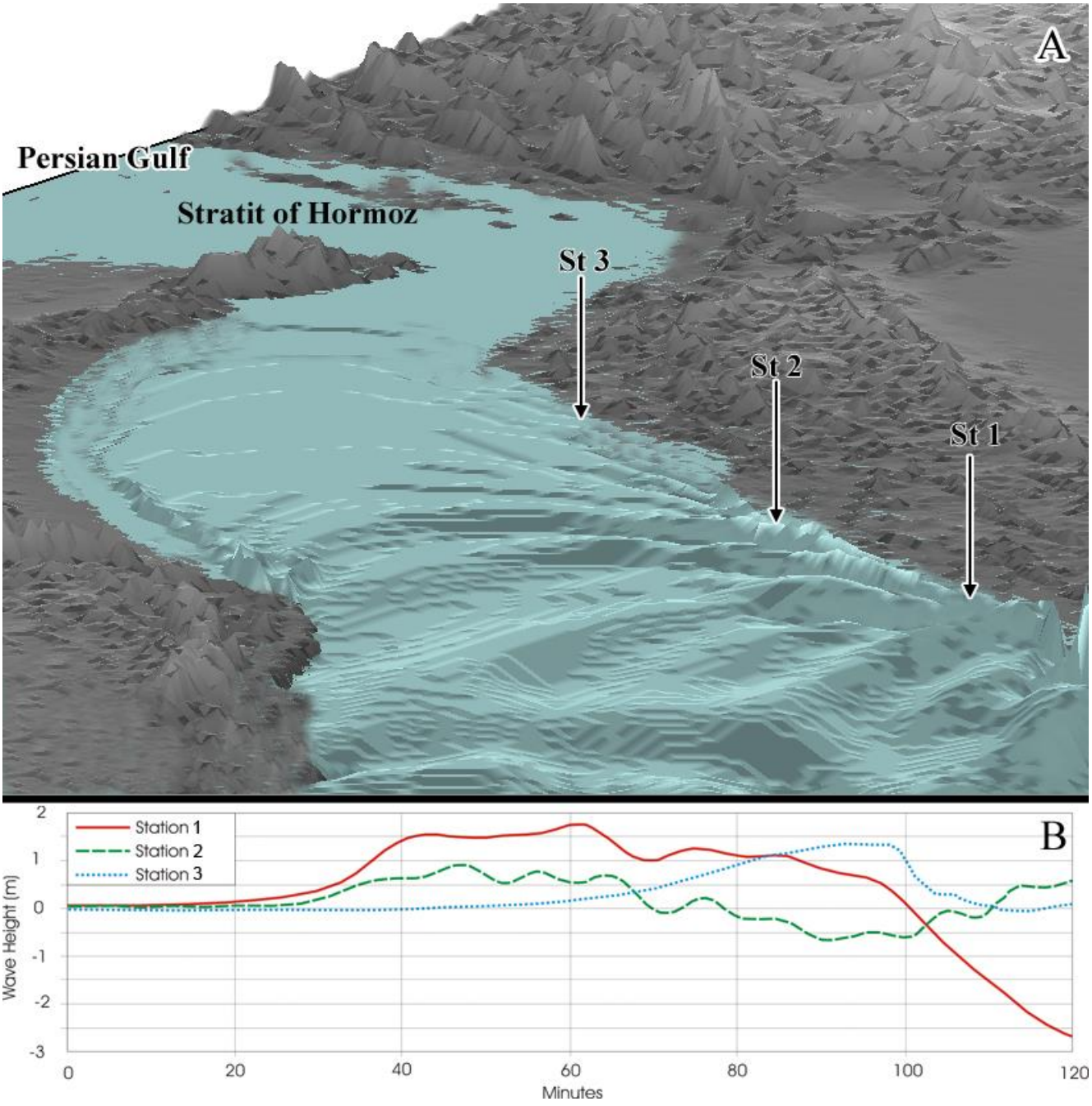

Figure 7. (a)- 3D close up of hypothetical tsunami propagation in the Oman Sea and Strait of Hormuz. (b)- Time series plot of tsunami wave height for three stations at the Iranian coastal areas.

at the central part of Arabian Sea and at the India and Pakistan coastal regions. Also, high waves will reach to these areas in less than 10 minutes (Fig 6D). A close up view of Strait of Hormuz for the tsunami propagation after 60 minutes is presented in Fig 7. This is an example of time series data extraction from the proposed data model for three points at the Iranian coasts of the Oman Sea. This shows that the first tsunami waves will reach to the Iranian coasts after 20 minutes following tsunami generation, and wave height will not be more than 2 meters during this hypothetical tsunami propagation. However, it is clear from the Figure 7A that the gentle slope at the neck of Strait of Hormuz acts as a barrier against tsunami propagation.

4. Conclusion

The process of computing the three stages of tsunami modeling, wave generation and propagation-inundation has been accelerated by generating a database of pre-computed scenarios. The pre-computed database represents the tsunami propagation information in the open ocean. An initial source is selected from the pre-computed database, while a tsunami event occurs. The appropriate scenario is selected from available propagation information to

compute the wave inundation. In order to get a reliable, strong and easy to use tsunami database for warning systems, it is accepted that the outputs of tsunami models must be converted to information. To do this, data management systems must be considered as one of the essential parts of the tsunami warning systems. Available tsunami models have an irregular data formats which are not in an international standard formats in operational data management systems. In addition, GIS is a powerful tool for data management and analysis that should be used in data management systems. The proposed data management system for the tsunami warning systems have at least three essential parts include: software convertor, GIS and relational database. The results of a database management system in the tsunami generation, propagation and inundation study should include information about the maximum wave height and maximum current speed as a function of location, maximum propagation/inundation line, time series of wave height indicating wave arrival time, and too many other analyses in upon the users' request. This information can be used by emergency managers and urban planners primarily to establish evacuation routes and location of vital infrastructure.

5. References

1- Bernard, E.N., F.I. González, and Titov V.V., (2005). The tsunameter and real-time tsunami forecasting. Chikyu Monthly, 27, 210–215

2- Titov, V.V., and Gonzalez F.I., (1997). Implementation and testing of the Method of Splitting Tsunami (MOST) model, NOAA Technical Memorandum ERL PMEL-112, 1-11.

3- Bernard, E.N., (2005). The U.S. National Tsunami Hazard Mitigation Program: A successful state–federal partnership. Nat. Hazards, Special Issue, U.S. National Tsunami Hazard Mitigation Program, 35, 5–24.

4- Harmancioglu, N.B., Alpaslan, M.N. and Ozkul, S.D., (1997). Conclusions and recommendations, Integrated approach to environmental data management systems, proceedings of the NATO advanced research workshop on integrated approach to environmental data management systems, Sept. 16-20, Izmir, Turkey, Kluwer academic publishers, NATO ASI Series, 2. Environment, 31, 35-48.

5- Harmancioglu, N.B., Alpaslan, M.N., Ozkul, S.D. and Singh, V.P., (1997). Integrated approach to environmental data management systems, proceedings of the NATO advanced research workshop on integrated approach to environmental data management systems, Sept. 16-20, Izmir, Turkey, Kluwer academic publishers, NATO ASI Series, 2. Environment, 31, 5-46.

6- Santos,M., (1997). Data management and the European Union information policy, Integrated approach to environmental data management systems, proceedings of the NATO advanced research workshop on integrated approach to environmental data management systems, Sept. 16-20, Izmir, Turkey, Kluwer academic publishers, NATO ASI Series, 2. Environment, vol. 31, pp., 35-48.

7- Young, I.R., (1999). Wind generated ocean waves. (Elsevier), 288 pp.

8- Singh, V.P., (1995). Computer models of watershed hydrology, water resources publications, (Littleton), 230 pp.

9- Berninghausen, (1996). W.H., Tsunamis and Seismic Seiches reported from regions adjacent to the Indian Ocean, BSSA, 56, 19-66.

10- Mokhtari, M. and Farahbod, A.M., (2005). Tsunami Occurrence in the Makran Region. Tsunami Seminar, Tehran, 26 February.

11- Qureshi R. M., (2006). Vulnerability of Pakistan Coast to Tsunami. Possible Applications/Role of Nuclear Techniques RCARO Workshop, 20 - 24 February, Daejon, Korea.

12- Pararas-Carayannis, G., (2006). The Earthquake and Tsunami of 28 November 1945 in Southern Pakistan, http://drgeorgepc.com/Tsunami1945Pakistan.html.

13- Quittmeyer, R.C., and Jacob, K.H., (1997). Historical and Modern Seismicity of Pakistan, Afghanistan, N.W. India and S.E. Iran, Bulletin of the Seismological Society of America, 69/3, 773-823.

14- Closs, H., Bungenstock, H., Hinz, K., (1969). Ergebnisse seismischer Untersuchungen im nrdlichen Arabischen Meer: ein Beitrag zur internationalen Indischen Ozean Expedition, GEOMAR Rep., 62, 292 pp.

15- White, R. S., Louden, K. E., (1983). The Makran Continental Margin: Structure of a Thickly Sedimented Convergent Plate Boundary, Am. Ass. Petrol. Geol., 34, 499-518.

16- Kopp C., Fruehn J., Flueh,E. R., Reichert, C., Kukowski N., Bialas J. and Klaeschen. D., (2000). Structure of the Makran subduction zone from wide-angle and reflection seismic data. Proceedings, 8th International Symposium on Deep Seismic Profiling of the Continents and Their Margins, 171-191.

17- Fruehn, J., White, R. S. and Minshull, T. A., (1997). Internal deformation and compaction of the Makran accretionary wedge, Terra Nova, 9, 101-104.

18- Platt, J. P., Leggett, J. K., Young, J., Raza, H. and Alam, S., (1985). Large-scale sediment underplating in the Makran accretionary prism, Southwest Pakistan, Geology, 13, 507-511.

19- Regard V. Bellier O., Thomas J.-C., Abbassi M.R., Mercier J. L., Shabanian E., Feghhi Kh., Soleymani Sh., Bonnet S., Bourlès D. L., Braucher R., and J. Martinod, (2003). Tectonics of a Lateral Transition Between Subduction and Collision:The Zagros-Makran Transfer Deformation Zone (SE IRAN), Geophysical Research Abstracts, 5, 200-210.

20- GEOMAR, (2000). Germany, the University of Cambridge and the National Institute of Oceanography, Pakistan, - Cruise (SONNE-123), 1997- 2000.

21- Hutchinson, I., Louden, K. E., White, R. S., (1981). Heat flow and age of the Gulf of Oman, Earth Planet. Sci. Lett., 56, 252-262.

22- Imamura, F. and Hashi, k., (2003). Re-examination of the Tsunami Source of the 1998 Papua New Guinea Earthquake Tsunami, Pure Appl. Geophys, 160, 2071-2086.

23- Satake, K. and Tanioka, Y., (2003). The July 1998 New Guinea Earthquake: Mechanism and Quantification of Unusual Tsunami Generation, Pure Appl. Geophys., 160, 1087-2118.

24- Lynett, P.J., Borrero, J.C., Liu, P.L.-F., and Synolakis, C.E., (2003). Field Survey and Numerical Simulations: A review of the 1998 Papua New Guinea Tsunami, Pure Appl. Geophys., 160, 2119-2146.

25- Imamura, F., Yalciner, A. and Ozyurt, G., (2006). TSUNAMI MODELLING MANUAL. The JCOMM/IODE Combined Modeling and Data Management Training Workshop Jamboree – II, Oostende, Belgium, 9 – 14 October.

26- Annunziato, A., Best, C., (2005). THE TSUNAMI EVENT ANALYSES AND MODELS. Institute for the Protection and Security of the Citizen Joint Research Centre, European Commission, Inter. Report.

27- Titov, V.V., González F.I., Bernard E.N., Eble M.C., Mofjeld, H.O., Newman J.C., and Venturato A.J., (2005). U.S. National Tsunami Hazard Mitigation Program, Nat. Hazards, , 35, 41–58.

28- Yalciner, A.C., Pelinovsky E., Zaytsev, A., Ozer C., Ozyurt G., Kurkin A., (2006). USER MANUAL OF TSUNAMI SIMULATION–VISUALIZATION SOFTWARE AVI-NAMI (version 2.0) for BEGINNERS. The JCOMM/IODE Combined Modeling and Data Management Training Workshop Jamboree – II, Oostende, Belgium, 9 – 14 October.

29- Kanbua, W., (2006). Siam Tsunami Propagation Simulator (SiTPros) model. The JCOMM/IODE Combined Modeling and Data Management Training Workshop Jamboree – II, Oostende, Belgium, 9 – 14 October.

30- Shuto, N., Goto, C., Imamura, F., (1990). Numerical simulation as a means of warning for near field tsunamis, Coastal. Engineering in Japan, 33, 173-193.

31- Goto, C. and Ogawa, Y., (1991). Numerical Method of Tsunami Simulation with the Leap-Frog Scheme, TIME Project Report, 220 pp.

32- Yalciner, A.C., Kanbua, W., Moradi, M., Sojisuporn, P. and Kirugara, D., (2006). SUMMARY REPORT FOR JAMBOREE-II ON NUMERICAL MODELING TSUNAMI GENERATION AND PROPAGATION. The JCOMM/IODE Combined Modeling and Data Management Training Workshop Jamboree – II, Oostende, Belgium, 9 – 14 October.

33- Carr, J., (2002) Data visualization in the geoscinces, Prentice Hall Inc., New Jersey, 266 pp.

34- Jeffy, A.H., Mary, B., Prescot, F.R. and McFadden, R. (2002). Modern database management. (Prentice Hall, New York, Sixth edition), 638 pp.

INTERNATIONAL JOURNAL OF
COASTAL & OFFSHORE ENGINEERING IJCOE Vol.6/No. 3/Summer 2021 (49-53)

Available online at: www. Ijcoe.org

Simulation of Tide in Khowr-e Musa by Using the TELEMAC Numerical Model

Nadia Talebpour[1], Mohammad Akbarinasab[2*], Masoomeh Rasoolian[3], Abolfazl Delbari[4]

[1] *MSc., Faculty of Marine and Oceanic Sciences, University of Mazandaran, Iran; n.talebpur@stu.umz.ac.ir*
[2*] *Associate Professor, Faculty of Marine and Oceanic Sciences, University of Mazandaran, Iran; m.akbarinasab@umz.ac.ir*
[3] *MSc., Faculty of Marine and Oceanic Sciences, University of Mazandaran, Iran; m.rasoolian@stu.umz.ac.ir*
[4] *Assistant Professor, Department of Physical Oceanography, Faculty of Marine Science, Khorramshahr University of Marine Science and Technology, Khorramshahr, Iran; abolfazl_delbari@yahoo.com*

ARTICLE INFO

Article History:
Received: 16 Nov. 2020
Accepted: 19 July. 2021

Keywords:
Khowr-e Musa
Tide
Water Level
TELEMAC Model

ABSTRACT

Khowr-e Musa at the northwestern terminus of the Persian Gulf sedimentary basin is the widest and longest inshore marine outcrop in the entire coast of the iran at present. In this research, the tidal Current velocity and tidal water level in the Khowr-e Musa estuary was modeled in a 15-day period from 18th of November 2006 by using the Telemac two-dimensional hydrodynamic software. For this purpose, the irregular mesh in two dimensions was selected from the smallest mesh of 70 meters to the largest mesh of 210 meters. The topography of the area was added to the grid of mesh by using an interpolation method. Then TPXO database tidal data applied along the boundary of model. The friction coefficient was calculated using the Stickler theory with the value of 40 m1/2s-1 and the model was executed with a time step of 10 seconds. After Sensitivity analysis and calibration, the model was validated by using measurement data that's provided by the ports and maritime organization. The results showed a good correlation of 94% between the results of the water surface level of modeling the tidal and measurement data and correlation of 73% between the results of the current velocity of modeling the tidal and measurement data, so the TELEMAC two-dimensional hydrodynamic model is suitable for studying the tidal current.

1. Introduction

In order to perform any engineering project or marine environment study, the prediction of currents is an essential task. Water currents in the Khowr-e Musa estuary are formed due to tidal fluctuations in Persian Gulf as well as the complicated geometric features of this multi branch estuary. Therefore, there are no regular streams in this multi branch estuary and the interaction between periodical behavior of tides of the Persian Gulf and the geometrical complexities of this estuary provides difficulties for prediction of the time dependent streams in the branches of the Khowr-e Musa [1].

Today Pacific basin scale and global scale tidal models are available on tidal inversion software or online sites (OTIS & FES) [2, 3, 4]. The global scale tides are suitable for describing the tides in large scale systems such as the Indian Ocean. However, in local or regional sites, the observation or ocean modeling of tides are still needed [5, 6, 7, 8, 9, 10, 11, 12].

Several researchers have used numerical modeling to assess tidal stream energy resources. Carballo et al. applied a two-dimensional horizontal finite element model to evaluate the tidal stream energy resources in the Ria de Muros, which is in the northwestern coast of Spain [13]. Sadrinasab and Shoaib employed a three-dimensional hydrodynamic model (COHERENS) to assess the tidal power of the Doragh estuary. Their simulation indicated that using one basin project at the estuary, where the average tidal range is 5 meters, can obtain about 30 MW of electrical power [14]. Blunden and Bahaj applied a two-dimensional tidally driven hydrodynamic numerical model (TELEMAC-2D) to estimate the available tidal stream energy resources at Portland Bill, UK [15]. Hashemi et al. investigated the influence of waves on tidal resource at Anglesey, showing that extreme wave-current interactions can reduce the tidal resource by 20% [16]. Wang et al. studied the seasonal variations of four principal tidal constituents [17]. Also, some studies have been conducted assessing locations for the available tidal

energy resource and the suitability for tidal stream extraction such as Robins et al., 2015 [18], Lewis et al., 2015 [19] and Neill et al., 2014 [20].

2. Objective

In this study, hydrodynamics tide of the Khowr-e Musa estuary modeled by TELEMAC-2D. Telemac-2D is an open-source computer numerical model that solves the shallow water equations using a finite element method [21] and also it has been carried out with Blue-Kenue (BK). BK is a pre and post-processor visualization program developed by the Canadian Hydraulics Centre of the National Research Council Canada [22].

The process of resource assessment involves the following stages:

1. Geometric layout and computational mesh preparation
2. Boundary condition definitions
3. Parameterisation of model
4. Model execution
5. Post-processing and analysis of output (Calibrate and validate by comparison with measurement data)

Figure 1 shows the process to undertake a resource assessment.

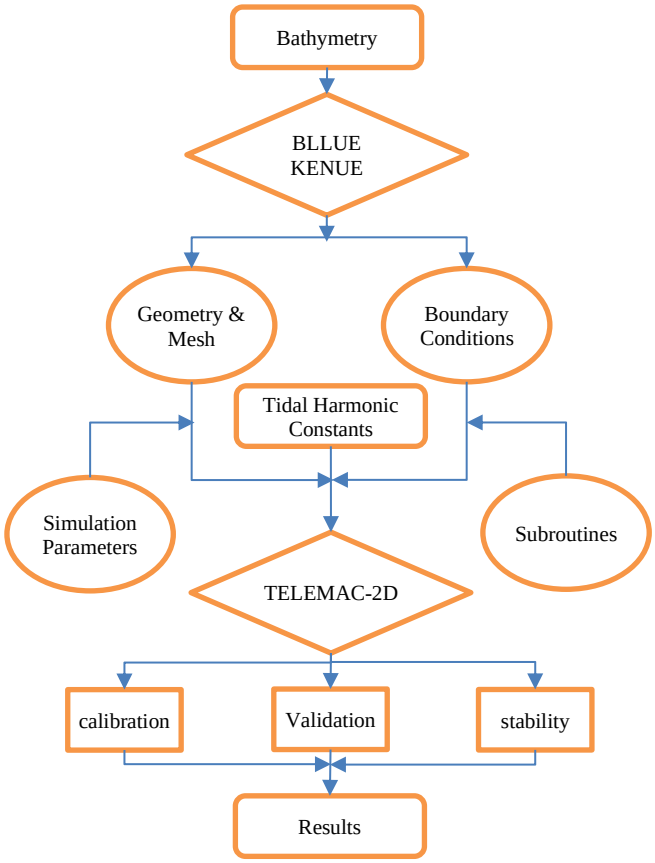

Figure 1: Model process with BK and Telemac-2D [23]

3. Site Description

Khowr-e-Musa estuary is located in the south-west of Iran and in the north-west of the Persian Gulf, at the approximate coordinates 30°28′ N 49°11′ E (Figure 2). The approximate area of Khowr-e Musa is 1350 km^2 [24]. The port of Imam Khomeini, the port city of Mahshahr and several important industrial enterprises are located in the vicinity of this estuary.

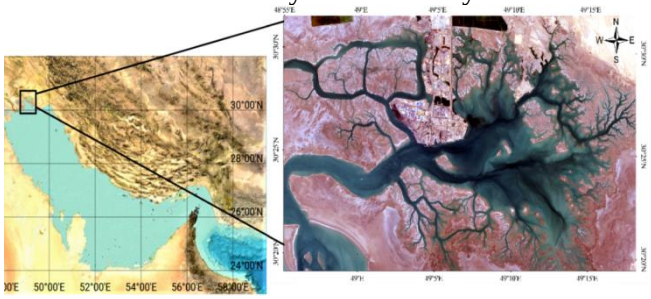

Figure 2: The position of the Khowr-e Musa estuary

4. data Description

Tidal data was received from the OSU[1] TPXO Tide Models [25]. The tidal level from the TPXO can be collected as predicted values, in which the tidal level is deduced from the harmonic constants, or observational values.

The bathymetry used to produce the mesh was provided by International Hydrographic Organization of Iran. Data resolution varies between 60 and 400 meters for Khowr-e Musa estuary with UTM coordinates system. The datasets used for the water level and flow velocity analysis are acquired from Iran Ports and Maritime Organization (PMO) at longitude 49.1° and latitude 30.42° for 15 days from 18-Nov-2006. Table 1 shows a summary of the input data.

Table 1. Input data

Initial data	Type of Data	Database	Time/ Duration	Resolution
Bed Bathymetry	Longitude Latitude Depth	IHO	-	varies between 60-400 m
Tidal data	Velocity components in the x and y directions Water height (h) Harmonic constants	TPXO database	2006/11/18 15 days	178 km
Measurement data	Flow velocity Water level	PMO	2006/11/18 15 days	-

4. Methods

Numerical model

The TELEMAC-2D code solves the second-order partial differential equations for depth-averaged fluid flow derived from the full three-dimensional Navier–Stokes equations. They are also called the Barre de Saint-Venant Equations. This gives a system consisting of an equation for mass continuity and two force-momentum equations. The equations at constant density are averaged over the vertical by integrating

[1] Organ State University

from the bottom to the surface. The averaged form of the continuity equation is:

$$\frac{\partial h}{\partial t}+\frac{\partial (hu)}{\partial x}+\frac{\partial (hv)}{\partial y}=0 \quad (1)$$

The average forms of the momentum equations are:

$$\frac{\partial (hu)}{\partial t}+\frac{\partial (hUU)}{\partial x}+\frac{\partial (hUV)}{\partial y} = -gh\frac{\partial z}{\partial x}+\frac{\partial}{\partial x}\left[hv_e\frac{\partial U}{\partial x}\right] + \frac{\partial}{\partial y}\left[hv_e\frac{\partial U}{\partial y}\right]+hF_x \quad (2)$$

$$\frac{\partial (hv)}{\partial t}+\frac{\partial (hVV)}{\partial y}+\frac{\partial (hUV)}{\partial x} = -gh\frac{\partial z}{\partial y}+\frac{\partial}{\partial x}\left[hv_e\frac{\partial V}{\partial x}\right] + \frac{\partial}{\partial y}\left[hv_e\frac{\partial V}{\partial y}\right]+hF_y \quad (3)$$

where U and V are depth average velocity components in x and y Cartesian directions, h is the depth, v_e is the coefficient of momentum diffusion (m^2s^{-1}), g is the gravitational acceleration, t is the time, Z is the elevation of free surface (m), Fx and Fy are some source terms of the momentum equation in U and V, respectively, which include friction, coriolis, and wind force.

The bed friction is represented as quadratic function of velocity, $\vec{\tau}=\rho C_f|U|\vec{U}$; where $\vec{U}=(U\cdot V)$. The friction coefficient (C_f) can be parameterised in terms of Strickler friction coefficients applying the respective equations (S is the Strickler coefficient) [26].

$$C_f=\frac{2g}{S^2h^{\frac{1}{3}}} \quad (4)$$

5. Results and Discussion

In the simulation, a mesh should be used that is able to properly simulate the geometric complexities of the bed and the environment. For this purpose, the mesh and the open boundary were made using the Blue-Kenue and are shown in Figure 3. At the mesh generation process, the optimal scale of the mesh was determined using the sensitivity of the network density by performing the model for different mesh scales for the whole area with a ratio of 1 to 3 and a minimum inter-node distance of 70m has been defined at the entrance of Khowr-e Musa to have a higher resolution for more accuracy and computation nodes near the open boundary. In areas farther from the open boundary and at the end of the estuary the grid size has been set up to 210 m to reduce the computation time. The final network used in the form of triangular irregular mesh consists of 75479 elements and 39745 nodes, which the depth is loaded in the mesh using linear interpolation. The model was run in a 15-day period from 18th of November 2006 with a time step of 10 s. The friction coefficient was calculated using the Stickler theory with the value of 40 m1/2s-1.

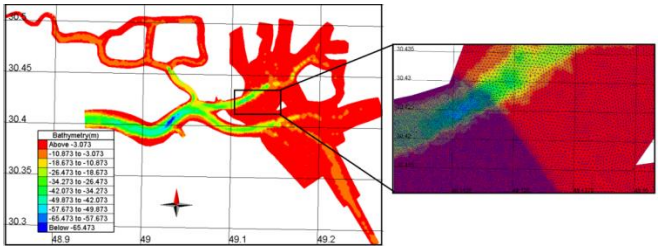

Figure 3: Bathymetry, open boundary and mesh of the study area

In order to achieve the desired accuracy and computational time, it is necessary to sensitize the model to the dimensions of the mesh and thus determine the optimal mesh. Table 2 shows the sensitivity of the model to the mesh and its execution time.

Table 2: sensitivity of the mesh

Mesh dimensions	20-60	40-120	60-180	70-210	80-240
Number of nodes	463214	117950	53142	39745	30693
Number of elements	912425	229017	101812	75479	57964
Running time	6 d	3 d	6 h	3 h	2 h
water level correlation	0.91	0.92	0.93	0.94	0.93
RMSE error of water level	0.3	0.28	0.26	0.25	0.26
current speed correlation	0.57	0.93	0.69	0.71	0.47
RMSE error of current speed	0.106	0.077	0.069	0.065	0.069

The tasks of both model calibration and validation require actual field (observed) data to complete. For calibration and validation of the model, one-hour time series data for water level and flow velocity were received from Iran Ports and Maritime Organization (PMO) at longitude 49.1° and latitude 30.42°, near the port of Imam Khomeini, for 15 days from 18-Nov-2006. Calibration is accomplished by changing the input parameters of the model for the purpose of having a simulation output similar to the observed values. For calibration, four coefficients including velocity range, tidal range, sea level and friction were investigated. Table 3 shows the selected coefficients for calibration.

Table 3: Selected calibration coefficients

Calibration coefficients	Value
velocity range	1.1
tidal range	2.7
sea level	3.26
friction	40

In order to evaluate the accuracy of the results of the numerical model, water surface levels and velocity values at a point in the middle of the estuary near the port of Imam Khomeini were compared with the field measurement data (Figures 4 and 5).

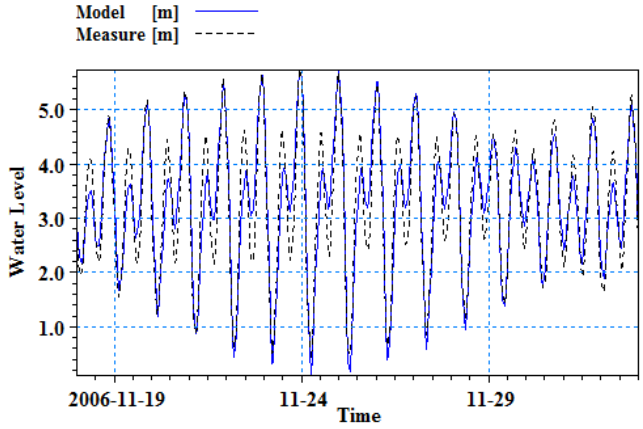

Figure 4: The result of the water surface level of the model compared with the measurement

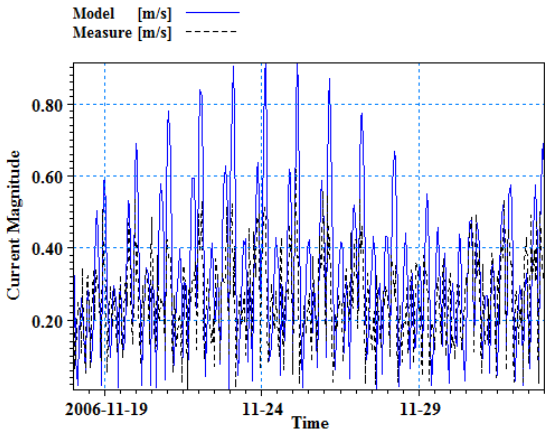

Figure 5: The result of the current velocity of the model compared to the measurement

Figures 6 and 7 show the correlation between measurement and results of the numerical model, water surface levels and current velocity values.

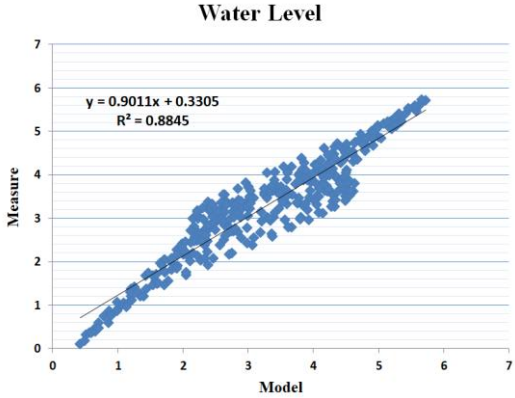

Figure 6: The correlation between measurement and the result of water surface level of model

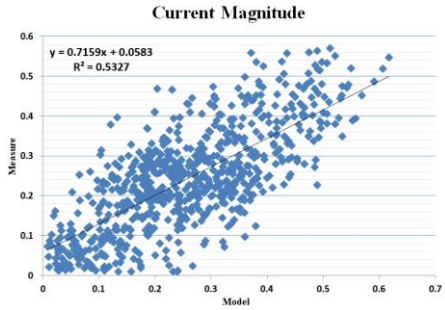

Figure 7: The correlation between measurement and the result of current velocity of model

6. Conclusions

In this study, the water surface levels and current velocity of the tidal currents was modeled by the two-dimensional hydrodynamic model TELEMAC in the Khowr-e Musa estuary region and the sensitivity and calibration of the model were investigated, then the model results were compared with the observed measurement data. The results showed that:

-The model is sensitive to the dimensions of the mesh, so mesh sensitivity is important in modeling and should be analyzed in the modeling process.

- The results of the numerical model presented in this study show a good correlation of 94% between the results of the water surface level of modeling the tidal and measurement data and correlation of 73% between the results of the current velocity of modeling the tidal and measurement data, so the TELEMAC two-dimensional hydrodynamic model is suitable for studying the tidal current.

8. References

1- Hashemi Aslani, Z., Niksokhan, M. H., and Montazeri Namin, M., (2017), *Assessment of the potential of harnessing tidal energy in the Khowr-e Musa estuary in the Persian Gulf*, Environmental Energy and Economic Research, 1(1), p.15-22.

2- Egbert, G. D., Bennett, A. F and Foreman, M.G.G., (1994), *TOPEX/POSEIDON tides estimated using a global inverse model*, J. Geophys. Res. 99, p.24821-24852.

3- Egbert, G. D., and Erofeeva, S. Y., (2002), *Efficient inverse modeling of barotropic ocean tides*. Journal of Atmospheric and Oceanic technology, 19(2), p.183-204.

4- Carrère, L., Lyard, F., Cancet, M., Guillot, A., Roblou, L., (2012), *A New Global Tidal Model Taking Advantage of Nearly 20 Years of Altimetry*, In Proceedings of the Meeting 20 Years of Altimetry, Venice, Italy, p.24–29.

5- Mayer-Gürr, T., Savcenko, R., Bosch, W., Daras, I., Flechtner, F., and Dahle, C., (2012), *Ocean tides from satellite altimetry and GRACE*, Journal of geodynamics, 59, p.28-38.

6- Pelling, H. E., Green, J. M., and Ward, S. L., (2013), *Modelling tides and sea-level rise: To flood or not to flood*, Ocean Modelling, 63, p.21-29.

7- Kumar, S. S., and Balaji, R., (2015), *Tidal Hydrodynamics along Gulf of Khambhat*, West Coast of India. Aquatic Procedia, 4, p.41-48.
8- Othmani, A., Béjaoui, B., Chevalier, C., Elhmaidi, D., Devenon, J. L., and Aleya, L., (2017), *High resolution numerical modelling of the barotropic tides in the Gulf of Gabes, eastern Mediterranean Sea (Tunisia)*, Journal of African Earth Sciences, 129, p.224-232.
9- Tazkia, A. R., Krien, Y., Durand, F., Testut, L., Islam, A. S., Papa, F., and Bertin, X., (2017), *Seasonal modulation of M2 tide in the Northern Bay of Bengal*, Continental Shelf Research, 137, p.154-162.
10- Pringle, W. J., Wirasaet, D., Suhardjo, A., Meixner, J., Westerink, J. J., Kennedy, A. B., and Nong, S., (2018), *Finite-element barotropic model for the Indian and Western Pacific Oceans: Tidal model-data comparisons and sensitivities*, Ocean Modelling, 129, p.13-38.
11- Deng, F., Jiang, W., Valle-Levinson, A., and Feng, S., (2019), *3D modal solution for tidally induced Lagrangian residual velocity with variations in eddy viscosity and bathymetry in a narrow model bay*, Journal of Ocean University of China, 18(1), p.69-79.
12- Setiawan, I., HaditiarA, Y., Ikhwan, M., Nufus, Z., Syukri, M., Ismail, N., and Rizal, S., (2020), *Modeling of M2-TIDE in the western waters of Aceh, Indonesia*, Journal of Sustainability Science and Management, 15(8), p.122-135.
13- Carballo, R., Iglesias, G., and Castro, A., (2009), *Numerical model evaluation of tidal stream energy resources in the Ría de Muros (NW Spain)*, Renewable Energy, 34(6), p.1517-1524.
14- Sadrinasab, M., and Shoaib, N., (2011), *The Potential of Tidal Power from the Doragh Estuary*, in 9 th Europaen wave and tidal energy conference.
15- Blunden, L. S., and Bahaj, A. S., (2006), *Initial evaluation of tidal stream energy resources at Portland Bill*, UK, Renewable Energy, 31(2), p.121-132.
16- Hashemi, M. R., Neill, S. P., Robins, P. E., Davies, A. G., and Lewis, M. J., (2015), *Effect of waves on the tidal energy resource at a planned tidal stream array*, Renewable Energy, 75, p.626-639.
17- Wang, D., Pan, H., Jin, G., and Lv, X., (2020), *Seasonal variation of the principal tidal constituents in the Bohai Sea*, Ocean Science, 16(1), p.1-14.
18- Robins, P. E., Neill, S. P., Lewis, M. J., and Ward, S. L., (2015), *Characterising the spatial and temporal variability of the tidal-stream energy resource over the northwest European shelf seas*, Applied Energy, 147, p.510-522.
19- Lewis, M., Neill, S. P., Robins, P. E., and Hashemi, M. R., (2015), *Resource assessment for future generations of tidal-stream energy arrays*, Energy, 83, p.403-415.
20- Neill, S. P., Hashemi, M. R., and Lewis, M. J., (2014), *Optimal phasing of the European tidal stream resource using the greedy algorithm with penalty function*, Energy, 73, p.997-1006.
21- Hervouet, J. M., (2007), *Hydrodynamics of free surface flows: modelling with the finite element method*, John Wiley and Sons.
22- Canadian Hydraulics Centre of the National Research Council Canada. Blue Kenue. [Online]. Available: http://www.nrccnrc.gc.ca/eng/solutions/advisory/blue_kenue_index.html.[Accessed: 12-Dec-2012].
23- Pérez-Ortiz, A., Pescatore, J., and Bryden, I., (2013, September), *A systematic approach to undertake tidal energy resource assessment with Telemac-2D*, In 10th European Wave and Tidal Energy Conference (EWTEC) (p. 9). Denmark: Aalborg.
24- Dehghan Madiseh, S., Esmaily, F., Marammazi, J. G., Koochaknejad, E., and Farokhimoghadam, S., (2012), *Benthic invertebrate community in Khur-e-Mussa creeks in northwest of Persian Gulf and the application of the AMBI (AZTI's Marine Biotic Index)*, Iranian Journal of Fisheries Sciences, 11(3), p.460-474.
25- OSU TPXO Tide Models, Service Home Page, Available online: https://www.tpxo.net/
26- Nolivos Alvarez, I., Choudhur, A., and Manbaliu, J., (2009), *N 2d hydrodynamic modelling of a tidal inlet using telemac, case study of "de ijzermonding*, Bachelor's thesis, Vrije Universiteit Brussel Belgium.